1997

Theoretical study: depth of small cracks (circa 100 microns) from photoinductive data

Ananth Sethuraman
Iowa State University

INFORMATION TO USERS

This manuscript has been reproduced from the microfilm master. UMI films the text directly from the original or copy submitted. Thus, some thesis and dissertation copies are in typewriter face, while others may be from any type of computer printer.

The quality of this reproduction is dependent upon the quality of the copy submitted. Broken or indistinct print, colored or poor quality illustrations and photographs, print bleedthrough, substandard margins, and improper alignment can adversely affect reproduction.

In the unlikely event that the author did not send UMI a complete manuscript and there are missing pages, these will be noted. Also, if unauthorized copyright material had to be removed, a note will indicate the deletion.

Oversize materials (e.g., maps, drawings, charts) are reproduced by sectioning the original, beginning at the upper left-hand corner and continuing from left to right in equal sections with small overlaps. Each original is also photographed in one exposure and is included in reduced form at the back of the book.

Photographs included in the original manuscript have been reproduced xerographically in this copy. Higher quality 6" x 9" black and white photographic prints are available for any photographs or illustrations appearing in this copy for an additional charge. Contact UMI directly to order.

UMI

A Bell & Howell Information Company
300 North Zeeb Road, Ann Arbor MI 48106-1346 USA
313/761-4700 800/521-0600

Theoretical study: Depth of small cracks (*circa* 100 microns) from photoinductive data

by

Ananth Sethuraman

A dissertation submitted to the graduate faculty

in partial fulfillment of the requirements for the degree of

DOCTOR OF PHILOSOPHY

Major: Electrical Engineering (Electromagnetics)

Major Professor: Hsiu C. Han

Iowa State University

Ames, Iowa

1997

Graduate College

Iowa State University

This is to certify that the doctoral dissertation of

Ananth Sethuraman

has met the dissertation requirements of Iowa State University

Signature was redacted for privacy.

Major Professor

Signature was redacted for privacy.

For the Major Department

Signature was redacted for privacy.

For the Graduate College

TABLE OF CONTENTS

ACKNOWLEDGEMENTS

There are many who have generously given their time, and made this dissertation possible. I wish to acknowledge my gratitude to them. Dr. James H. Rose suggested the dissertation problem and indicated several references. Most important of all, he gave me a number of perspectives on how to carry out research. I had useful discussions with Dr. Hsiu C. Han. Dr. Robert J. Weber, Dr. Lalita Udpa and Dr. Michael W. Smiley critically reviewed the project. Dr. Norio Nakagawa offered advice on the formulation and made available his boundary element program. Dr. John C. Moulder and Cheng-Chi Tai showed me the photoinductive apparatus. Parts of the work were presented at conferences and the feedback given by the audiences there -- particularly Dr. Harold A. Sabbagh, Dr. J.R. Bowler, Brian Lepine, Dr. Lester W. Schmerr and Dr. Donald O. Thompson -- was useful. The project was sponsored by the NSF Industry/University Center for NDE at ISU. Finally, I thank my wife for her support.

CHAPTER 1. INTRODUCTION

Scope of the Chapter

This chapter states the dissertation problem and explains its significance. It indicates the essential idea behind the approach adopted. It gives a brief statement of the findings. The chapter closes with the arrangement of the dissertation.

The Dissertation Problem

The photoinductive method is a relatively new method of nondestructive evaluation [14-15, 18-19] offering fine spatial resolution, *e.g.*, of the order of tens of microns. The dissertation problem is to devise a numerical method that reconstructs the shape and size of a crack in a (nonmagnetic) metallic test specimen from given photoinductive data. The focus is on a particular category of cracks, namely, tight surface-breaking cracks.

Significance of the Dissertation Problem

Tight surface-breaking cracks are rather difficult to reconstruct, particularly if their linear dimensions are small, say, of the order of hundreds of microns. The tightness of such cracks tends to defeat x-ray inspection, as x-ray inspection looks for a difference in the atomic number. Likewise, the smallness of such cracks tends to defeat ultrasound inspection, as ultrasound inspection depends on a good temporal resolution. In contrast, the photo inductive method is expected to be well-suited for characterizing such cracks, because of its fine spatial resolution.

Approach to the Dissertation Problem

Our approach is based on three facts:

(i) Each photoinductive measurement can be interpreted as the square of an electric field.

(ii) The electric field mentioned in (i) is a function of a quantity known as the current dipole density.

(iii) The support of the current dipole density -- the set of points where the current dipole density is non-zero -- can be identified as the crack.

From (i) and (ii), the square of the electric field, *i.e.*, the photoinductive measurement, is also a function of the current dipole density. If this function has an inverse, the current dipole density can be computed from the photoinductive measurement. The crack then emerges from (iii).

The Findings of the Dissertation

Using (synthetic) photoinductive measurements, we have shown that in principle it is possible to reconstruct cracks whose size is on the order of tenths of a millimeter in nonmagnetic metals, subject to the question of ill-posedness. Ill-posedness manifests itself as a kind of non-uniqueness: there exist a number of cracks such that photoinductive measurements for them differ only by a few per cent. An additional criterion -- that of seeking a crack with the least perimeter -- helps to select a unique crack.

The photoinductive method also stably determines the geometry of larger cracks, with lengths of the order of a millimeter or more.

Arrangement of the Dissertation

We begin by delineating the specific category of cracks we wish to reconstruct: small, tight, surface-breaking cracks. Next we review the a.c. field measurement method and the standard eddy current method, which have been described in the literature in connection with crack characterization. While covering the eddy current method, we stress the concept of the current dipole density, as it is useful in the photoinductive method. We then examine the photoinductive method. After this, we explain our numerical method for reconstructing the

crack from photoinductive measurements. Applying the numerical method to (synthetic) photoinductive measurements, we analyze the successes and the limitations of the numerical method. The limitations are mainly due to the ill-posedness inherent in the dissertation problem. This brings us to the conclusion.

CHAPTER 2. THE TIGHT CRACK MODEL

Scope of the Chapter

This chapter sets out certain assumptions used to model tight cracks. It also explains the rationale for the assumptions. The chapter closes by mentioning certain nondestructive methods of characterizing cracks.

Assumptions of the Tight Crack Model

By the phrase "tight crack model", we mean a set of assumptions that simplify the geometry of the crack, thereby making the reconstruction of the crack a little easier. The assumptions are as follows.

(i) The crack is so thin that it can be modeled as a two-dimensional figure.

(ii) The two-dimensional figure mentioned in (i) lies in a given vertical cross-section of the test specimen.

(iii) The crack is an electrical insulator. In particular, it is impossible for an electric current to pass normal through the two-dimensional figure mentioned in (i).

Motivation for Assumption (i)

A crack may be either surface-breaking or buried. The distinction is that if the crack is surface-breaking, its boundary intersects the top surface of the test specimen. The first step in reconstructing the crack is to know whether the crack is surface-breaking or buried. The tight crack model supposes that this first step has already been carried out and that the crack is known to be surface-breaking.

A surface-breaking crack gives rise to an opening on the top surface of the test specimen (Figure 2.1). The very word "crack" suggests that width of the opening is small in some sense. The tight crack model supposes that the width of the opening tends to zero.

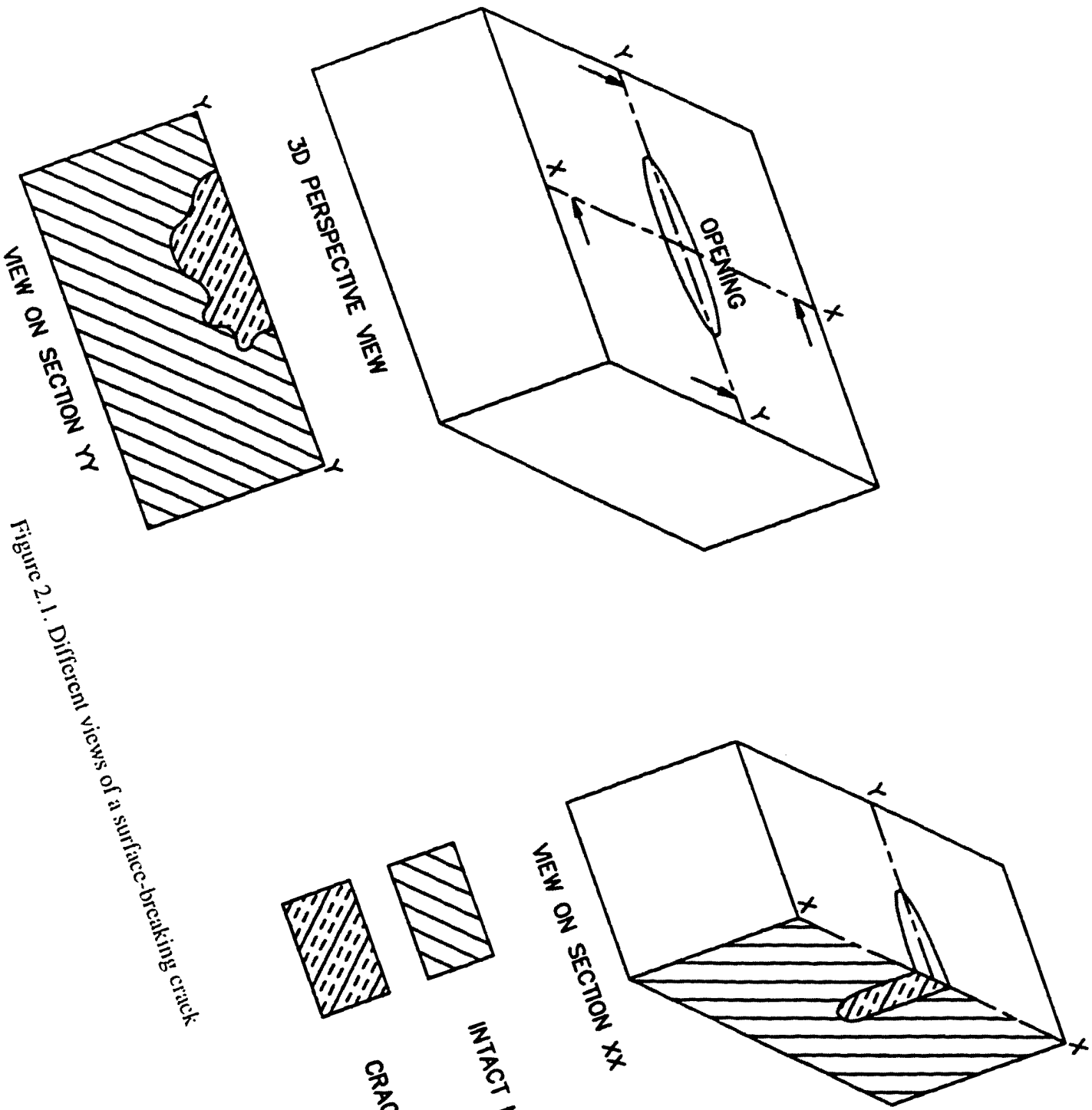

Figure 2.1. Different views of a surface-breaking crack

This statement reduces the opening to a line, and the crack as a whole to a two-dimensional figure. This leads to the assumption (i) of the tight crack model.

Motivation for Assumption (ii)

There are some possibilities concerning the two-dimensional figure mentioned above. It may lie in a vertical cross-section of the test specimen, or in a plane inclined at some angle to the top surface, or in a curved surface rather than a plane. The mathematical model supposes that the two-dimensional figure lies in a vertical cross-section of the test specimen.

There may more than one crack in the test specimen. If so, these cracks may lie in different vertical cross-sections of the test specimen. The tight crack model ignores this possibility by assuming that, if there is more than one crack, all the cracks are present in one, and the same, vertical cross-section of the test specimen (Figure 2.2).

Consider a series of vertical cross-sections of the test specimens. One of these contains the crack(s). But which one? Fortunately, this question need not be considered as a complication, as the photoinductive method has the ability to directly determine which vertical cross-section of the test specimen contains the crack(s). In fact, the particular vertical cross-section containing the crack(s) can be considered a given piece of information. This leads to the assumption (ii) of the tight crack model.

Motivation for Assumption (iii)

Even a crack is a material of some kind. As the crack is surface-breaking, there is a path from the air above to the interior of the crack, and it is logical to suppose that the material of the crack is air. Another possibility is that the material of the crack may be the oxide of the metal [4, page 261]. Therefore there are two possibilities for the material of the crack -- air or the oxide of the metal. In either case, the material of the crack is an electrical insulator. This leads to the assumption (iii) of the mathematical model.

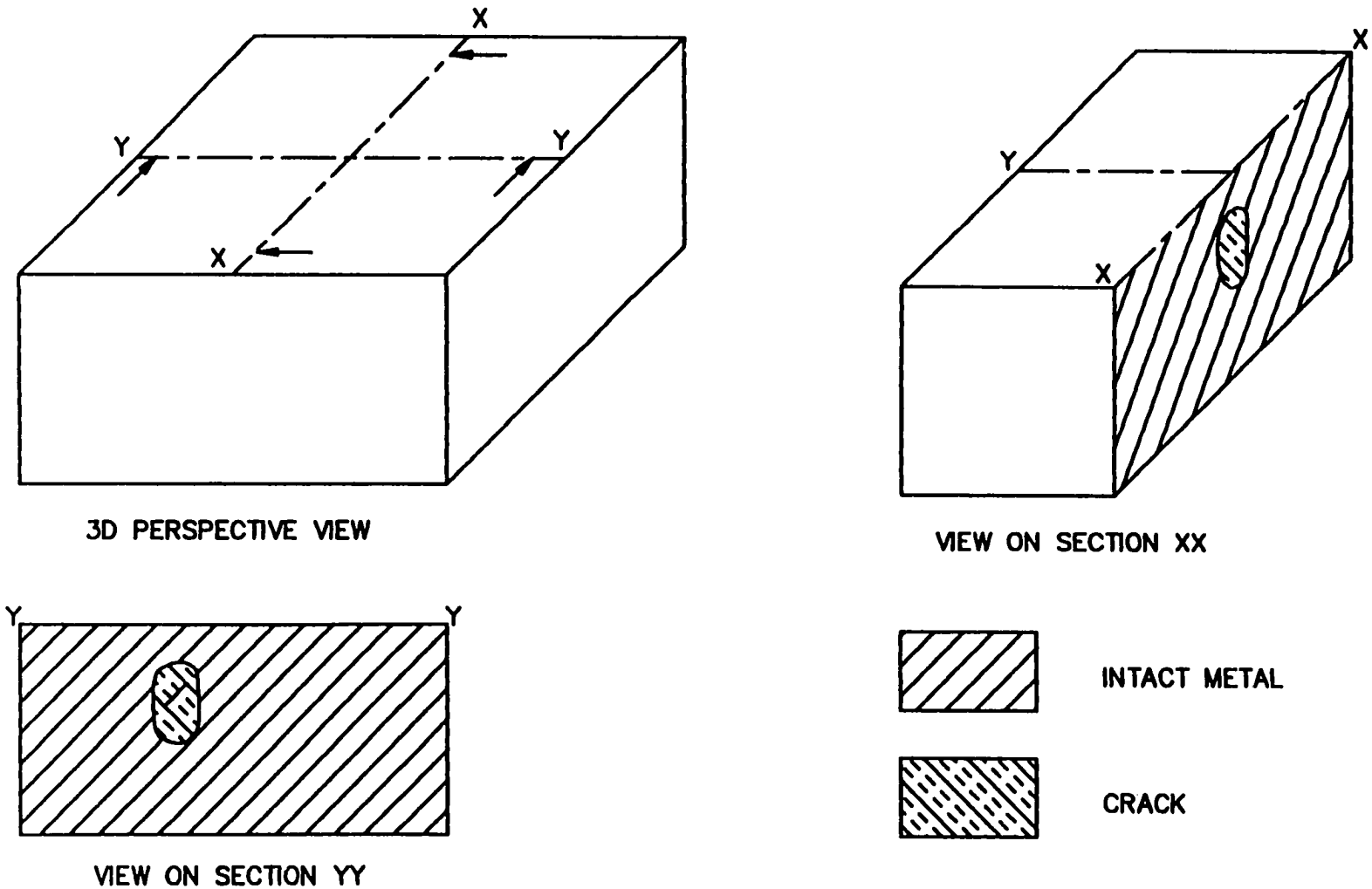

Figure 2.2. All the cracks lie in a single cross-section

Some Nondestructive Methods for Characterizing Cracks

The very phrase "electrical insulator" occurring in assumption (iii) suggests that electromagnetic methods will be useful for characterizing the cracks we are interested in. In Chapter 3, we shall discuss an electromagnetic method known as the a.c. field measurement method. In Chapter 4, we shall discuss another electromagnetic method known as the standard eddy current method. However, the main subject of this dissertation is yet another electromagnetic method, known as the photoinductive method.

CHAPTER 3. CRACK RECONSTRUCTION USING THE A.C. FIELD MEASUREMENT METHOD

Scope of the Chapter

This chapter explains how the a.c. field measurement method operates. It describes the working of the a.c. field measurement method in connection with two kinds of cracks: a one-dimensional infinite through crack and a crack with finite length, with a sketch of the relevant derivations. The chapter closes with some results on crack reconstruction.

Operation of the A.C. Field Measurement Method

The a.c. field measurement method, also known as the a.c. potential drop method [3, page 272], characterizes cracks by injecting current into the metallic test specimen, and measuring voltages. The frequency of the injected current is relatively high and the cracks are relatively large, so that the skin depth is much less than the crack depth.

The apparatus is shown in Figure 3.1. A current source is used to inject current at the point M into the metallic test specimen, and collect it at N. The current travels by diverse paths through the metal from M to N (Figure 3.1). Let p,q,P,Q be points on the top surface of the test specimen such that p,q,P are on one side of the crack $ABCD$ while Q is on the other side. Let $pq = PQ = \Delta$. Let v,V be the voltages across pq and PQ respectively. These voltages are measured. In general $v \neq V$. The task is to characterize the crack from the measured voltages v and V.

Intuitive Reason the Crack can be Reconstructed

As a voltage is the line integral of an electric field, v depends on a number Δ, denoting the average length of the paths down which the current flows when the crack is absent. Similarly, V depends on a number L, denoting the average length of the paths

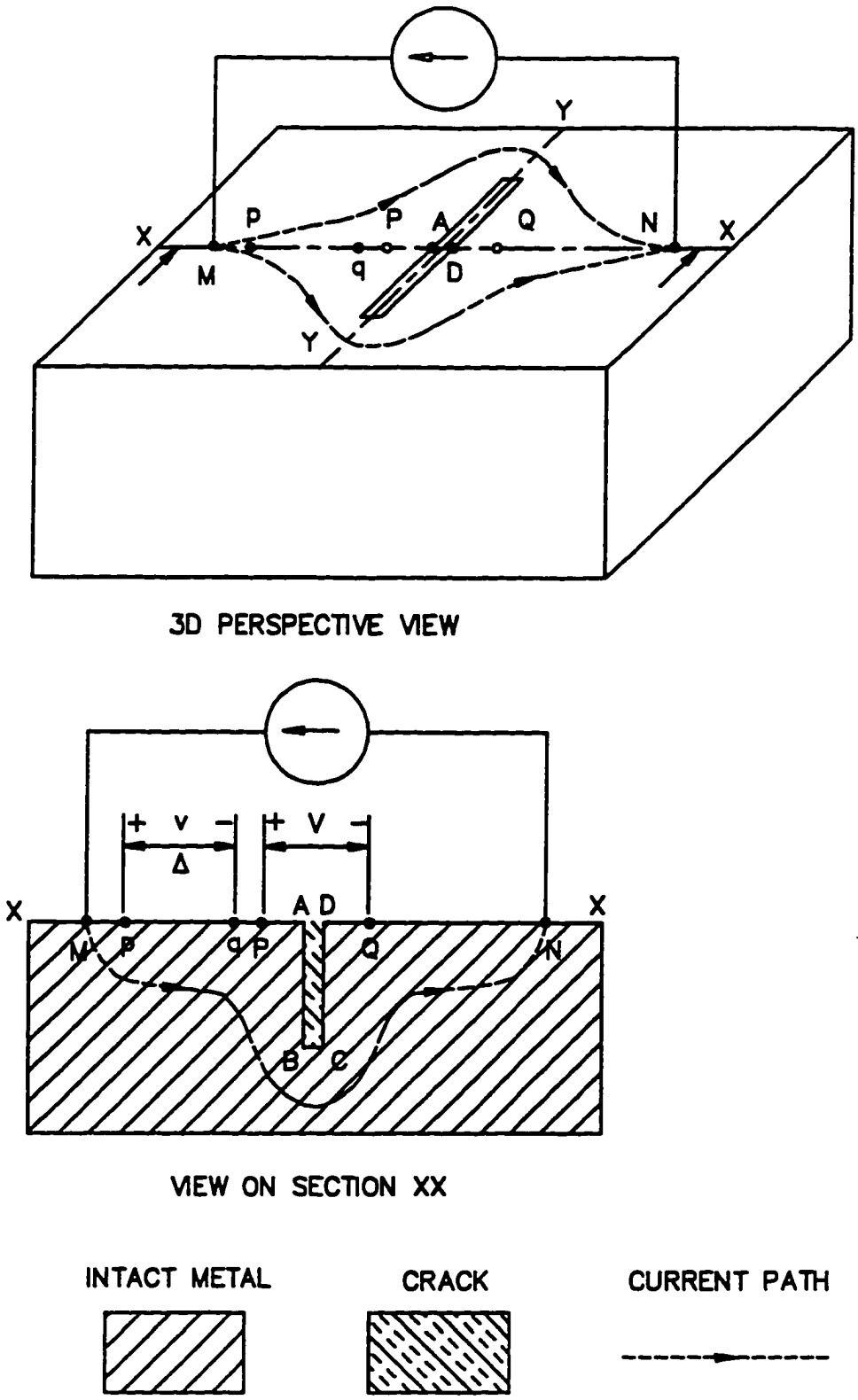

Figure 3.1. The apparatus of the a.c. field measurement method

down which the current flows when the crack is present. The difference between v and V depends on the difference between Δ and L. But the difference between Δ and L is of the order of the dimensions of the crack. Therefore, by studying the voltages v and V, we expect to estimate the dimensions of the crack.

Assumptions of the One-Dimensional Crack

The intuition indicated above is verified with a simple example of a crack termed the one-dimensional crack [3, page 255] Assume that the statements (i)-(iv) given below are true.

(i) The leads of the voltmeter are twisted into a braid. Twisting the leads is a precaution against spurious components in the voltage [3, page 260].

(ii) The crack is covered by the tight crack model of Chapter 2.

(iii) The crack and the test specimen extends to an infinite length in the direction perpendicular to the plane of the paper, or, equivalently, the crack and the test specimen have translational symmetry.

(iv) The a.c. frequency tends to infinity, or, equivalently, the skin depth tends to zero.

Derivations for a One-Dimensional Crack

By the statements (i) and (ii), the area formed by the voltmeter probes, the wiring internal to the voltmeter, and the curve $PABCDQ$ is small, ideally zero. To keep the derivation simple, let us say that the area is indeed zero. Therefore the magnetic flux cutting this area is also zero. By the law of electromagnetic induction

$$\int_{\text{voltmeter}} \mathbf{E} \cdot d\mathbf{l} = \int_{PABCDQ} \mathbf{E} \cdot d\mathbf{l}. \tag{3.1}$$

The left-hand side can be identified as V. In the right-hand side, we use Ohm's law to replace the integrand $\mathbf{E}$ by $\mathbf{J}/\sigma$, where $\mathbf{J}$ is the current density and σ the current density. Therefore

$$V = \frac{1}{\sigma} \int_{PABCDQ} \mathbf{J} \cdot d\mathbf{l}. \tag{3.2}$$

In the same way

$$v = \frac{1}{\sigma} \int_{pq} \mathbf{J} \cdot d\mathbf{l}. \tag{3.3}$$

Next, by the translational symmetry -- assumption (iii) -- the current does not have a component perpendicular to the plane of the paper. And, by the thin skin limit -- assumption (iv) -- the current behaves like a current sheet. As a result, the current density is uniform. Equations 3.2 and 3.3 become

$$V = \frac{J}{\sigma}(PA + AB + BC + CD + DQ) \tag{3.4}$$

$$v = \frac{J}{\sigma}(pq) \tag{3.5}$$

Therefore

$$\frac{V}{v} = \frac{PA + AB + BC + CD + DQ}{pq}. \tag{3.6}$$

But

$$PA + BC + DQ = PA + AD + DQ = PQ = \Delta \tag{3.7}$$

$$AB = CD = d \tag{3.8}$$

$$pq = \Delta \tag{3.9}$$

Therefore,

$$\frac{V}{v} = \frac{\Delta + 2d}{\Delta}. \tag{3.10}$$

Or

$$d = \frac{1}{2}\left(\frac{V}{v} - 1\right)\Delta. \tag{3.11}$$

As all the quantities on the right-hand side can be measured, d can be computed. In this simple one-dimensional situation, d is the only dimension of the crack to be determined. Therefore the crack is completely characterized.

Assumptions of the Unfolding Model

In many situations, cracks do not satisfy the statement (iii), *i.e.*, there is no question of translational symmetry. Such cracks are termed finite aspect ratio cracks [12, page 180]. For finite aspect ratio cracks, the derivation given above does not apply. Instead, a theory known as the unfolding model is used [7, 12, 13]. Its assumptions are as follows.

(i) Consider the crack shown in Figure 3.2. Draw *abcdef* parallel to *ABCDEF*. Let the thickness of the space between *abcdef* and *ABCDEF* be a few skin depths. Let an a.c. current be injected into the test specimen. This current flows practically only in the space between *abcdef* and *ABCDEF*. In the space between the surfaces ab, AB, the current has no component normal to AB. In the space between the surfaces bc, BC, the current has no component normal to BC. In the space between the

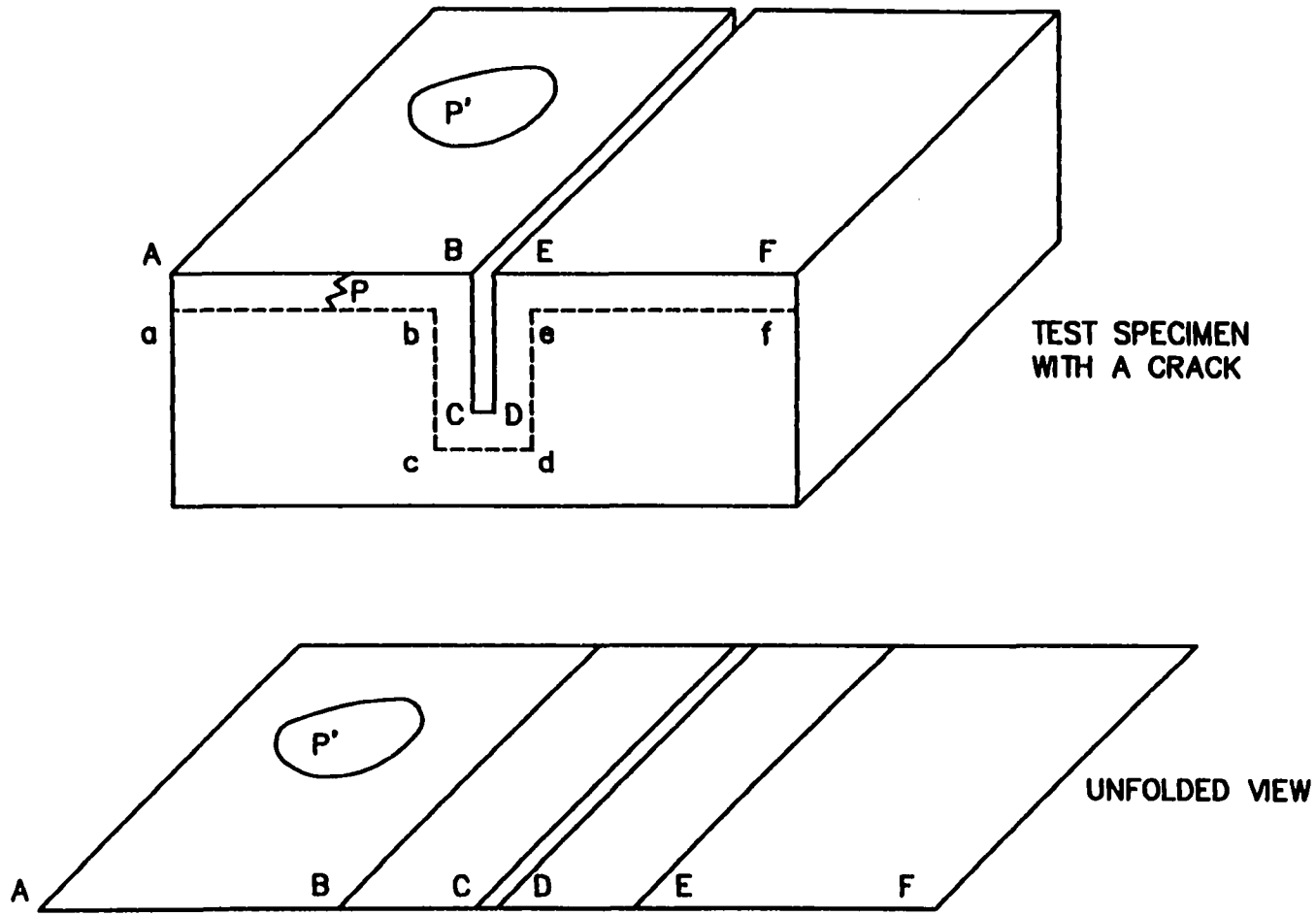

Figure 3.2. The unfolding of a crack

surfaces cd, CD, the current has no component normal to CD. In the space between the surfaces de, DE, the current has no component normal to DE. In the space between the surfaces ef, EF, the current has no component normal to EF. Therefore the current density reduces to a two-component vector. By Ohm's law the same is true of the electric field [12, Equation 2.2].

(ii) Consider a path starting from the surface $ABCDEF$ and ending on the surface $abcdef$ (the path P in Figure 3.2). Each of the two components of the electric field decays exponentially, due to the effect of the skin depth [12, Equation 2.2].

(iii) No charge accumulates in the space between $abcdef$ and $ABCDEF$ [12, Equation 2.3].

(iv) Consider any closed path drawn on $ABCDEF$ (the path P' in Figure 3.2). The line integral of the electric field on any such path is zero [12, Equation 2.3]. Or using the law of electromagnetic induction, the magnetic flux cutting the area enclosed by the closed path is zero.

(v) Consider the following five spaces:

$$ab, AB; bc, BC; cd, CD; de, DE; ef, EF$$

The electric fields in these five spaces are analytical continuations of one another. To give a vivid illustration, suppose that these spaces were to laid out straight (Figure 3.2). The five spaces would collapse into one long space. One, and the same, formula would hold for the electric field. This vivid manner of illustrating the property of analytical continuation is the reason for terming the model an unfolding model.

Sketch of the Derivations in the Unfolding Model

Let a coordinate system be introduced into the unfolded view (Figure 3.2) such that the XY plane is the unfolded surface $ABCDEF$. According to statement (ii) of the unfolding model, the electric field has only XY components, $E_X(X,Y,Z), E_Y(X,Y,Z)$. Putting $Z=0$, we obtain $E_X(X,Y,0), E_Y(X,Y,0)$, which define a two-dimensional vector field depending on two variables XY. By statement (iv), this vector field is conservative, *i.e.*, there exists a function $\Phi(X,Y)$ such that

$$E_X(X,Y,0)=\frac{\partial \Phi}{\partial X}, E_Y(X,Y,0)=\frac{\partial \Phi}{\partial Y}. \tag{3.12}$$

From statement (iii), $\Phi(X,Y)$ is harmonic. Since Φ is a harmonic function of only two variable, rather than three, it is possible to introduce complex variable theory. Specifically, there exists a function $\Psi(X,Y)$ such that Φ, Ψ satisfy the Cauchy-Riemann equations:

$$E_X(X,Y,0)=\frac{\partial \Phi}{\partial X}=\frac{\partial \Psi}{\partial Y} \tag{3.13}$$

$$E_Y(X,Y,0)=\frac{\partial \Phi}{\partial Y}=-\frac{\partial \Psi}{\partial X} \tag{3.14}$$

Or if

$$Z=X+iY \tag{3.15}$$

$$W(Z)=\Phi(X,Y)+i\Psi(X,Y) \tag{3.16}$$

then

$$\frac{dW}{dZ}=\frac{\partial(\Phi+i\Psi)}{\partial X}=\frac{\partial(\Phi+i\Psi)}{i\partial Y}=E_X-iE_Y \tag{3.17}$$

Consider those points (X,Y) on the unfolded view where the current is flowing. For such points (X,Y), the components of the electric field $E_X(X,Y,0), E_Y(X,Y,0)$ cannot both be zero, since the current is flowing. Therefore, dW/dZ cannot be zero. Therefore, Z, W are connected by a conformal mapping. This means that Z can be considered as a function of W. Equivalently, it is meaningful to speak of the functions $X(\Phi,\Psi), Y(\Phi,\Psi)$. The importance of this comment is as follows.

The current does not flow at a tangent to the surface-breaking edge nor at a tangent to the buried edge of the crack. By Ohm's law, the electric field does not have a component at a tangent to these edges. Therefore both the surface-breaking edge and the buried edge of the crack are characterized by a constant value of Φ. This constant value can be chosen to be zero. Therefore the locus

$$X = X(\Phi,\Psi)|_{\Phi=0} \tag{3.18}$$

$$Y = Y(\Phi,\Psi)|_{\Phi=0} \tag{3.19}$$

can be identified as the union of the buried and the surface-breaking edges of the crack. The strategy of reconstructing the crack is therefore to use the measured voltages to determine Φ, Ψ, X, Y, and hence the buried edge of the crack. The derivations are based on Plemelj's formula [12][13, page 368]. Omitting the details of the derivations, let us pass on to the results presented by McIver [12].

Achievements with the Unfolding Model

Using the unfolding model, it has been possible to reconstruct semicircular, semielliptical and triangular cracks whose aspect ratios is of the order of 1.5 to 5.0. The accuracy of the reconstruction is good wherever the buried edge has a single well-defined tangent. For example, semicircular and semielliptical cracks -- which have a tangent -- have

been reconstructed accurately. Triangular cracks have been reconstructed accurately everywhere except in a small neighborhood of the vertex. But at the vertex, the buried edge does has two tangents, and not one clear-cut tangent.

CHAPTER 4. CRACK RECONSTRUCTION USING THE STANDARD EDDY CURRENT METHOD

Scope of the Chapter

This chapter first describes the operation of the standard eddy current method. Next, it introduces the concept of the current dipole density. Then it covers the properties of the current dipole density. It also covers certain equations in which the current dipole density has a role. The chapter describes a crack reconstruction procedure used by Bowler, Norton and Harrison [2] touching on the subject of ill-posedness. The chapter closes with some results obtained with this reconstruction procedure.

The Principle of the Standard Eddy Current Method

The standard eddy current method operates by inducing a current in the test specimen and measuring an impedance. The apparatus is shown in Figure 4.1. A current source is connected to an air-core coil of cylindrical cross-section, set on the test specimen with axis vertical. In this condition, the test specimen is separated from the coil by the insulating case that houses the coil. Therefore, unlike the a.c. field measurement method, current cannot be injected into the test specimen. Rather, current is induced to flow in the test specimen by transferring power in a non-contact manner. This is described next.

The time-varying current in the coil gives rise to a time-varying magnetic field directed roughly normal to the test specimen. The time-varying magnetic field, according to the law of electromagnetic induction, gives rise to an electric field in the test specimen. By Ohm's law, a current, known as the eddy current, flows in the test specimen (Figure 4.1). The power for the eddy current, in the final analysis, comes from the current source driving the coil.

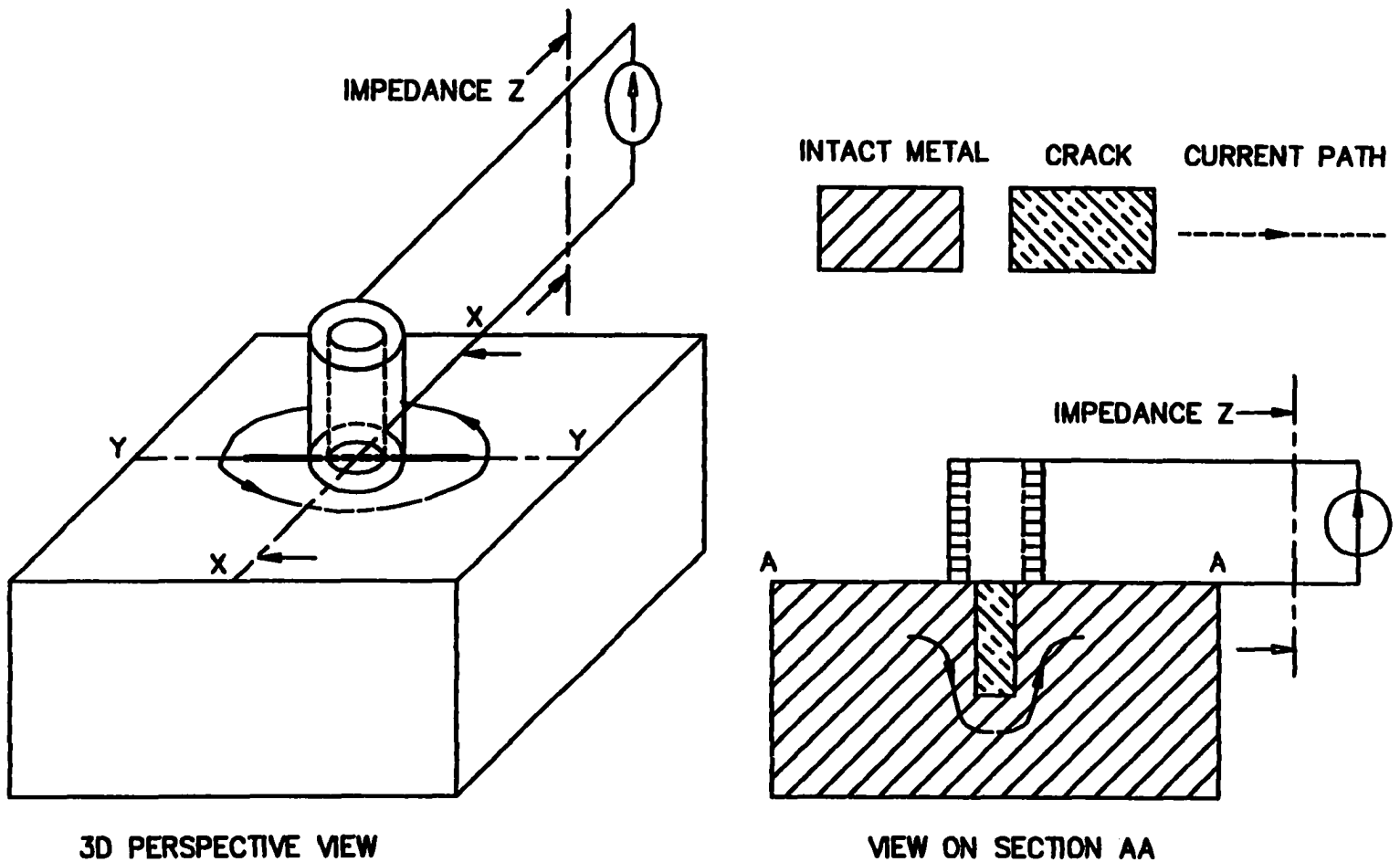

Figure 4.1. The apparatus of the standard eddy current method

The Importance of the Impedance

If the current of the current source is $\sqrt{2}I\cos\omega t$, and the impedance facing the current source is Z, the power provided by the current source is I^2Z. By the design of the current source I is a constant, so that monitoring Z is equivalent to monitoring the power.

The impedance Z is measured using an impedance analyzer (not shown in Figure 4.1). After this, the coil is moved a considerable distance from the crack and the impedance is measured again. This is a new number, Z_0. It indicates what the impedance would be in the absence of the crack and is termed the reference impedance.

As the very word "reference" suggests, the standard eddy current method compares the numbers Z and Z_0. If the test specimen does not have a crack, we would expect that $Z = Z_0$. On the other hand, if the test specimen does have a crack, we would expect the difference $Z - Z_0$ to be relatively large. In short, the difference $Z - Z_0$ is sensitive to the presence or the absence of the crack. Conversely, we expect that a study of the difference $Z - Z_0$ will help to reconstruct the crack.

It is possible to move the coil down the length of the crack (Figure 4.2). This would give rise to multiple values of Z, one for each coil position, and hence to multiple values of $Z - Z_0$. All these values may be used for crack reconstruction.

The Current Dipole Density

As explained by Bowler [1], a key step in the reconstruction of the crack is to introduce a concept called current dipole density. To define this concept, the crack is first visualized as a three-dimensional figure whose thickness is eventually allowed to tend to zero (Figure 4.3). Before the thickness tends to zero, the crack has two faces, S_+, S_-. Let $\mathbf{r}$ be a position vector lying on either face. The electric field $\mathbf{E}(\mathbf{r})$ can be represented as

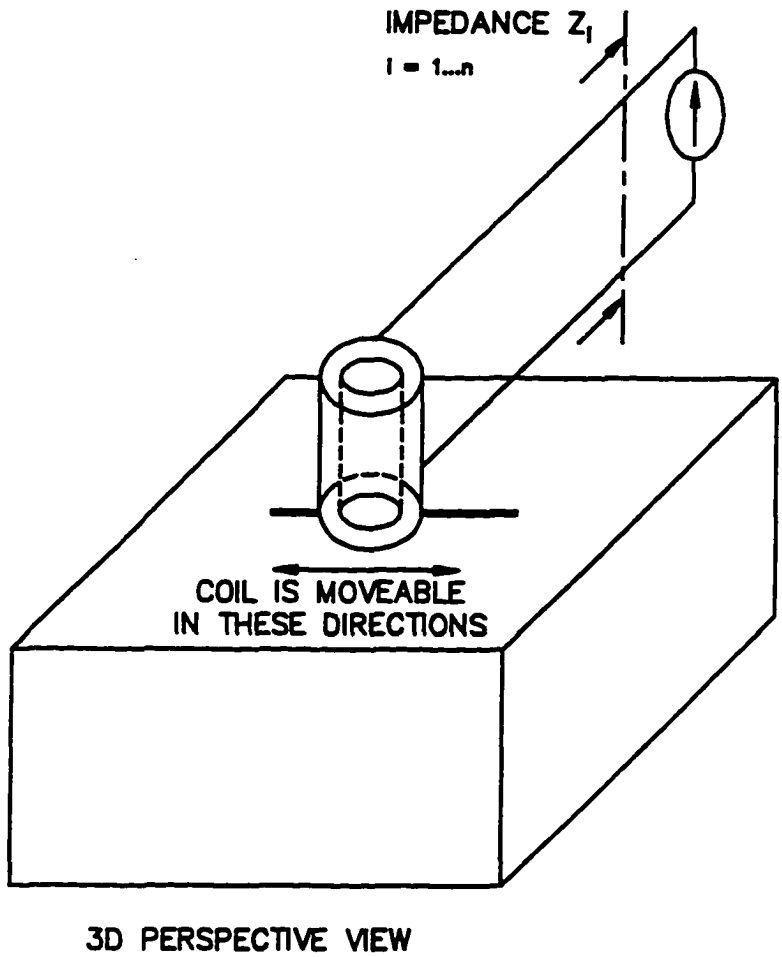

Figure 4.2. The coil can be set at any position down the length of the crack

$$\mathbf{E}(\mathbf{r}) = \nabla\phi(\mathbf{r}) + \nabla\times[U(\mathbf{r})\mathbf{n}] \tag{4.1}$$

where $\phi(\mathbf{r})$ and $U(\mathbf{r})$ are scalar fields defined on the crack faces S_+, S_- and $\mathbf{n}$ is the unit vector normal to the crack faces. Let $\mathbf{r}_+, \mathbf{r}_-$ be two position vectors on S_+, S_- respectively, such that each position is a mirror image of the other, the plane of symmetry being the midplane between S_+, S_- (Figure 4.3). Putting $\mathbf{r} = \mathbf{r}_+, \mathbf{r} = \mathbf{r}_-$ in Equation 4.1,

$$\mathbf{E}(\mathbf{r}_+) = \nabla\phi(\mathbf{r}_+) + \nabla\times[U(\mathbf{r}_+)\mathbf{n}] \tag{4.2}$$

$$\mathbf{E}(\mathbf{r}_-) = \nabla\phi(\mathbf{r}_-) + \nabla\times[U(\mathbf{r}_-)\mathbf{n}] \tag{4.3}$$

As the thickness of the three-dimensional crack tends to zero, the two faces of the crack, S_+, S_-, approach one another and define a two-dimensional figure, which is merely the tight crack of Chapter 2. The position vectors $\mathbf{r}_+, \mathbf{r}_-$ tends to a common limit, $\mathbf{r}$. It is shown by Bowler [1] that there exists a finite scalar-valued function of $\mathbf{r}$, $p_n(\mathbf{r})$, such that

$$\phi(\mathbf{r}_+) \to \phi(\mathbf{r}_-) + \frac{p_n(\mathbf{r})}{\sigma} \tag{4.4}$$

Multiplying $p_n(\mathbf{r})$ by the unit normal vector $\mathbf{n}$, we obtain a vector field defined on the tight crack. This vector field is termed the current dipole density.

Properties of the Current Dipole Density

The current dipole density possesses a number of properties that are useful not only in the standard eddy current method, but also in the photoinductive method. Therefore we shall describe these properties in some detail.

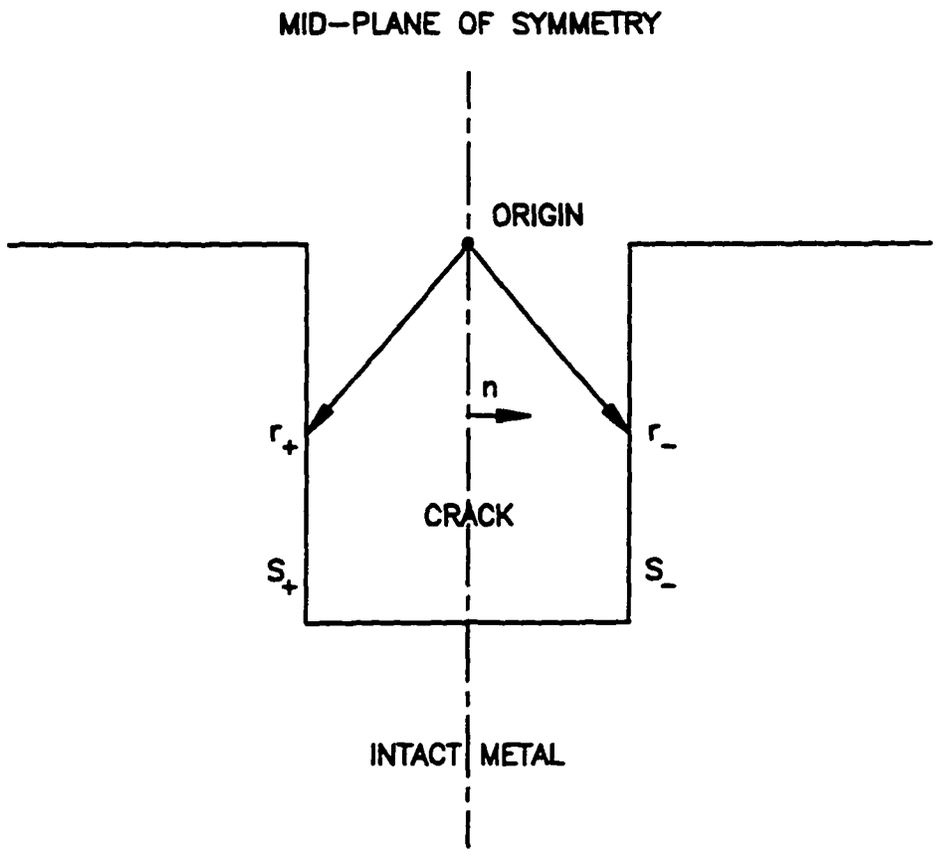

Figure 4.3. A tight crack is the limit of crack as the width tends to zero

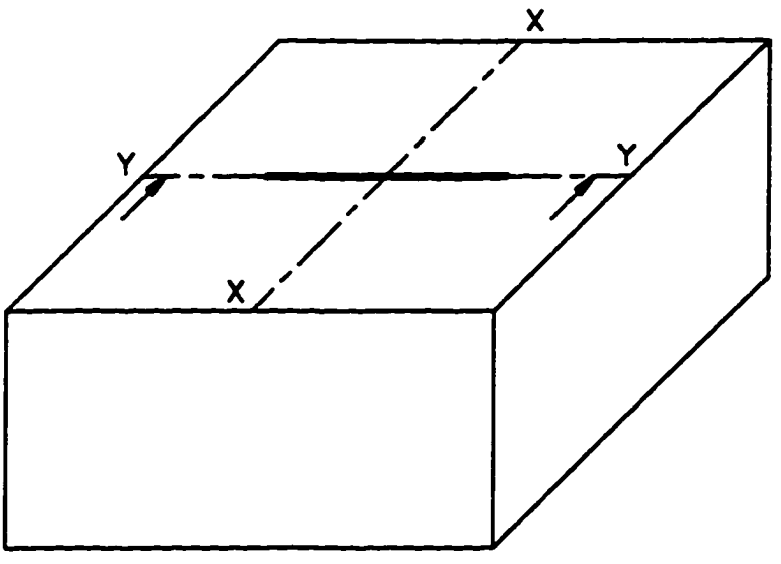

3D PERSPECTIVE VIEW

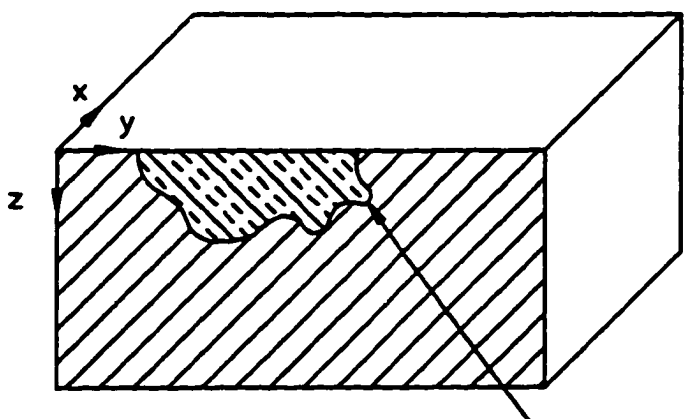

VIEW ON SECTION YY $z = f(y)$

INTACT METAL $p_x = 0$

CRACK $p_x \neq 0$

Figure 4.4. A coordinate system for the test specimen

To describe these properties, it is convenient to choose a coordinate system such that the top surface of the test specimen is the xy plane (Figure 4.4). The vertical plane containing the crack is yz plane. Let the positive z-axis point into the test specimen. The current dipole density possesses the properties (i)-(v) given below.

(i) The dimension of the current dipole density is current divided by length.

(ii) The current dipole density is a vector, and therefore can be projected into x, y, z components.

(iii) The y, z components of the current dipole density are zero. Only the x-component, p_x, is nonzero. In general, the components of the current dipole density at a tangent to the crack are zero, while the normal component is nonzero.

(iv) This x-component p_x varies as a function of y and z.

(v) Half the yz plane is embedded in the test specimen (Figure 4.5). This half can be divided into two parts -- the cracked part and the intact part (Figure 4.6). The current dipole density is defined on the cracked part However, we may extend the domain of definition so as to include the intact part also: if (y, z) is a point in the intact part, we set $p_x = 0$.

Important Equations Involving the Current Dipole Density

The current dipole density appears as a factor in a number of equations that are useful in not only the standard eddy current method, but also in the photoinductive method.

(i) If (x,y,z) is a point in the test specimen, the electric field is given by

$$\mathbf{E}(x,y,z) = \mathbf{E}_0(x,y,z) + \iint_{crack} \mathbf{G}_1(x,y,z,0,y',z') p_x(y',z') dy'dz' \qquad (4.5)$$

or, equivalently,

$$E_x(x,y,z) = E_{0x}(x,y,z) + \iint_{crack} G_{1x}(x,y,z,0,y',z')p_x(y',z')dy'dz', \quad (4.6)$$

$$E_y(x,y,z) = E_{0y}(x,y,z) + \iint_{crack} G_{1y}(x,y,z,0,y',z')p_x(y',z')dy'dz', \quad (4.7)$$

$$E_z(x,y,z) = E_{0z}(x,y,z) + \iint_{crack} G_{1z}(x,y,z,0,y',z')p_x(y',z')dy'dz' \quad (4.8)$$

In Equations 4.5-4.8, $\mathbf{E}_0$ denotes the electric field in the absence of the crack. An explicit formula for it has been published by Dodd and Deeds [5, put $\alpha_1 = \alpha_2$ in Equation 75] and by Bowler [1, Equations 23-27]. The function $\mathbf{G}_1$ is the first column of a dyadic (3×3 matrix) Green's function. An explicit formula for it has been published by Raiche and Coggon [20] and by Bowler [1, Equations 17-20 and the Appendix].

(ii) As the crack is an electrical insulator, the normal component -- the x-component -- of the current density is zero at any point (y,z) of the crack:

$$J_x(0,y,z) = 0. \quad (4.9)$$

By Ohm's law,

$$E_x(0,y,z) = 0. \quad (4.10)$$

Combining Equations 4.6 and 4.10,

$$E_{0x}(0,y,z) + \iint_{guessed\_crack} G_{1x}(0,y,z,0,y',z')p_x(y',z')dy'dz' = 0. \quad (4.11)$$

(iii) The formula for the change in the impedance is

$$Z - Z_0 = -\iint_{crack} p_x(y,z)E_{0x}(0,y,z)dydz \quad (4.12)$$

Crack Reconstruction Procedure

The reconstruction procedure described by Bowler, Norton and Harrison [2] is as follows. First, a guess is made as to the shape of the crack. Next, the p_x corresponding to the guessed crack is determined by solving Equation 4.11. Then Equation 4.12 is used to calculate $Z - Z_0$. This should agree with the measured value of $Z - Z_0$, if the guessed crack is the correct one.

It was noted earlier that it is possible to move the coil down the length of the crack, measuring $Z - Z_0$ for each coil position. These are used as follows. For each coil position, Equation 4.11 is solved to obtain the p_x corresponding to the guessed crack, and this p_x is substituted in Equation 4.12 to compute $Z - Z_0$. The computed $Z - Z_0$ is compared with the $Z - Z_0$ which was measured for that particular coil position. The two should be equal for each, and every, coil position, if the guessed crack is the correct one.

If the measured and the computed $Z - Z_0$ disagree, a new guess must be made as the crack and the steps mentioned above on the new guess.

From the above outline, it is clear that the procedure to reconstruct the crack is an optimization procedure. The objective function is

$$\sum_{all\_coil\_positions} \left| (Z - Z_0)_{measured} - (Z - Z_0)_{calculated} \right|^2 \qquad (4.13)$$

while the unknowns to be determined are the shape and the size of the crack. The crack is considered to be the area between the y-axis and the curve $z = f(y)$ in the yz plane (Figure 4.6). Knowing the function f is equivalent to knowing the crack. The objective function just mentioned is therefore considered to be a functional whose argument is f. The details of the optimization are given by Bowler, Norton and Harrison [2].

The problem is inherently ill-posed for reasons given in Chapter 9. In the work of Bowler, Norton and Harrison [2], the ill-posedness was averted by adjoining the constraint

that the area of the crack should be as small as possible. This constraint adds one more term to the objective functional and is a stabilizing functional in the sense of Tikhonov [24, page 59].

Achievements of the Reconstruction Procedure

The procedures given by Bowler, Norton and Harrison [2] have been used to reconstruct semielliptical cracks as well as cracks of fairly irregular shape. In the case studies presented by these authors, the crack sizes were on the order of millimeters.

CHAPTER 5. THE GREEN'S FUNCTION

Scope of the Chapter

This chapter describes the partial differential equations whose Green's function was mentioned in the Chapter 5. It sketches the main ideas behind the derivation of the Green's function, touching in particular on the gauge conditions. The chapter then quotes the formula for the Green's function. The chapter concludes with the near field asymptotic development of the Green's function.

The Partial Differential Equations

Let a cartesian coordinate system be adopted, and suppose that the half-space $z > 0$ is occupied with a metal, while the half-space $z < 0$ is free space. Combining Maxwell's laws with the identity

$$\nabla \times \nabla \times \mathbf{E} = \nabla(\nabla \cdot \mathbf{E}) - \nabla^2 \mathbf{E} \tag{5.1}$$

we obtain the following equations. In the metal,

$$\begin{aligned} &(\nabla^2 + k^2)\mathbf{E} = \mathbf{0}, \\ &k = \frac{1+i}{\delta} \end{aligned} \tag{5.2}$$

where δ is the skin depth. In air,

$$\nabla^2 \mathbf{E} = \mathbf{0} \tag{5.3}$$

Equation 5.2 is valid only if the metal is not cracked. Suppose that there is a crack. Let σ_{crack} denote the conductivity of the crack and σ_{metal} the conductivity of the metal. Define a new quantity $\sigma_{correction}(\mathbf{r})$ as follows. If $\mathbf{r}$ is a position vector in the crack,

$$\sigma_{correction}(\mathbf{r}) = \sigma_{crack} - \sigma_{metal} \tag{5.4}$$

Thus if the crack is modeled as an insulator, $\sigma_{crack} = 0$ and $\sigma_{correction} = -\sigma_{metal}$. If $\mathbf{r}$ is a position vector in the intact metal,

$$\sigma_{correction}(\mathbf{r}) = 0 \tag{5.5}$$

The formula

$$\sigma(\mathbf{r}) = \sigma_{metal} + \sigma_{correction}(\mathbf{r}) \tag{5.6}$$

gives the conductivity of any position vector $\mathbf{r}$, whether $\mathbf{r}$ is in the crack or in the intact metal. The governing differential equation for the electric field can be shown to be

$$(\nabla^2 + k^2)\mathbf{E} = -i\omega\mu_0\sigma_{correction}\mathbf{E} \tag{5.7}$$

in the half-space $z > 0$. For the half-space $z < 0$, Equation 5.3 continues to be valid even if the metal is cracked.

The Green's function for Equations 5.3 and 5.7 is a dyadic, or more simply, a 3×3 matrix. The first column of the matrix defines a vector $\mathbf{G}_1$. In the metal, $\mathbf{G}_1$ satisfies

$$(\nabla^2 + k^2)\mathbf{G}_1 = -\mathbf{i}i\omega\mu_0\delta_{3D}(\mathbf{r} - \mathbf{r}') \tag{5.8}$$

where $\mathbf{i}$ is the unit vector down the x axis. In air, $\mathbf{G}_1$ satisfies

$$\nabla^2 \mathbf{G}_1 = \mathbf{0} \tag{5.9}$$

It is this $\mathbf{G}_1$ which was referred to in Chapter 5.

Main Steps in the Derivation

The derivation of the formula for $\mathbf{G}_1$ is given in [1], [2], [20] and the references cited therein. As $\mathbf{G}_1$ has the interpretation of being an electric field, it is legitimate to write $\mathbf{G}_1$ terms of a vector potential and a scalar potential. The main steps in the derivation are:

(i) To introduce a gauge.

(ii) To write a set of partial differential equations for the vector potential.

(iii) To write a set of partial differential equations for the scalar potential.

(iv) To derive a Green's function, $\mathbf{G}_{1-vec-pot}$, for the vector potential.

(v) To use the gauge condition and the function $\mathbf{G}_{1-vec-pot}$ to derive the formula for the scalar potential.

(vi) To use the formulas for the vector potential and the scalar potential derived in (iv) and (v) to obtain $\mathbf{G}_1$.

Owing to the length of the derivation, we shall not cover it here. However, we shall mention that the gauge is neither Coulomb's nor Lorentz's. Instead it is the equation

$$\phi = -\frac{\nabla \cdot \mathbf{A}}{\mu_0 \sigma} \tag{5.10}$$

where $\mathbf{A}, \phi$ denote the vector and scalar potential respectively.

The Formula for $\mathbf{G}_1$

The formula for the x component of $\mathbf{G}_1$ is given below:

$$G_{1x} = \frac{T_1 + T_2 + T_3 + T_4 + T_5}{4\pi\sigma} \tag{5.11}$$

where

$$\begin{aligned}
T_1 &= \frac{\exp(ikr_1)}{r_1^3}\left[k^2\left(r_1^2 - X^2\right) + \left(1 - ikr_1\right)\left(\frac{3X^2}{r_1^2} - 1\right)\right] \\
T_2 &= \frac{\exp(ikr_2)}{r_2^3}\left(\frac{Y^2}{r_2^2} - \frac{Z_2^2}{r_2^2}\right)\left(3 - 3ikr_2 - k^2 r_2^2\right) \\
T_3 &= \frac{k^2 Z_2}{r_2^2}\left[I_0 K_0\left(\frac{3Y^2}{r_2^2} - 1\right) + I_1 K_1\left(\frac{2X^2}{\rho^2} - \frac{3Y^2}{r_2^2} - 1\right)\right] \\
T_4 &= \frac{ik}{r_2^2} I_1 K_0\left[\left(1 - \frac{Z_2}{r_2}\right)\left(\frac{3Y^2}{r_2^2} - 1\right) + \frac{k^2 y^2 Z_2}{r_2}\right] \\
T_4 &= \frac{ik}{r_2^2} I_0 K_1\left[\left(1 + \frac{Z_2}{r_2}\right)\left(\frac{3Y^2}{r_2^2} - 1\right) - \frac{k^2 y^2 Z_2}{r_2}\right] \\
X &= x' - x \\
Y &= y' - y \\
Z_1 &= |z' - z| \\
Z_2 &= z' + z \\
\rho &= \sqrt{\left(X^2 + Y^2\right)} \\
r_1 &= \sqrt{\rho^2 + Z_1^2} \\
r_2 &= \sqrt{\rho^2 + Z_2^2}
\end{aligned} \tag{5.12}$$

The quantities I_0, I_1 are the modified Bessel's functions I_0, I_1 with argument $\frac{1}{2}\sqrt{\omega\mu\sigma}\left(r_2 - z_2\right)\exp\left(-\frac{1}{4}i\pi\right)$. The quantities K_0, K_1 are the modified Bessel's functions K_0, K_1 with argument $\frac{1}{2}\sqrt{\omega\mu\sigma}\left(r_2 + z_2\right)\exp\left(-\frac{1}{4}i\pi\right)$.

The formula for the y component of the Green's function is given below:

$$G_{1y} = \frac{XY\left[S_1 + S_2 + S_3 + S_4 + S_5\right]}{4\pi\sigma} \tag{5.13}$$

where

$$\begin{aligned}
S_1 &= \frac{\exp(ikr_1)}{r_1^5}\left(3 - 3ikr_1 - k^2 r_1^2\right), \\
S_2 &= -\frac{\exp(ikr_2)}{r_1^5}\left(3 - 3ikr_2 - k^2 r_2^2\right), \\
S_3 &= \frac{k^2 z_2}{r_2^4}\left[I_1 K_1\left(3 + \frac{2r_2^2}{\rho^2}\right) - 3I_0 K_0\right] \\
S_4 &= -\frac{ik}{r_2^4} I_1 K_0\left[3\left(1 - \frac{z_2}{r_2}\right) + k^2 Z_2 r_2\right] \\
S_4 &= -\frac{ik}{r_2^4} I_0 K_1\left[3\left(1 + \frac{z_2}{r_2}\right) - k^2 Z_2 r_2\right]
\end{aligned} \tag{5.14}$$

The formula for the z component of $\mathbf{G}_1$ is given below:

$$G_{1z} = \frac{-X}{4\pi\sigma}\left[tA(r_1) - A(r_2)\right] \tag{5.15}$$

where

$$\begin{aligned}
t &= \frac{z - z'}{|z - z'|} \\
A(r_j) &= \frac{Z_j}{r_j^5}\exp\left(ikr_j\right)\left[3 - 3ikr_j - k^2 r_j^2\right]
\end{aligned} \tag{5.16}$$

The Near Field Asymptotic Development

If r_1 is small in comparison with the skin depth, all the factors of the type $kr_1, kX, kY, \ldots$ are small in comparison with 1. Therefore it is safe to make the approximations

$$\begin{aligned} &\exp(ikr_1) \approx 1 \\ &3 - 3ikr_1 - k^2 r_1^2 \approx 3 \end{aligned} \tag{5.17}$$

and so on. The formulas for G_{1x}, G_{1y} can be quoted as follows:

$$\begin{aligned} G_{1x} &\approx \frac{1}{4\pi\sigma}\frac{1}{r_1^3}\left(\frac{3X^2}{r_1^2} - 1\right) \\ G_{1y} &\approx \frac{3XY}{4\pi\sigma r_1^5} \end{aligned} \tag{5.18}$$

CHAPTER 6. THE PHOTOINDUCTIVE METHOD

Scope of the Chapter

This chapter first describes some of the circumstances surrounding this dissertation problem. Next it explains why it is useful to measure the square of a particular electric field. The chapter then describes the operation of the photoinductive method, showing that a photoinductive measurement yields what is essentially the square of the electric field. By way of interest, the chapter points out a delicate feature of the measurement. The chapter closes by noting an adjustment necessary to achieve fine spatial resolution.

Background

The photoinductive method is being developed at the Center for Nondestructive Evaluation and is intended to detect and characterize very small cracks whose size is on the order of 0.1-0.5 mm. This project has both an experimental and a theoretical component. The experimental side of the work has been described by Tai and Moulder [24]. The experiments reported by these authors are concerned with small cracks at the periphery of bolt-holes (corner cracks) and sensitivity has been demonstrated for cracks as small as 0.175 mm. The present thesis summarizes the state of the theoretical work, which is primarily concerned with crack characterization, *i.e.*, the problem of determining the shape and the size of the crack, once the crack has been detected.

In this chapter, we will describe the use of the photoinductive method for cracks in bolt-holes and thus maintain contact with the experimental work. However, this geometry will prove to be too difficult for a complete analysis of the problem. Consequently, the rest of the thesis will focus on a simpler geometry, namely, a surface-breaking crack in a thick metal plate -- a problem of considerable technological interest in its own right.

The Sensitivity of E^2 to Cracks

Suppose, for instance, that the test specimen is a metal plate with four bolt holes (Figure 6.1), such that three bolt holes are in good condition, while one bolt hole has a crack. Let us consider how the photoinductive method characterizes the crack.

One of the items in the photoinductive apparatus is an air-core coil of circular cross-section (Figure 6.2). This coil is designed and manufactured in the same way as the coil used in the standard eddy current method. The coil is inserted into one of the bolt holes.

The coil is connected to an alternating current source whose current is $\sqrt{2}I\cos\omega t$, where I is a constant and the frequency ω is adjustable. Due to this current, the coil causes an eddy current to flow in the test specimen. The path of the eddy current is sketched in Figures 6.2 - 6.3. Let us compare these figures.

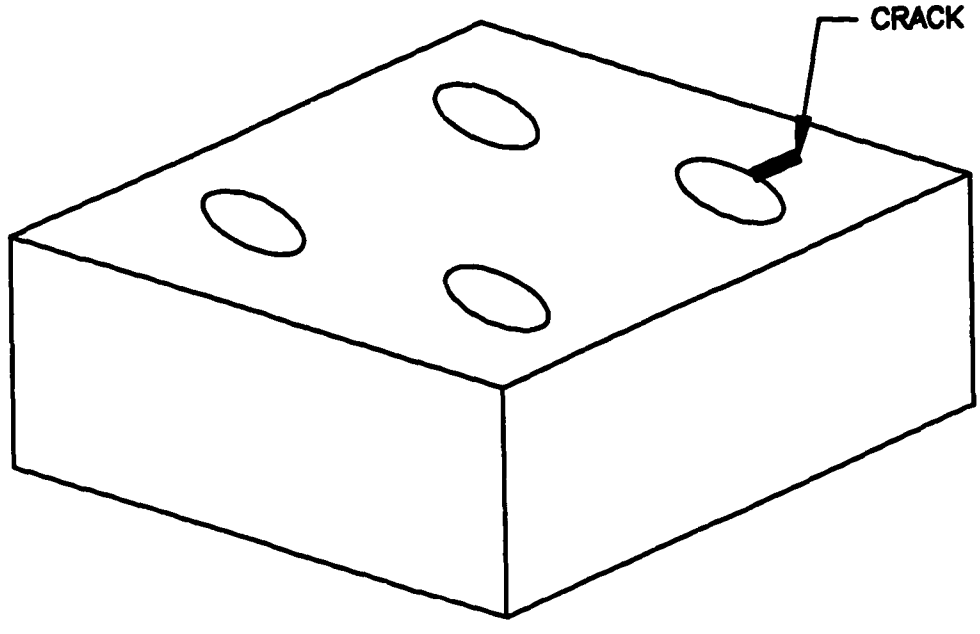

Figure 6.1. A test specimen with bolt holes

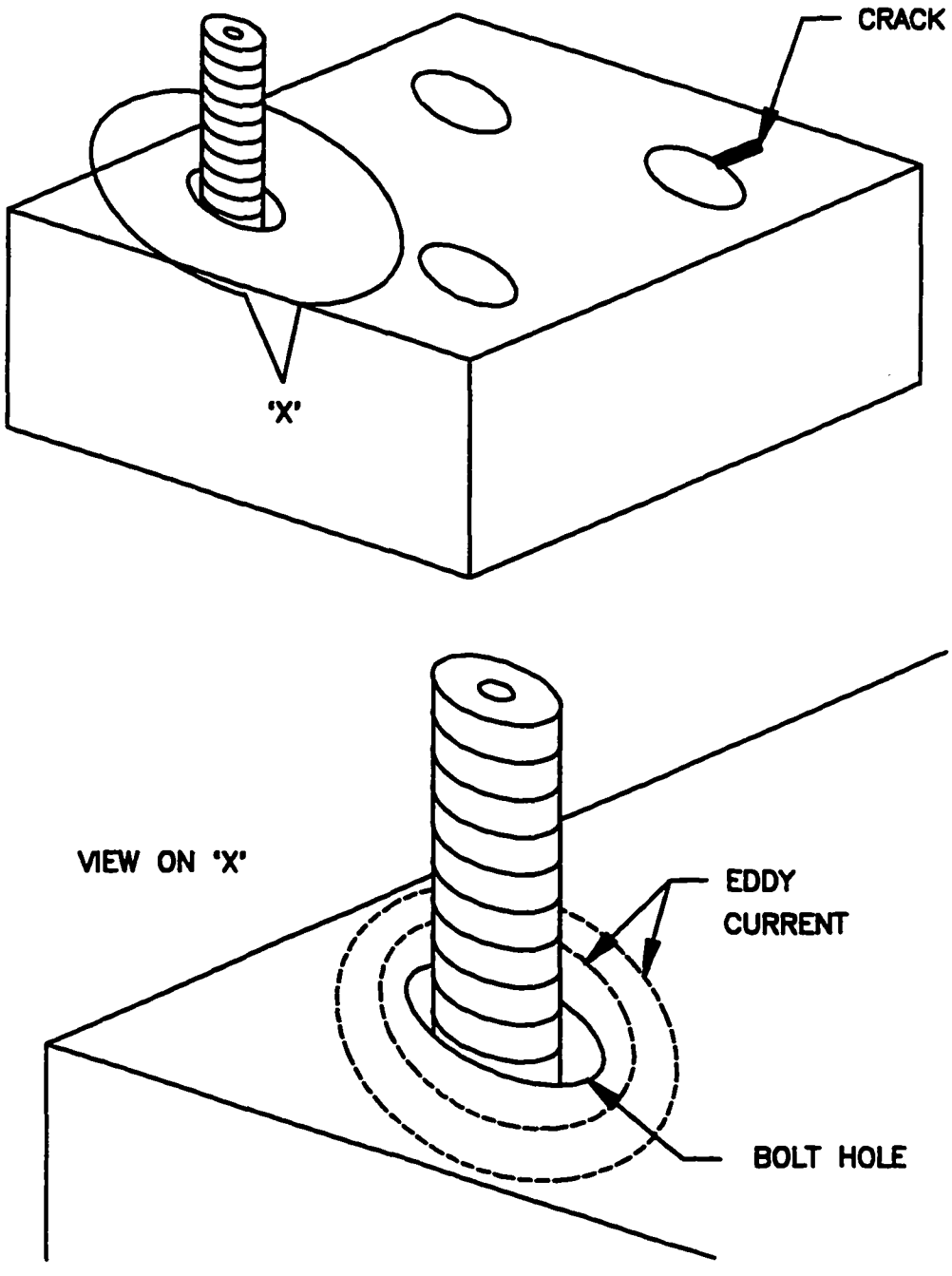

Figure 6.2. A coil is inserted into a crack-free bolt hole

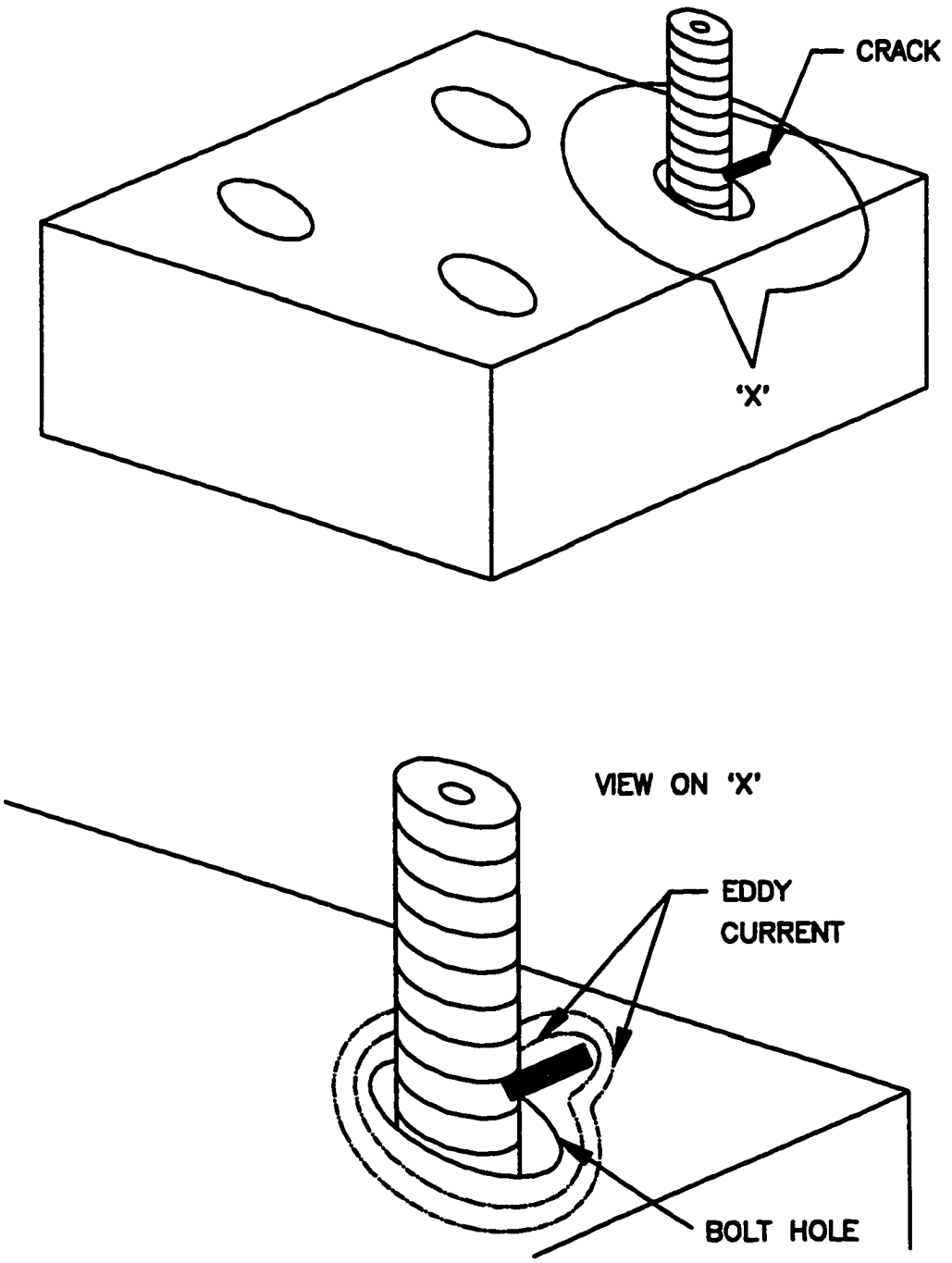

Figure 6.3. The coil is inserted into a cracked bolt hole

In Figure 6.2, the coil is inserted a good bolt hole, and the eddy current flows in a particular set of paths. In Figure 6.3, on the other hand, the coil is inserted into the bolt hole with the crack, and the eddy current in the test specimen is constrained to flow around the crack. This is a consequence of assumption (iii) of Chapter 2, which says that the crack is an electrical insulator.

Let $\mathbf{J}$ denote the current density of the eddy current. Figures 6.2-6.3 show that $\mathbf{J}$ is sensitive to the presence or absence of the crack. By Ohm's law, the electric field, $\mathbf{E}$ is also sensitive to the presence or absence of the crack. Squaring the electric field, we expect that $\mathbf{E}^2$ is sensitive to the presence or absence of the crack. Conversely, we hope that if measurements of $\mathbf{E}^2$ at the surface of the test specimen are available, it will be possible to reconstruct the crack. As we shall see below, these measurements of $\mathbf{E}^2$ are exactly what the photoinductive method provides.

$\mathbf{E}^2$ is in the Frequency Domain

One point should be clarified at this juncture. In electromagnetic theory the electric field $\mathbf{E}$ can be expressed either in the time domain or in the frequency domain. Accordingly $\mathbf{E}$ is a vector whose three components E_x, E_y, E_z are real or complex. Accordingly, $\mathbf{E}^2 = E_x^2 + E_y^2 + E_z^2$ is a real scalar or a complex scalar. In the photoinductive method, only the frequency domain representation is used. What the photoinductive method measures is the complex scalar $\mathbf{E}^2$.

The Role of the Laser

So far we have only spoken of one item in the photoinductive apparatus, the coil. We now examine the other items. Let one set of lines be drawn be drawn parallel to a tangent to the bolt hole (Figure 6.4), and another set of lines be drawn at right angles to the first set. The

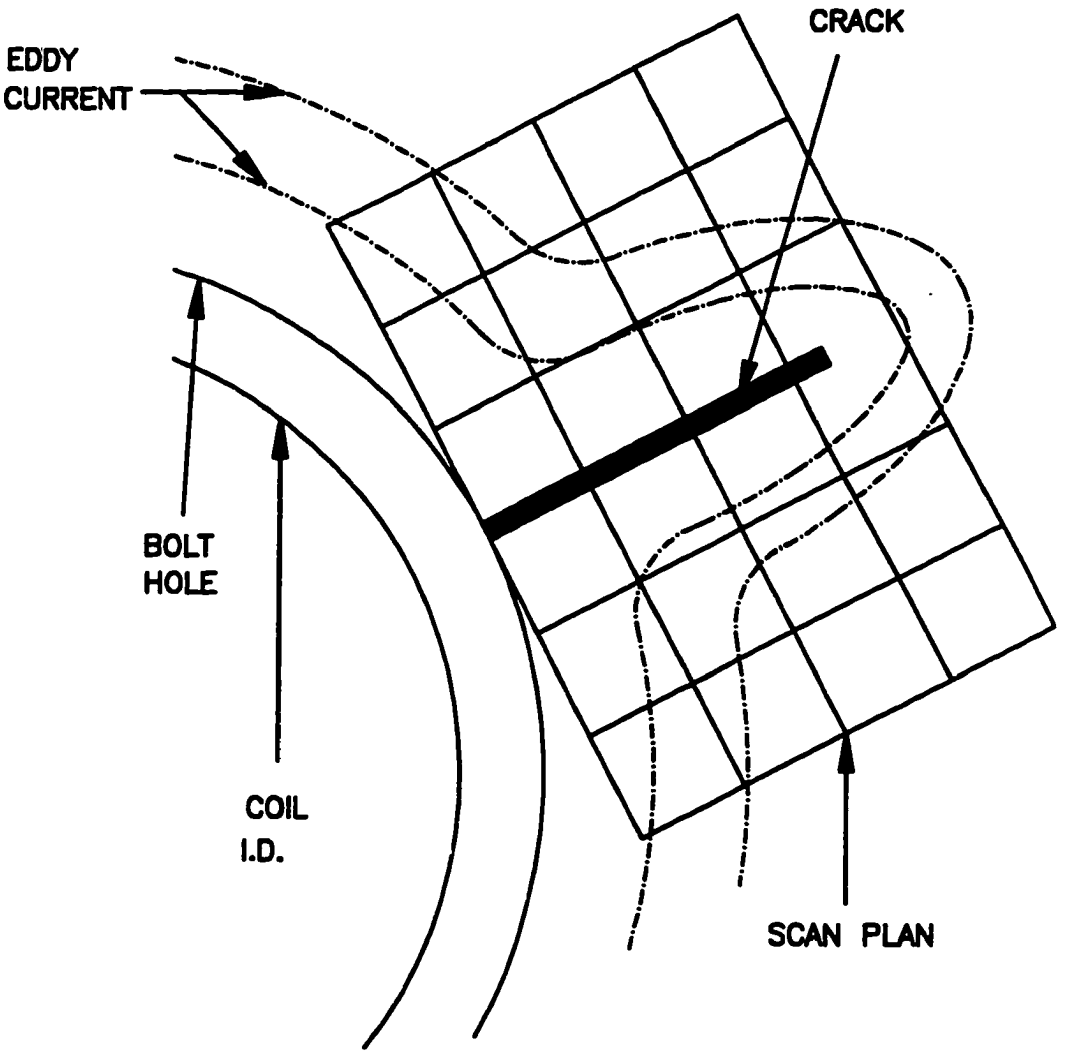

Figure 6.4. A scan plan around the periphery of a bolt hole

intersection of the two sets of lines gives rise to a set of points. It will be convenient to use two technical terms for these points -- laser focus points and scan points.

We pick any one of these points, and focus a laser on it (Figure 6.5). As a result the following parameters change in a related way:

(i) The temperature at the laser focus point (or scan point) changes from T_{off} when the laser is off to T_{on} when the laser is on.

(ii) Since the conductivity of a metal depends on the temperature, the conductivity changes from σ_{off} to σ_{on}.

(iii) We saw that the current density of the eddy current, $\mathbf{J}$, is altered by the presence of the crack. In addition, the change in the conductivity from σ_{off} to σ_{on} also causes $\mathbf{J}$ to change from $\mathbf{J}_{off}$ to $\mathbf{J}_{on}$, as the current tends to avoid a region of low conductivity.

(iv) The electric field changes from $\mathbf{E}_{off}$ to $\mathbf{E}_{on}$.

(v) The complex power consumed by the test specimen changes.

(vi) The complex power supplied by the current source changes.

Why a Photoinductive Measurement is a Measurement of $\mathbf{E}^2$

Let the voltage and the current of the current source be $\sqrt{2}U\cos(\omega t+\theta)$ and $\sqrt{2}I\cos(\omega t)$ respectively. The complex power supplied by the current source is UI. According to (vi) above, the power UI is different when the laser is off and when the laser is on. By the definition of the current source, the factor I cannot change. Therefore it is the voltage U that must change. Let it change from U_{off} to U_{on}.

It can be shown that (Appendix A) for small $T_{on}-T_{off}$,

$$U_{on}-U_{off}\approx-\frac{\sigma_{off}\alpha(T_{on}-T_{off})V}{I}\mathbf{E}_{off}^2, \tag{6.1}$$

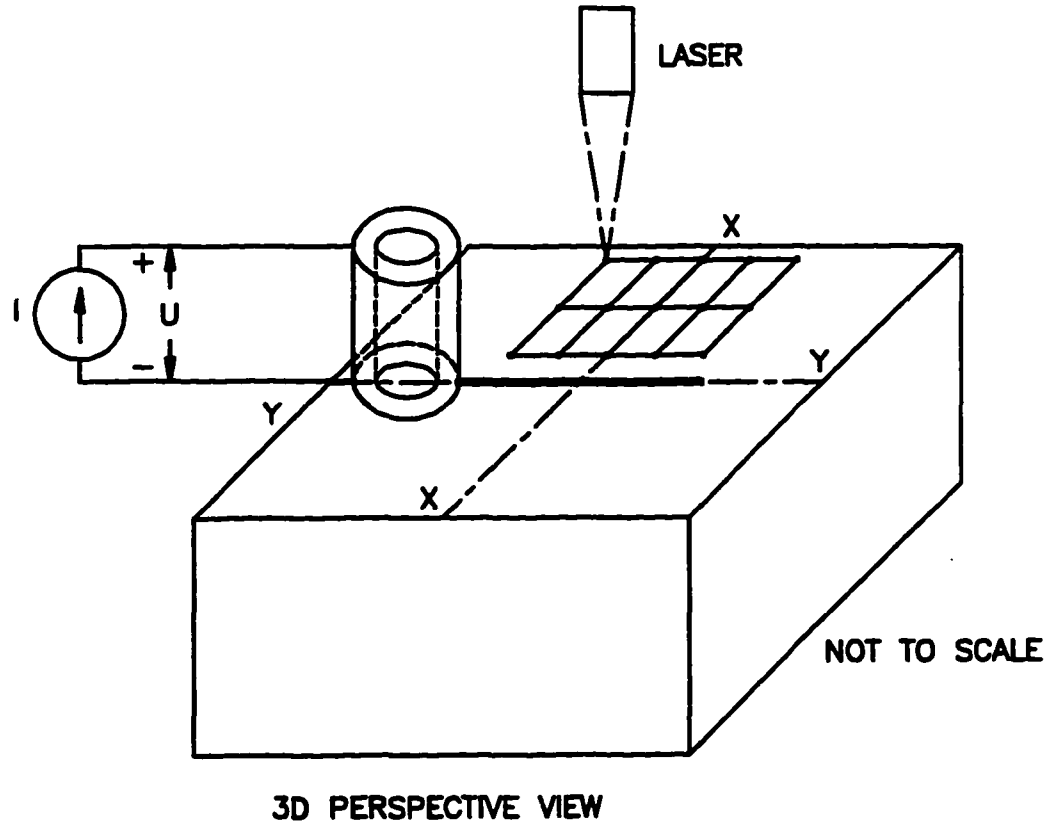

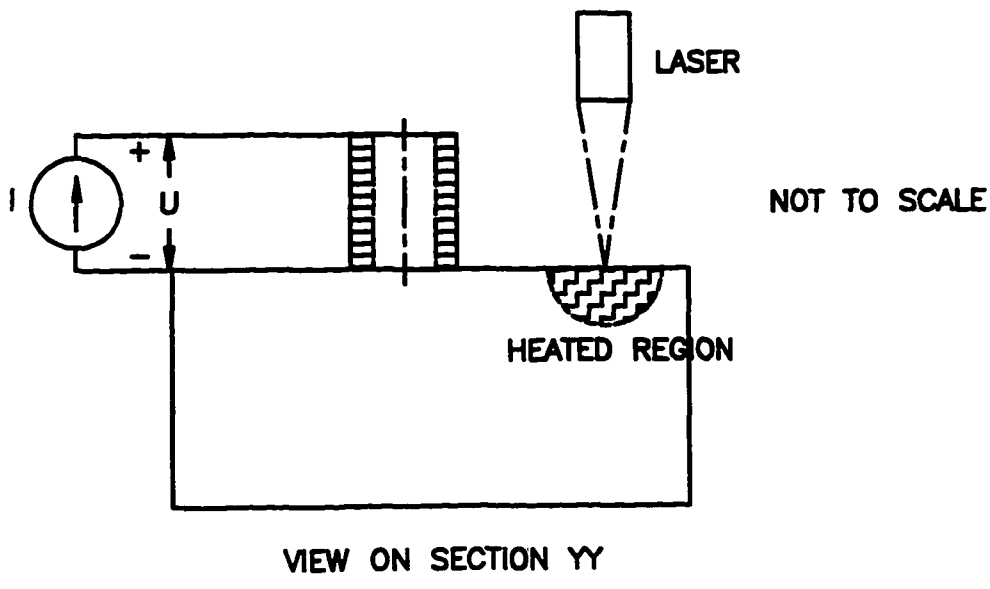

Figure 6.5. The apparatus of the photoinductive method

where α denotes the thermal conductivity of the metal and V is the volume of the heated region in the test specimen. This formula may be termed a Born approximation as terms of the order $O\left(T_{on}-T_{off}\right)^2$ are neglected. From this formula,

$$\mathbf{E}_{off}^2 \approx \frac{-I}{\sigma_{off}\alpha(T_{on}-T_{off})V}\left(U_{on}-U_{off}\right) \tag{6.2}$$

Moreover the quantity

$$\frac{-I}{\sigma_{off}\alpha(T_{on}-T_{off})V} \tag{6.3}$$

is independent of whether the inspected bolt hole is the one with the crack. This quantity can be determined by a calibration. With the calibration done, we can say that $\mathbf{E}_{off}^2$ is directly proportional to $U_{on}-U_{off}$. To measure $U_{on}-U_{off}$ is to measure $\mathbf{E}_{off}^2$. In this way a photoinductive measurement is equivalent to a measurement of $\mathbf{E}^2$.

Delicacy of Measuring $U_{on}-U_{off}$

The naive approach to measuring $U_{on}-U_{off}$ is to measure the voltage twice -- once with the laser off, getting U_{off} and once with the laser on, getting U_{on}. Subtracting, we get $U_{on}-U_{off}$. However the measurement error in U_{off} or in U_{on} is itself of the order of the difference $U_{on}-U_{off}$, and, therefore, this approach is not accurate.

The practical approach is to the operate the laser in a chopped mode, so that its light flashes on and off at the laser focus point (or scan point) at some frequency. Consequently the voltage U becomes an almost periodic function of time, with a component at the laser chopping frequency and a component at the frequency of the current source. The former component alternates between U_{off} and U_{on} Filtering this component, we obtain an accurate measurement of $U_{on}-U_{off}$.

Adjustments to Achieve Fine Spatial Resolution

We close this chapter by drawing attention to the heated region shown in Figure 6.5. For the photoinductive measurements to have a meaning, it is necessary that the electric field $\mathbf{E}_{eff}$ should be practically constant in the heated region. This condition will be satisfied if the user ensures that the heated region is small compared to the inner radius of the coil. Let us consider what the user can adjust to meet this requirement.

The size of the heated region depend on the thermal skin depth. The concept of the thermal skin depth states that if heat impinges on a point P, the temperature at another point P' falls off exponentially as the distance PP' increases. A formula for the thermal skin depth has been quoted by Moulder *et al* [15, Equation 6]:

$$\delta_{thermal} = \frac{\sqrt{2}}{\left(\omega_{chop}^2 \alpha^2 + \beta^2\right)^{1/4}} \tag{6.4}$$

were $\delta_{thermal}$ denotes the thermal depth, ω_{chop} is the (radian) frequency of chopping, α is the thermal conductivity of the metal and β is a coefficient for the heat emission from the test specimen to the environment.

This formula shows that the thermal conductivity of the metal and the laser chopping frequency are among the factors that determine the thermal skin depth, and, hence, the size of the heated region. An additional factor is the laser beam diameter. If possible, the user should adjust these factors to keep the heated region small.

The thermal conductivity of the metal cannot be adjusted. The laser chopping frequency can be adjusted. The laser beam diameter can be adjusted in principle by having several interchangeable lenses, and introducing one or other of these lenses in the path of the laser beam. In short, the user should choose the laser chopping frequency and the lens such

that the heated region is small compared to the inner radius of the coil. Then only does the photoinductive measurement achieve a fine spatial resolution.

CHAPTER 7. AN IDEA FOR ATTACKING THE PROBLEM

Scope of the Chapter

This chapter first describes a test specimen with a simple geometry. Next it presents the photoinductive measurement as a function of the current dipole density. The chapter then considers whether it is meaningful to invert this functional relationship so as to determine the current dipole density from the photoinductive measurement. The chapter shows why it is worthwhile to determine the current dipole density. The chapter concludes by pointing out an additional equation, embodying the electrical insulating property of the crack, that must be satisfied.

A Test Specimen with a Half-Space Geometry

The test specimen in the previous chapter was a metallic plate with four bolt holes. But in this chapter, we shall discuss a test specimen with a simpler geometry.

This test specimen has the geometry of a half-space without bolt holes (Figure 7.1). The top surface has a small, tight surface-breaking crack obeying the assumptions of the tight crack model of Chapter 2. Taking a vertical cross-section, we obtain a complete view of the crack (Figure 7.1). The dissertation problem is to reconstruct this complete view nondestructively, without physically taking a vertical cross-section.

Set the eddy current coil as shown in Figure 7.2, and focus the laser on the scan points. The photoinductive method gives us measurements of $\mathbf{E}_{off}^2$ at the scan points. Using these measurements, we are to reconstruct the complete view of the crack.

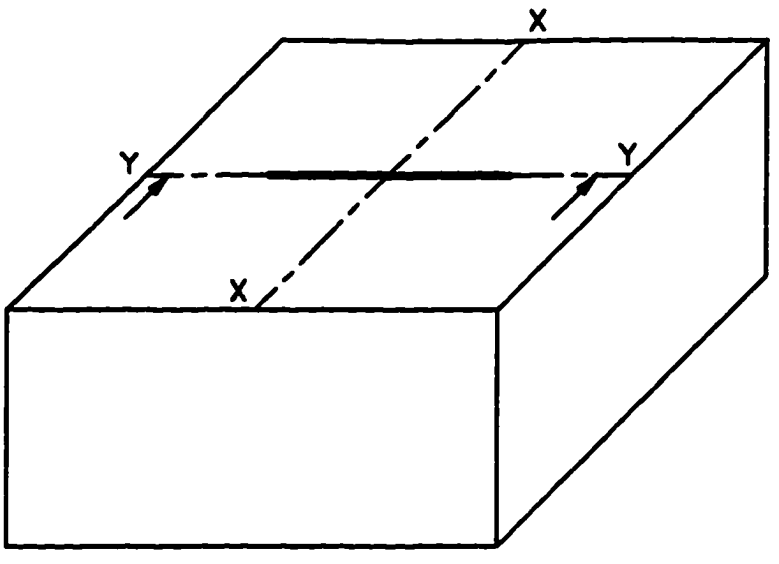

3D PERSPECTIVE VIEW

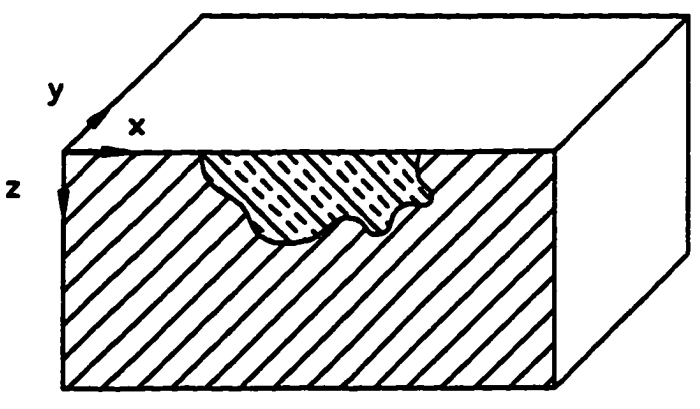

VIEW ON SECTION YY

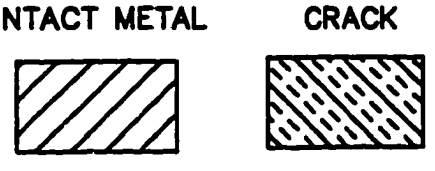

Figure 7.1. A test specimen with the geometry of a half-space

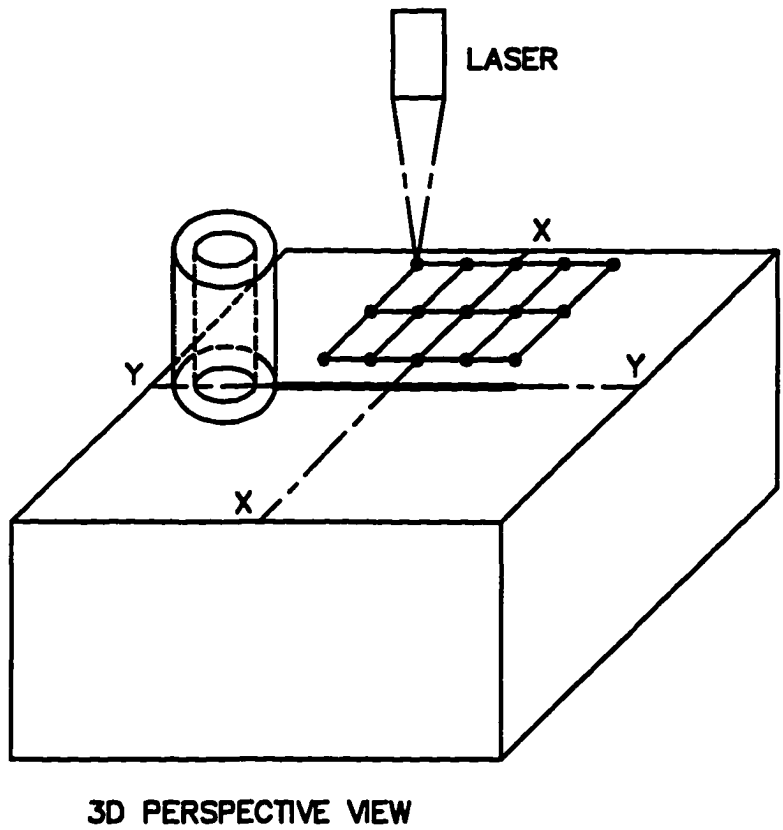

Figure 7.2. The scan plan for a half-space test specimen

A Formula for $\mathbf{E}_{off}^2$

The geometry shown in Figures 7.1-7.2 is identical to the one shown in Figures 4.1-4.3. Indeed when the laser is turned off, the photoinductive method reduces to the standard eddy current method. Therefore the quantity $\mathbf{E}_{off}$ in the photoinductive method is merely the electric field $\mathbf{E}$ in the standard eddy current -- the same electric field for which we quoted Equation 4.5. Therefore

$$\mathbf{E}_0(x,y,z) + \iint_{crack} \mathbf{G}_1(x,y,z,0,y',z')\, p_x(y',z')\, dy'dz' = \mathbf{E}_{off}(x,y,z) \qquad (7.1)$$

Squaring,

$$\left(\mathbf{E}_0(x,y,z) + \iint_{crack} \mathbf{G}_1(x,y,z,0,y',z')\, p_x(y',z')\, dy'dz' \right)^2 = \mathbf{E}_{off}^2(x,y,z) \qquad (7.2)$$

The right-hand side is precisely the photoinductive measurement.

The Knowns and the Unknowns in Equation 7.2

In the left-hand side, $\mathbf{E}_0$ and $\mathbf{G}_1$ are known, as analytical formulas for them have been published, while the current dipole density, p_x, is unknown. In the right-hand side, the quantity $\mathbf{E}_{off}^2$ is known from the photoinductive data. Another unknown is the domain over which the double integral must be computed, since that domain defines the crack that is to be reconstructed. Thus there appear to be two unknown items.

However a simple manipulation turns the domain of the double integral into a known item. We change Equations 7.1-7.2 as follows:

$$\mathbf{E}_0(x,y,z) + \int_{-\infty}^{\infty} dy' \int_{0}^{\infty} dz' \mathbf{G}_1(x,y,z,0,y',z')\, p_x(y',z') = \mathbf{E}_{off}(x,y,z) \qquad (7.3)$$

$$\left[\mathbf{E}_0(x,y,z)+\int_{-\infty}^{\infty}dy'\int_{0}^{\infty}dz'\mathbf{G}_1(x,y,z,0,y',z')p_x(y',z')\right]^2=\mathbf{E}_{on}^2(x,y,z) \quad (7.4)$$

These equations differ from Equations 7.2-7.3 in that the domain of the double integral has been changed from the crack to the entire cross-section, *i.e.*, to the half of the yz plane that lies in the metal (Figure 7.1). The change of the domain is legitimate because, according to the property (v) in Chapter 4, p_x is zero on the intact part.

Now that even the domain of the double integral is known, the only unknown is the current dipole density p_x. We therefore hope to determine p_x.

Why it is Useful to Determine the Current Dipole Density

Assuming that this hope of determining p_x is realized in practice, we divide the points (y,z) of the cross-section containing the crack into two sets, I and C, as follows:

$$I = \text{the set of points } (y,z) \text{ such that } p_x(y,z)=0. \quad (7.5)$$

$$C = \text{the set of points } (y,z) \text{ such that } p_x(y,z)\neq 0. \quad (7.6)$$

Using the property (v) of Chapter 4 again, C can be identified as the cracked region(s), while I is the intact region(s). This is the importance of the quantity p_x.

An Additional Equation

A simple equation can now be deduced. For all points (y,z) in the cross-section,

$$p_x(y,z)\left[E_{0_x}(0,y,z)+\int_{-\infty}^{\infty}dy'\int_{0}^{\infty}dz'G_{1_x}(0,y,z,0,y',z')p_x(y',z')\right]=0. \quad (7.7)$$

To deduce this equation, we note that the factor in the square brackets is, by Equation 4.6, merely $E_x(0,y,z)$. Proving Equation 7.7 is therefore equivalent to proving that

$$p_x(0,y,z)E_x(0,y,z) = 0. \tag{7.8}$$

Any point (y,z) must belong to either I or to C. If it belongs to I, p_x must be zero by the property (v) of Chapter 4, and Equation 7.8 is satisfied. If, on the other hand, (y,z) belongs to C, $E_x(0,y,z)$ must be zero by Equation 4.10, and Equation 7.8 is again satisfied. Therefore Equation 7.7 is also proved.

Any numerical method to determine p_x must ensure that Equation 7.7 is satisfied. Only then is it safe to identify the set C as the crack region(s).

CHAPTER 8. FIRST SET OF NONLINEAR EQUATIONS

Scope

This chapter essentially reformulates Equation 7.4. First it changes the domain of the double integral in Equation 7.4 from an infinitely large figure to a finite rectangle. Next it introduces the notion of a pixel, similar to the pixel of a television screen. This notion leads to certain changes in the double integral. Finally it introduces a notation for the items needed to specify a photoinductive measurement. This further leads to further changes in the double integral.

Reducing the Domain of the Double Integral

Equations 7.3-7.4 contain double integrals computed over an infinitely large domain. To make the computations manageable, we shall suppose that the crack is known to lie in a given rectangle *OABC* (Figure 8.1). Therefore the domain of the double integrals need not be the entire cross-section, but merely the rectangle *OABC*. With this, Equations 7.3-7.4 change into

$$\mathbf{E}_0(x,y,z)+\int_0^{y_A} dy' \int_0^{z_B} dz' \mathbf{G}_1(x,y,z,0,y',z')\, p_x(y',z') = \mathbf{E}_{off}(x,y,z) \qquad (8.1)$$

$$\left[\mathbf{E}_0(x,y,z)+\int_0^{y_A} dy' \int_0^{z_B} dz' \mathbf{G}_1(x,y,z,0,y',z')\, p_x(y',z')\right]^2 = \mathbf{E}_{off}^2(x,y,z) \qquad (8.2)$$

where y_A denotes the y coordinate of A and z_B denotes the z coordinate of B.

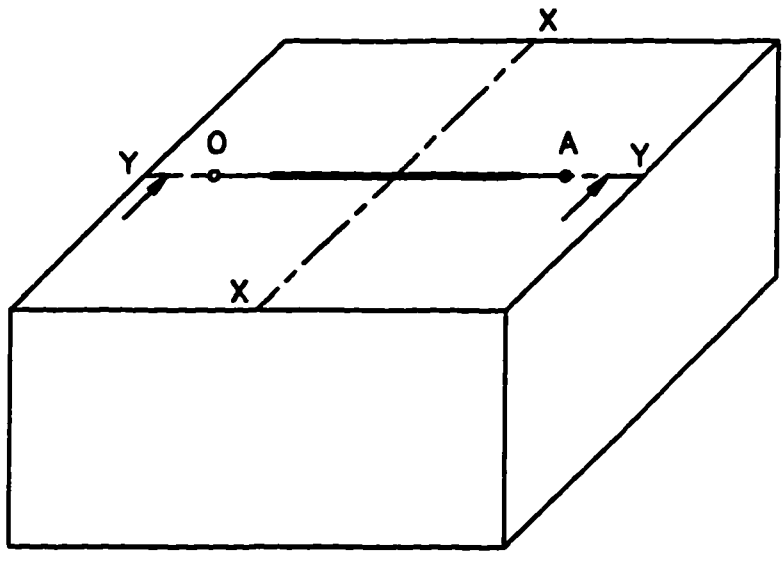

3D PERSPECTIVE VIEW

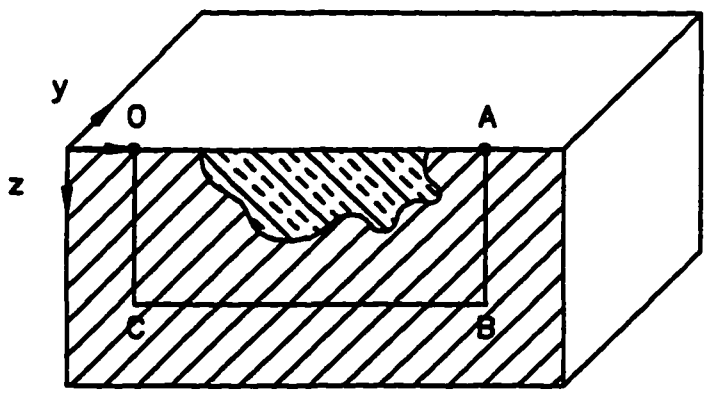

VIEW ON SECTION YY

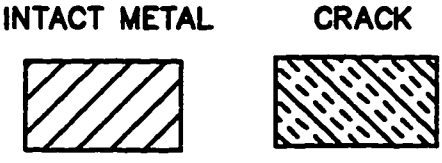

Figure 8.1. The crack is postulated to lie inside a given rectangle *OABC*

Discretizing the Rectangle *OABC* into Pixels

The rectangle *OABC* is divided into squares (Figures 8.2), just as a television screen is divided into pixels. Since the pixels of a television screen can depict even a complex figure, the squares of the rectangle *OABC* should be able to depict tight cracks with a complex shape. We shall use the term pixels for the squares of *OABC* to emphasize this depicting ability.

Let the pixels be numbered in the same way as the elements of matrix. Thus the pixel i, j is the pixel in the ith row and the jth column. We shall suppose that each pixel is so small that $p_x(y,z)$ is practically a constant in it. Let $p_x(y,z) = p_{i,j}$ for all points (y,z) that lie in the pixel i, j. Equations 8.1-8.2 are equivalent to

$$\mathbf{E}_0(x,y,z) + \sum_{i=1}^{m}\sum_{j=1}^{n} p_{i,j} \iint_{square\_i,j} \mathbf{G}_1(x,y,z\,0,y',z')dy'dz' = \mathbf{E}_{off}(x,y,z) \tag{8.3}$$

$$\left(\mathbf{E}_0(x,y,z) + \sum_{i=1}^{m}\sum_{j=1}^{n} p_{i,j} \iint_{square\_i,j} \mathbf{G}_1(x,y,z,0,y',z')dy'dz' \right)^2 = \mathbf{E}_{off}^2(x,y,z) \tag{8.4}$$

where m is the number of rows of pixels in the rectangle *OABC* (Figure 8.2), and n denotes the number of columns.

A Notation for the Particulars of a Measurement

A measurement is fully described by providing the following particulars:

(i) The xy coordinates of the laser focus point (or scan point). Note that the z coordinate of the laser focus point is always zero, as the point lies on the top surface of the test specimen which is nothing but the xy plane.

(ii) The y coordinate of the axis of the coil. Note that we are planning to move the coil only up and down the y axis only -- never off the y axis. In contrast, the laser will be moved up and down both the x and y axes.

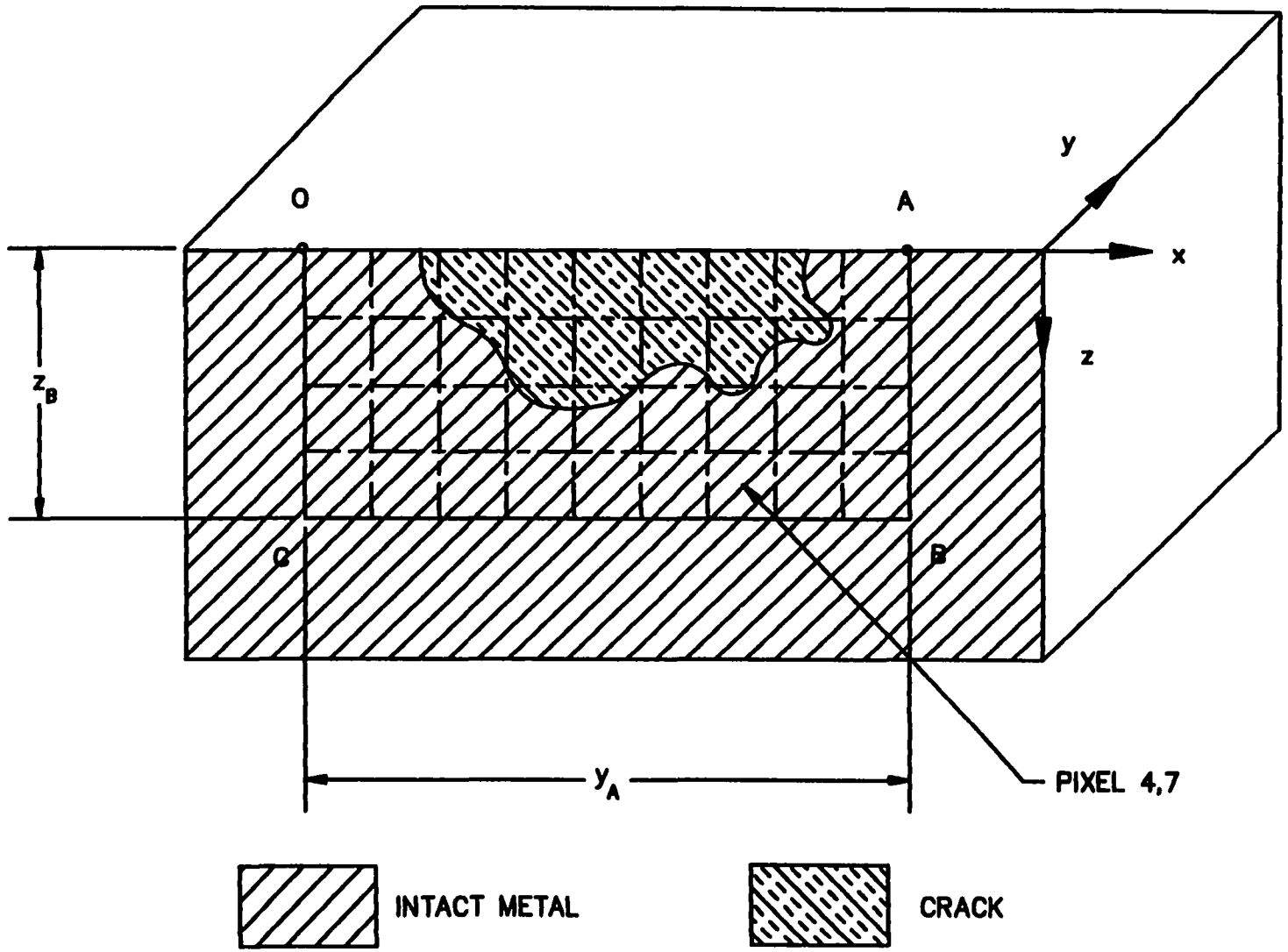

Figure 8.2. The bounding rectangle *OABC* is divided into pixels

(iii) The frequency of the current source. We are contemplating that the frequency is adjustable.

(iv) The value of $\mathbf{E}_{off}^2$ obtained in the measurement.

These particulars will be discussed further in Chapters 14-15. In this chapter, we will merely introduce the following notation:

(i) Λ = the number of photoinductive measurements

(ii) $(\xi_\alpha, \eta_\alpha)$ = the xy coordinates of the laser focus point in the αth measurement, where α is a index that runs from 1 through Λ

(iii) f_α = the frequency of the current source in the αth measurement

(iv) π_α = the value of $\mathbf{E}_{off}^2$ obtained in the αth measurement.

Rewriting Equation 8.4 with the Foregoing Notation

With this notation, Equation 8.4 is equivalent to

$$\left(\mathbf{E}_0(\xi_\alpha, \eta_\alpha, 0) + \sum_{i=1}^{m} \sum_{j=1}^{n} p_{i,j} \iint_{square\_i,j} \mathbf{G}_1(\xi_\alpha, \eta_\alpha, 0, 0, y', z') dy' dz' \right)^2 = \pi_\alpha \qquad (8.5)$$

Since the index α runs from 1 through Λ, this equation actually amounts to a set of Λ equations.

This set is the first set of nonlinear equations that our numerical procedure needs to solve.

CHAPTER 9. THE SECOND SET OF NONLINEAR EQUATIONS

Scope

Just as Chapter 8 reformulated Equation 7.4 in terms of pixels, this chapter reformulates Equation 7.7 in terms of pixels. Next it discusses the adequacy of the resulting equation. Finally it reformulates the sets I' and C' in terms of pixels.

Rewriting Equation 7.7 in Terms of Pixels

Equation 7.7 must be satisfied at all points of the cross-section containing the crack. The cross-section can be split into two regions -- the region inside rectangle $OABC$ and the region outside the rectangle $OABC$ (Figure 9.1). Equation 7.7 is automatically satisfied in the region outside the rectangle $OABC$, as p_x is defined to be zero there. Therefore it is sufficient to ensure that Equation 7.7 is satisfied in the region inside the rectangle $OABC$.

But there are infinitely many points inside the rectangle $OABC$. It is probably impossible to ensure that Equation 7.7 is satisfied for all these points. We adopt a more modest objective: let us merely ensure that Equation 7.7 is satisfied at the center of each, and every, pixel inside the rectangle $OABC$. If $(Y_{i,j}, Z_{i,j})$ denote the yz coordinates of the center of the pixel i, j, our more modest objective reduces Equation 7.7 to

$$p_{i,j}\left[E_{0x}(0, Y_{i,j}, Z_{i,j}) + \sum_{r=1}^{m}\sum_{s=1}^{n} p_{r,s} \iint_{Square\_r,s} G_{1x}(0, Y_{i,j}, Z_{i,j}, 0, y', z')dy'dz'\right] = 0 \quad (9.1)$$

Since the index i runs $1...m$ and the index j $1...n$, this equation amounts to a set of mn equations. This set is the second set of nonlinear equations that our numerical procedure needs to solve.

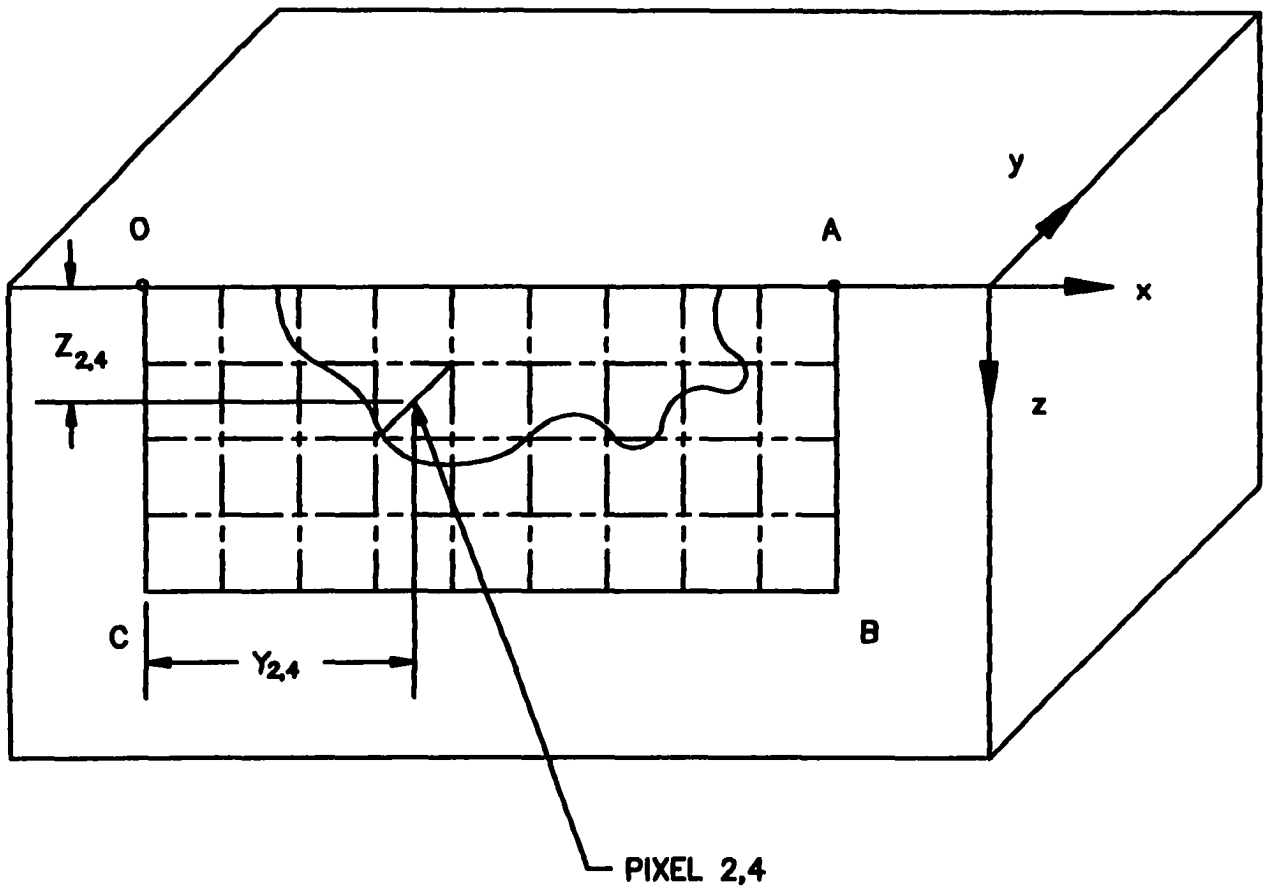

Figure 9.1. Enforcing Equation 9.1 is equivalent to enforcing Equation 7.7 at the centers of the pixels

By satisfying Equation 9.1, we satisfy Equation 7.7 only at the centers of the pixels, and not necessarily at all the points of the cross-section. Therefore it is worthwhile asking whether this will be prevent us from reconstructing the crack. If all the pixels are small, their centers will define a dense grid of points at which Equation 7.7 will be satisfied. In the limit that the pixel size tends to zero, the grid will be so dense as to cover the cross-section, and Equation 7.7 will be satisfied everywhere on the cross-section. Therefore, with a very small pixel size, satisfying Equation 9.1 -- satisfying Equation 7.7 at only a grid of points, rather than everywhere -- should not prevent us from reconstructing the crack.

Further confidence comes from noting that Equation 9.1 is similar to an equation used by Bowler [1, Equation 32].

Reformulating the Sets I' and C' in Terms of Pixels

Our numerical procedure must solve Equations 8.5 and 9.1 for the unknowns $p_{i,j}$, where $i = 1...m$ and $j = 1...n$. This done, the pixels i,j ($i = 1...m$ and $j = 1...n$) are divided into two sets, I' and C'. according to the following criteria:

$$I' = \text{the set of pixels } i,j \text{ such that } p_{i,j} \text{ is zero.} \tag{9.2}$$

$$C' = \text{the set of pixels } i,j \text{ such that } p_{i,j} \text{ is non-zero.} \tag{9.3}$$

The sets I' and $C'$are equivalent to the sets I and C defined in Equations 8.4-8.5, but, given that we have introduced the notion of a pixel, are more convenient to use. The crack to be reconstructed is merely the set C'.

CHAPTER 10. ILL-POSEDNESS

Scope of the Chapter

This chapter examines whether the Equations 8.5 and 9.1 are well-posed. The chapter first presents the definition of ill-posedness. Next it gives an intuitive explanation, based on the skin effect, to show that the dissertation problem is ill-posed. Then, using the theory of Fredholm equations of the first kind and the Riemann-Lebesgue lemma, it notes that ill-posedness is connected to the smoothing of rapid oscillations. The chapter presents an analogy from signal processing. It also shows that compact operators tend to smooth out rapid oscillations. The chapter shows that Equation 8.5 particularly has the structure indicative of smoothing of rapid oscillations. The chapter closes with the topic of regularization.

Ill-Posedndess

The concept of ill-posedness can be approached by first defining well-posedness. A system of equations is said to be well-posed if:

(i) A solution exists.

(ii) The solution is unique.

(iii) The solution changes only a little if the right-hand sides or the coefficients of the equations are altered slightly to reflect manufacturing tolerances and measurement errors.

The absence of well-posedness is ill-posedness.

Intuitive Explanation Why Equations 8.5 and 9.1 are Ill-Posed

The Green's function occurring in Equation 8.5 possesses an exponentially decaying factor of the form

$$\exp\left[(1+i)\frac{|\mathbf{r}-\mathbf{r}'|}{\delta}\right]$$

where δ denotes the skin depth, $\mathbf{r}$ the position vector of the field point and $\mathbf{r}'$ the position vector of the source point. To interpret this observation, suppose that there is a crack at $\mathbf{r}'$. The current dipole density at $\mathbf{r}'$, being nonzero, sets up an electric field at $\mathbf{r}$, which decays as the distance $|\mathbf{r}-\mathbf{r}'|$ increases. This may be viewed as an instance of the skin effect.

Suppose that $\mathbf{r}$ is a point on the top surface of the metal and that $|\mathbf{r}-\mathbf{r}'|$ is very large. The current dipole density at $\mathbf{r}'$ can only contribute a *small* term to the electric field at $\mathbf{r}$, and hence to a photoinductive measurement -- the square of the electric field -- at $\mathbf{r}$. Therefore a photoinductive measurement at $\mathbf{r}$ is practically insensitive to the current dipole density at $\mathbf{r}'$. Conversely, the current dipole density at $\mathbf{r}'$ is not well-determined from a photoinductve measurement at $\mathbf{r}$, if the distance $|\mathbf{r}-\mathbf{r}'|$ is very large.

Consider a crack whose depth is much greater than its surface length. If $\mathbf{r}'$ is a position vector in the deepest part of the crack, $|\mathbf{r}-\mathbf{r}'|$ cannot but be very large, as $\mathbf{r}$ is constrained to lie on the top surface. Therefore the current dipole density at $\mathbf{r}'$ deep down the cross-section is not well-determined from any photoinductive measurement. Therefore the deepest parts of the crack are not reflected in the photoinductive measurements. It would be impossible uniquely to reconstruct the deepest parts of the crack, meaning that the dissertation problem is ill-posed.

Ill-Posedness of A Fredholm Equation of the First Kind

The intuitive argument presented above may be supported by another argument which is described next. A Fredholm integral equation of the first kind is an equation of the form

$$\int_a^b K(x,x')f(x')dx' = g(x) \qquad (10.1)$$

where the kernel, $K(x,x')$, the limits of the integral, a,b, and the right-hand side, $g(x)$, are given, while the unknown function $f(x')$ is to be determined. For simplicity, we suppose that the kernel $K(x,x')$ is continuous, apart from an integrable singularity.

Suppose that $f(x') = f_1(x')$ is an exact solution to Equation 10.1:

$$\int_a^b K(x,x') f_1(x') dx' = g(x) \tag{10.2}$$

Then for sufficiently large values of the integer n, $f(x') = f_1(x') + \cos(nx')$ comes very close to being a solution to Equation 10.1:

$$\int_a^b K(x,x')\{f_1(x') + \cos(nx')\}dx' \approx g(x) \tag{10.3}$$

This follows from the Riemann-Lebesgue lemma discussed below.

The Riemann-Lebesgue Lemma

The Riemann-Lebesgue lemma says that for sufficiently large integers n

$$\int_a^b K(x,x') \cos(nx') dx' \approx 0 \tag{10.4}$$

the relation becoming exact in the limit as n tends to infinity. It is easy to see why this lemma is true if the kernel is continuous.

Suppose that the range of integration $[a,b]$ is partitioned into pieces of the length of the period of $\cos(nx')$.

$$\int_a^b K(x,x')\cos(nx')dx' = \sum_{all\_pieces}\int K(x,x')\cos(nx')dx' \qquad (10.5)$$

For large n, the period of $\cos(nx')$ becomes very short, so that each piece of the interval $[a,b]$ is very short. Suppose that the kernel is continuous; it will behave approximately like a constant function of x' in each piece. Therefore, for an approximate calculation, the kernel can be taken out of the integral as a constant factor in each piece of the interval $[a,b]$, leaving $\cos(nx')$ in the integrand.

$$\int K(x,x')\cos(nx')dx' \approx K(x,x') \int_{each\_piece}\cos(nx')dx' \qquad (10.6)$$

Integrating this over each piece -- essentially one period of $\cos(nx')$ -- gives zero. Therefore the integral is practically zero on each piece. Summing over all the pieces in the interval $[a,b]$, the integral over $[a,b]$ is also practically zero.

If the kernel has an integrable singularity, it cannot be continuous everywhere; all the same, the statements just made are still valid.

Implications for the Fredholm Equation of the First Kind

The Riemann-Lebesgue lemma shows the truth of (the approximate) Equations 10.3-10.4. The implication is as follows.

In view of manufacturing tolerances, measurement errors and the finite precision of computer arithmetic, the coefficients and the right-hand sides of Equation 10.1 are known only with a certain error. Therefore it is appropriate to seek an approximate solution to Equation 9.1, rather than an exact one. Once we decide to seek approximate solutions, both $f(x') = f_1(x')$ and $f(x') = f_1(x') + \cos(nx')$ (for all large integers n) must be accepted as solutions. As these solutions are *widely* different, Equation 10.1 cannot but be ill-posed.

Smoothing of Rapid Oscillations

The graph $y = f_1(x') + \cos(nx')$ looks like the graph $y = f_1(x')$ with a high frequency oscillation superimposed. Yet when the operations of multiplication by $K(x,x')$ and integration over $[a,b]$ are performed, both functions give rise to practically the same output $g(x)$. This fact shows that if an unknown function is multiplied by a reasonably well-behaved kernel and integrated, there is an effect of smoothing out any rapid oscillations that may be present in the unknown function. The corresponding integral equation is automatically ill-posed.

An Analogy from Signal Processing

An analogy from signal processing may be presented. Smoothing out rapid oscillations amounts to low-pass filtering. The function $f(x')$ can be conceived as the input to a low pass filter, while the function $g(x)$ is the output. Solving Equation 10.1 is akin to reconstructing the input to a low pass filter from the output. Therefore Equation 10.1 is ill-posed.

Compact Operators and Smoothing of Rapid Oscillations

In some books [9, Theorem 15.4, page 224], ill-posedness is associated with compact operators. Evans has remarked that, thinking intuitively, a compact operator is an operator that smoothes out any rapid oscillation in the input function [8, page 468, text between Equations 20-21]. To elaborate on this remark, suppose that

$$f_1(x), f_2(x), f_3(x), \ldots \tag{10.7}$$

is a complete orthonormal system of functions. Subject to certain technical conditions, any function $f(x)$ can be expanded in an infinite series of the form

$$f(x) = a_1 f_1(x) + a_2 f_2(x) + a_3 f_3(x) + \cdots \tag{10.8}$$

Applying a compact operator Γ to both sides of Equation 10.8,

$$\Gamma f(x) = \Gamma[a_1 f_1(x) + a_2 f_2(x) + a_3 f_3(x) + \cdots] \tag{10.9}$$

Let us stop the infinite series in Equation 10.7 after , say, the lth term, and the infinite series in Equation 10.8 after, say, the m th term. This yields the following approximations:

$$f(x) \approx a_1 f_1(x) + a_2 f_2(x) + \cdots + a_l f_l(x) \tag{10.10}$$

$$\Gamma f(x) \approx \Gamma[a_1 f_1(x) + a_2 f_2(x) + \cdots + a_m f_m(x)] \tag{10.11}$$

The characteristic property of a compact operator is that, independent of the approximation in Equation 10.10, the approximation in Equation 10.11 can be made good by having a sufficiently large number m [23, Vol. V, Art. 134, pages 402-405]. In short, the terms with subscripts larger than m can be discarded with little error if the intention is to apply the compact operator Γ.

The subscript has the following significance. Common examples of complete orthonormal systems, such as the trigonometric functions and Chebyshev functions [10], are characterized by the property that they oscillate rapidly if the subscript is large. Thus we have the heuristic rule that the functions listed in Equation 10.6 oscillate rapidly as the subscript increases. To discard the terms with subscripts greater than, say, m is to discard rapidly oscillating terms. Thinking intuitively, compact operators smooth out any rapid oscillation in the input function. Therefore the theory of ill-posedness based on compact operators is really a theory about the smoothing of rapid oscillations.

Similarity of the Fredholm Equation to Equation 8.5

Equation 8.5 contains an integral in which the Green's function $\mathbf{G}(\mathbf{r},\mathbf{r}')$ is like the kernel $K(x,x')$ and the current dipole density $p_x(y',z')$ is like the unknown function $f(x')$. Just as the rapid oscillations (if any) in $f(x')$ are smoothed out, so are the rapid oscillations (if any) in the current dipole density $p_x(y',z')$. Therefore the integral in Equation 8.5 can only reflect the coarse variations in the current dipole density $p_x(y',z')$.

After adding the term $\mathbf{E}_0$ to the integral and squaring, we obtain the left-hand side of Equation 8.5; this will reflect the coarse variations in the current dipole density $p_x(y',z')$.

Consider two cracks such that $p_x(y',z')=p_{x1}(y',z')$ for one crack and $p_x(y',z')=p_{x2}(y',z')$ for the other. Suppose that the difference $p_{x1}-p_{x2}$ be a rapidly oscillating function of y',z', *e.g.*, $\cos\{n(y'+z')\}$ with a large integer n. The operation of multiplying by the Green's function and computing the double integral will smooth out the rapidly oscillating difference. Therefore both cracks will give rise to practically the photoinductive measurements $\mathbf{E}^2$. When we use photoinductive measurements $\mathbf{E}^2$ to reconstruct the crack, we should obtain both p_{x1},p_{x2}, meaning that we should reconstruct both cracks, not merely one. Moreover these current dipole densities, p_{x1},p_{x2}, are *widely* different. This is the fundamental reason for thinking that the problem is ill-posed.

Lack of Uniqueness in a Practical Sense

The discussion just presented shows that Equations 8.5 and 9.1 should be considered, for practical purposes, as equations that have multiple solutions. One of the multiple solutions will be the crack actually present in the given test specimen. But we cannot tell which one, and so Equations 8.5 and 9.1 are only partially adequate for reconstructing the crack.

Regularization of Ill-Posed Problems

Tikhonov and Arsenin [25] suggest that ill-posed equations can be supplemented with an additional equation or constraint in an effort to remove ill-posedness. Such equations or constraints are said to regularize (or stabilize) the problem. In the work by Bowler, Norton and Harrison [2], an additional constraint was introduced: the area of the crack should be a minimum. Another example of such an constraint is that the perimeter of the crack should be a minimum.

Tikhonov and Arsenin [25] invoke the concept of compactness in theorems on regularizing ill-posed problems. This shows that regularizing an ill-posed problem is, at bottom, connected to the smoothing of rapid oscillations.

CHAPTER 11. AN OBJECTIVE FUNCTION

Scope

This chapter shows how Equations 8.5 and 9.1 can be turned into an objective function for minimization. The chapter concludes by indicating briefly how ill-posedness manifests itself in the minimization exercise.

An Objective Function

Equations 8.5 and 9.1 are nonlinear equations. One way to solve them is to convert them into an objective function which is to be minimized. Let M_α denote the difference between the left-hand side and right-hand side of Equation 8.5:

$$M_\alpha = \left(E_0(\xi_\alpha, \eta_\alpha, 0) + \sum_{i=1}^{m} \sum_{j=1}^{n} p_{i,j} \iint_{square\_i,j} G_1(\xi_\alpha, \eta_\alpha, 0, 0, y', z') dy' dz' \right)^2 - \pi_\alpha \tag{11.1}$$

Here the index α runs from 1 through Λ, and for each α, M_α should be zero. Let $N_{i,j}$ denote the left-hand side of Equation 9.1:

$$N_{i,j} = p_{i,j} \left[E_{0x}(0, Y_{i,j}, Z_{i,j}) + \sum_{r=1}^{m} \sum_{s=1}^{n} p_{r,s} \iint_{Square\_r,s} G_{1x}(0, Y_{i,j}, Z_{i,j}, 0, y', z') dy' dz' \right] \tag{11.2}$$

Here the indices $i = 1 \ldots m$ and $j = 1 \ldots n$ and for each i, j, $N_{i,j}$ should be zero.

Consider the quantity

$$F = \sum_{\alpha=1}^{\Lambda} |M_\alpha|^2 + \sum_{i=1}^{m} \sum_{j=1}^{n} |N_{i,j}|^2 \tag{11.3}$$

Making this zero is equivalent to satisfying Equations 8.5 and 9.1. On the other hand, if Equations 8.5 and 9.1 are not satisfied, then $F > 0$. Therefore F is a minimum when Equations 8.5 and 9.1 are solved.

The plan of solving Equations 8.5 and 9.1 is to think of F as the objective function to be minimized, with $p_{i,j}$, $i = 1...m$ and $j = 1...n$, as the unknowns. After the minimization is done, we form the sets I' and C' described earlier and report C' as the crack which was to be reconstructed.

How Ill-Posedness Manifests Itself

According to Chapter 10, ill-posedness means that for practical purposes, Equations 8.5 and 9.1 should be regarded as equations with nonunique solutions. Nonunique solutions emerge as multiple minima of the objective function. We will find in Chapters 16-17 that there are alternative ways to generate multiple minima:

(i) We can add a small, random quantity to the photoinductive data to simulate noise and repeat the optimization.

(ii) Adopting a Monte Carlo algorithm for the optimization, we can change an input known as the seed to the Monte Carlo algorithm and repeat the optimization.

The different minima corresponding to different cracks that give rise to practically the same photoinductive data.

CHAPTER 12. HEURISTIC ESTIMATE FOR THE CURRENT DIPOLE DENSITY

Scope of the Chapter

This chapter first explains the need for a heuristic estimate for the current dipole density of a pixel. Next it provides a heuristic estimate, together with the rationale. Finally it analyzes the heuristic estimate for the qualitative behavior of the current dipole density. The chapter closes with a comment on what the user can adjust to make each photoinductive measurement useful.

Need for a Heuristic Estimate

In Chapter 10 we showed that solving Equations 8.5 and 9.1 could be reduced to an optimization exercise. Therefore the computer program we would be writing would amount to an optimization routine. A number of optimization routines have been described in the literature. In this dissertation, we choose the Monte Carlo optimization routine [4], as it does not require us to differentiate the objective function with respect to the unknowns. The Monte Carlo routine has a good chance of succeeding if we can provide a heuristic starting point for the $p_{i,j}$'s that is close to the actual answers.

Our Heuristic Estimate

Numerical experimentation showed that the following formula gives a good starting point. For each i, j, there are two alternatives:

$$\text{either } p_{i,j} = 0, \tag{12.1}$$

$$\text{or } p_{i,j} \approx -E_{0x}(0, Y_{i,j}, Z_{i,j}) \Big/ \iint_{Square\_i,j} G_{1x}(0, Y_{i,j}, Z_{i,j}, 0, y', z')\, dy'\, dz' \tag{12.2}$$

Accordingly, the pixel i, j is in the set I' or in the set C'.

Rationale for Equations 12.1-12.2

The pixel i, j must be in the set I' or in the set C'. Suppose that it is in I'. Then Equation 12.1 is true. On the other hand, if the pixel i, j is in C', then there is a rationale for Equation 12.2 to be true.

Consider Figure 12.1. Here the rectangle $OABC$ has been divided into two pixels - the number of rows $m = 2$ and the number of columns $n = 1$. Let both pixels be cracked. Thus the crack is completely given. Such a situation - where the crack is completely given - is useful to understand why Equation 12.2 is true.

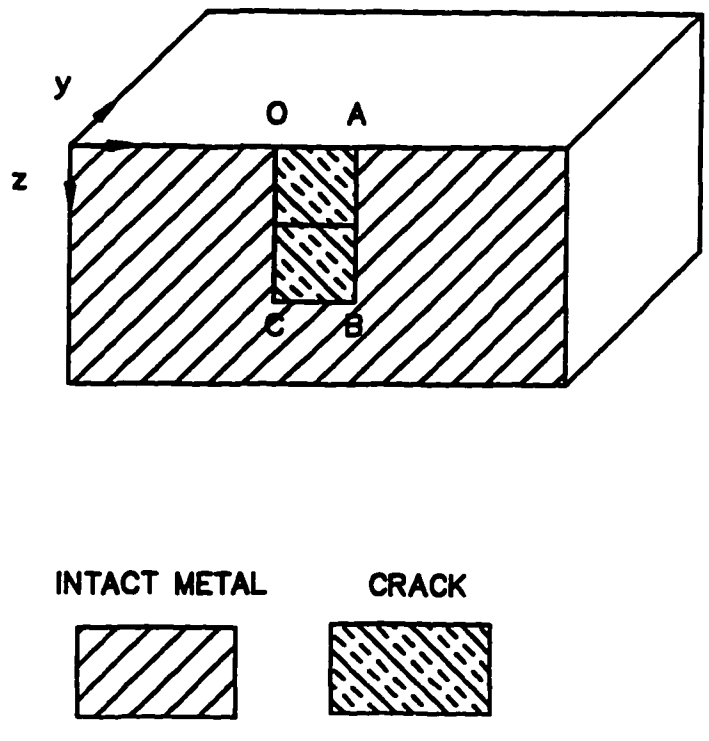

Figure 12.1. A situation where the crack geometry is given helps to arrive at the heuristic estimate

Since the pixels (1,1) and (2,1) are cracked, they belong to the set C'. Therefore $p_{1,1}, p_{2,1}$ are both nonzero. The second set of nonlinear equations, Equation 9.1, reduces to

$$p_{1,1} \iint_{Square\_1,1} G_{1x}(0, Y_{1,1}, Z_{1,1}, 0, y', z')dy'dz' + p_{2,1} \iint_{Square\_2,1} G_{1x}(0, Y_{1,1}, Z_{1,1}, 0, y', z')dy'dz' = -E_{0x}(0, Y_{1,1}, Z_{1,1})$$

$$p_{1,1} \iint_{Square\_1,1} G_{1x}(0, Y_{2,1}, Z_{1,1}, 0, y', z')dy'dz' + p_{2,1} \iint_{Square\_2,1} G_{1x}(0, Y_{2,1}, Z_{2,1}, 0, y', z')dy'dz' = -E_{0x}(0, Y_{2,1}, Z_{2,1})$$

or, in matrix notation,

$$\begin{bmatrix} \iint_{Square\_1,1} G_{1x}(0, Y_{1,1}, Z_{1,1}, 0, y', z')dy'dz', & \iint_{Square\_2,1} G_{1x}(0, Y_{1,1}, Z_{1,1}, 0, y', z')dy'dz' \\ \iint_{Square\_1,1} G_{1x}(0, Y_{2,1}, Z_{1,1}, 0, y', z')dy'dz', & \iint_{Square\_2,1} G_{1x}(0, Y_{2,1}, Z_{2,1}, 0, y', z')dy'dz' \end{bmatrix} \begin{bmatrix} p_{1,1} \\ p_{2,1} \end{bmatrix} = \begin{bmatrix} -E_{0x}(0, Y_{1,1}, Z_{1,1}) \\ -E_{0x}(0, Y_{2,1}, Z_{2,1}) \end{bmatrix}$$

The important property of the 2×2 matrix is that the entries in the main diagonal are a good deal larger (in terms of the absolute value) than the off-diagonal entries. Since we are only interested in a rough estimate for $p_{1,1}, p_{2,1}$, we discard the off-diagonal entries. The matrix equation reduces to

$$p_{1,1} \iint_{Square1,1} G_{1x}(0, Y_{1,1}, Z_{1,1}, 0, y', z')dy'dz' = -E_{0x}(0, Y_{1,1}, Z_{1,1})$$

$$p_{2,1} \iint_{Square2,1} G_{1x}(0, Y_{2,1}, Z_{2,1}, 0, y', z')dy'dz' = -E_{0x}(0, Y_{2,1}, Z_{2,1})$$

Taking the double integrals to the right-hand side, we obtain Equation 12.2. This gives the rationale for the heuristic estimate.

Qualitative Behavior of the $p_{i,j}$

The numerator of the right-hand side of Equation 12.2 is essentially a component of the electric field set up by the coil. Thinking intuitively, the numerator should be large, in terms of absolute value, for a pixel near the coil and small for a pixel far away far away. Numerical evaluations confirm this intuition. Suppose, for example, that the pixel nearest the coil is characterized by $i=1, j=1$ (Figure 12.2). The numerator is a maximum (in terms of absolute value) for these subscripts.

The denominator of the right-hand side of Equation 12.2 can be interpreted as follows. If the pixel i, j is cracked and its current dipole density is $p_{i,j} = 1$A/m, Equation 4.6 says that there would be a term

$$\iint_{Square\_i,j} G_{1x}(0, Y_{i,j}, Z_{i,j}, 0, y', z')dy'dz'$$

in the electric field at the center of the pixel i, j. We note that the subscripts i, j are the same for the second and third argument of the Green's function -- $Y_{i,j}, Z_{i,j}$ -- as well as for the pixel over which the double integral is being computed, square i, j. Thinking intuitively, the double integral would be roughly the same for all i, j. This is confirmed by numerical evaluations.

From the behavior of the numerator and denominator, we infer that, among the cracked pixels, those relatively near the coil tend to have a relatively large current dipole density. This is intuitively acceptable, as such pixels tend to intercept a relatively large fraction of the current induced by the coil.

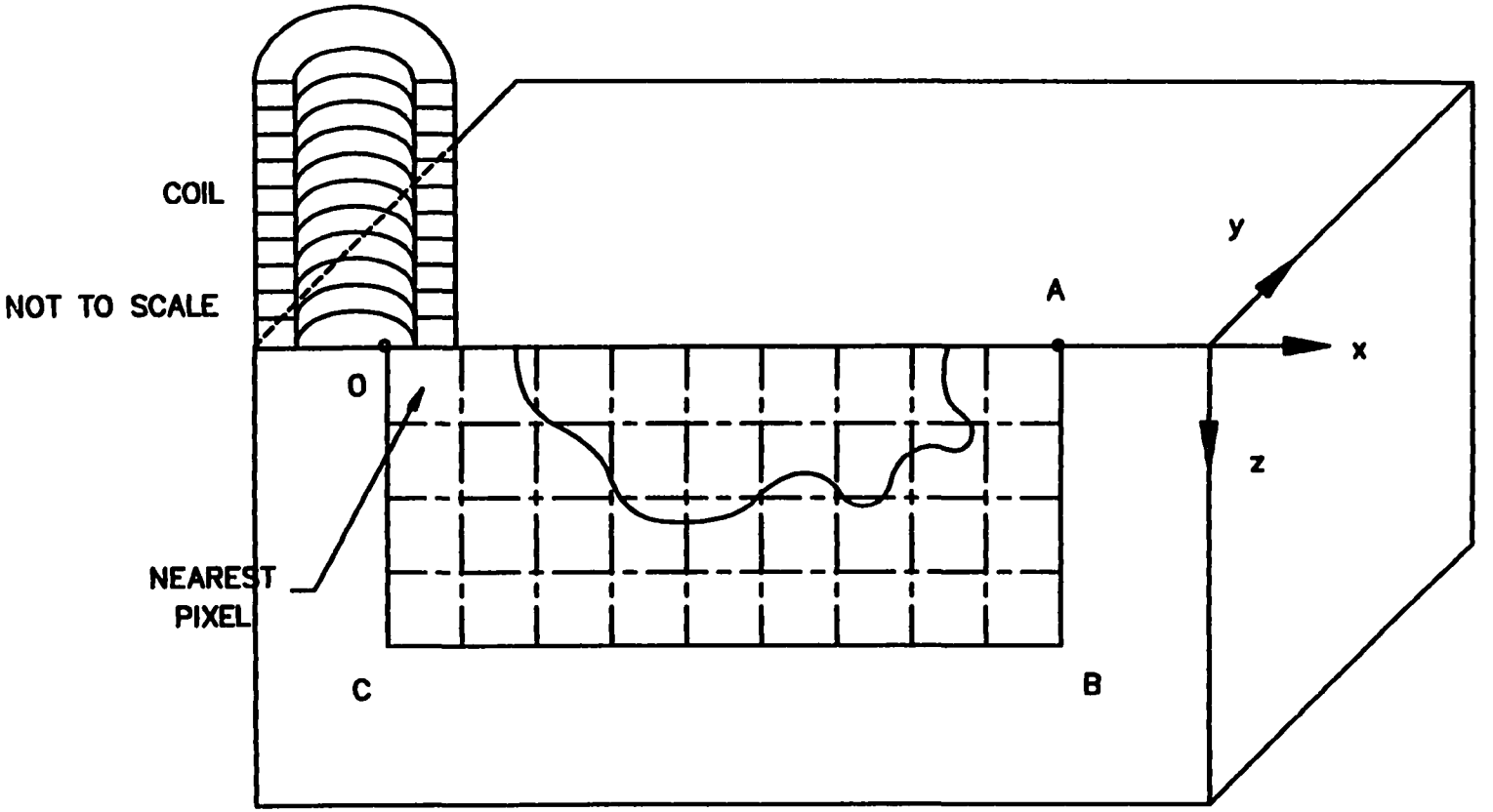

Figure 12.2. The pixel (1, 1) is the pixel nearest the coil

CHAPTER 13. THE IMPORTANCE OF A PARTICULAR DOUBLE INTEGRAL

Scope of the Chapter

This chapter first describes a case where all photoinductive measurements are useless for reconstructing the crack. The analysis of this case yields a criterion for judging whether a photoinductive measurement will be useful for reconstructing the crack.

A Case Where All Photoinductive Measurements are Useless

Suppose that all the laser focus points (or scan points) are far away from the top edge of the crack. It is intuitively obvious that, because of the distance, the photoinductive measurements π_α will not be helpful in reconstructing the crack. Equation 7.5 justifies this intuition. By Equation 8.5

$$\left(\mathbf{E}_0(\xi_\alpha, \eta_\alpha, 0) + \sum_{i=1}^{m} \sum_{j=1}^{n} p_{i,j} \iint_{square\_i,j} \mathbf{G}_1(\xi_\alpha, \eta_\alpha, 0, 0, y', z') dy' dz' \right)^2 = \pi_\alpha \quad (13.1)$$

The quantity $|\xi_\alpha|$ is large as the laser focus point is far from the crack. This causes the function $\mathbf{G}_1$ to be very small, because $\mathbf{G}_1$ contains the factor

$$\exp(ikr)/r^3, \quad (13.2)$$

$$r = \sqrt{(\xi_\alpha - 0)^2 + (\eta_\alpha - y')^2 + (0 - z')^2} \quad (13.3)$$

Therefore the double integrals are also small. The smallness of the double integrals causes the double sum to be small. Meanwhile, $\mathbf{E}_0$ is still quite large, as it does not decrease as rapidly as $\mathbf{G}_1$. Therefore, Equation 13.1 amounts to

$$\mathbf{E}_0^2 \approx \pi_\alpha \tag{13.4}$$

This equation shows that the measurement π_α has little or no dependence on $p_{i,j}$. Consequently, the measurement π_α is not useful in reconstructing the crack. In this way the mathematics justifies our intuition that laser focus points (or scan points) that are far from the top edge of the crack are not useful.

Criterion for Judging the Usefulness of Photoinductive Measurements

The analysis just presented not only confirms intuition, but also provides a criterion for judging whether a photoinductive measurement will be useful. If the double integrals are small for all the indices i, j in the double sum, the measurement is not useful. If, on the other hand, the double integral is large for some value of i, j, the measurement is useful.

In fact $\mathbf{G}_1(\xi, \eta, 0, 0, y', z')$ indicates how sensitive the electric field at $(\xi, \eta, 0)$ is to the presence or absence of a crack at $(0, y', z')$. The double integral over the pixel i, j indicates how sensitive the electric field is to the presence or absence of a crack in the pixel i, j. The larger the double integral, the greater is the sensitivity of the photoinductive measurement to the presence or absence of a crack.

What the User can Adjust for Maximum Sensitivity to Cracks

Values can be assigned to the following quantities at our discretion:

(i) Λ = the number of photoinductive measurements

(ii) $(\xi_\alpha, \eta_\alpha)$ = the xy coordinates of the laser focus point in the αth measurement, where α is a index that runs from 1 through Λ

(iii) f_α = the frequency of the current source in the αth measurement

The requirement is to assign values such that the double integral of the Green's function is as large as possible. To give a sense of how large this double integral can be, we note that, from numerical evaluations, the double integral occurring in Equation 12.2

$$\iint_{Square\_i,j} G_{1x}(0,Y_{i,j},Z_{i,j},0,y',z')dy'dz' \tag{13.5}$$

acts as an upper bound.

The behavior of the double integral is covered in Chapter 14.

CHAPTER 14. THE BEHAVIOR OF A PARTICULAR DOUBLE INTEGRAL

Scope of the Chapter

The results and discussion are split into two chapters. In this chapter the focus is on the behavior of the double integral whose importance was pointed out in Chapter 13. The chapter first presents an array of laser focus points. Next it considers how the double integral varies from point to point. Then it considers varying the frequency. In varying the frequency two conditions have to be met. The chapter explains the trade-off between the two conditions. The chapter concludes by connecting ill-posedness with the failure to meet the second condition.

An Array of Laser Focus Points

As a typical example, we considered the rectangle $OABC$ shown in Figure 14.1, which was divided into $m = 3$ rows and $n = 5$ columns of pixels. We considered an array of points

$$P_{1,1}, P_{1,2}, P_{1,3}, P_{1,4}, P_{1,5}$$
$$P_{2,1}, P_{2,2}, P_{2,3}, P_{2,4}, P_{2,5}$$
$$P_{3,1}, P_{3,2}, P_{3,3}, P_{3,4}, P_{3,5}$$

on the top surface of the metal. Let $(\xi_{r,s}, \eta_{r,s})$ denote the xy coordinates of the point $P_{r,s}$. (In passing, we note that, unlike the previous chapters, in this chapter it will be convenient to use double subscripts for ξ, η.) The numerical values of these coordinates are given in Figure 14.1 in terms of the parameter a, denoting the size of each pixel.

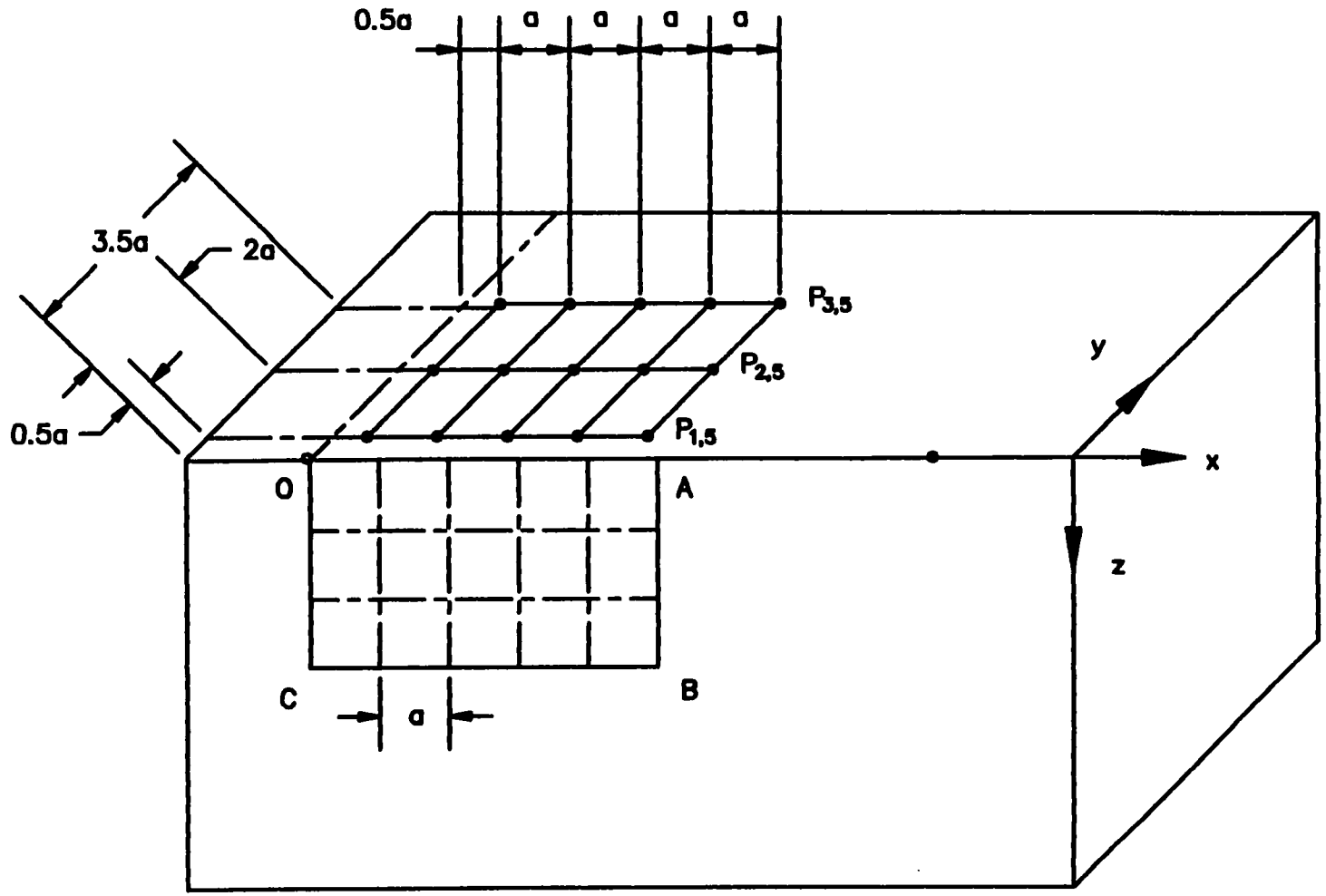

Figure 14.1. An array of laser focus points

Numerical Evaluations Carried Out on a Specific Point

Taking a specific laser focus point, say, $P_{r,s}$, we carried out the following steps:

(i) We evaluated the double integral of the Green's function over the pixel (i,j) for all indices (i,j). Note that the indices (i,j) denote the pixels, while the indices r,s denote the laser focus (or scan) points. We varied (i,j), keeping r,s fixed.

(ii) We sorted these double integrals in descending order in terms of the absolute value.

(iii) We determined what indices (i,j) gave the largest double integral, the largest but one, the largest but two, and so on.

(iv) Let $\iota_1, \iota_2, \iota_3, \ldots$ denote the largest double integral, the largest but one, the largest but two and so on. We examined whether ι_1 was, say, an order of magnitude larger than $\iota_2, \iota_3, \ldots$, or only moderately greater than them.

(v) We repeated the steps (i)-(iv) for several values of the current source frequency.

Discussion of the Point $P_{1,1}$

We began with the point $P_{1,1}$, so that $(r,s) = (1,1)$. Carrying out the steps (i)-(v), we found that the double integral was a maximum when the indices $(i,j) = (1,1)$. The maximum value ι_1 was almost an order of magnitude greater than $\iota_2, \iota_3, \ldots$ These observations were true at both low and high frequencies.

As the double integral was much larger for $(i,j) = (1,1)$ than for other indices, we concluded that the measurement at $P_{1,1}$ is sensitive to the presence or absence of a crack in the pixel (1,1). In mathematical terms, Equation 8.5 reduces approximately to

$$\left[\mathbf{E}_0(\xi_{1,1}, \eta_{1,1}, 0) + p_{1,1} \iint_{Square\_1,1} \mathbf{G}_1(\xi_{1,1}, \eta_{1,1}, 0, 0, y', z') dy' dz' \right]^2 \approx \mathbf{E}^2(\xi_{1,1}, \eta_{1,1}, 0) \quad (14.1)$$

an equation in which only $p_{1,1}$ occurred. Suppose that the right-hand side of this equation were measured with the photoinductive method. We would have an equation in which $p_{1,1}$ is the only unknown. Therefore $p_{1,1}$ could be determined. Although Equation 14.1 is only approximately true, it is good enough to judge whether $p_{1,1}$ is zero or non-zero, *i.e.*, whether the pixel (1,1) was intact or cracked.

Discussion of the Point $P_{1,s}$

In the same way, we set $(r,s) = (1,s)$, $s = 1...n$, and carried out the steps (i)-(v). We found that the measurement at the point $P_{1,s}$ is useful for determining the condition, whether intact or cracked of the pixel $(1,s)$.

The results obtained so far show that the points $P_{1,s}$, $s = 1...n$ are well-suited to be scan points (or laser focus points). They can help us to infer the condition, whether intact or cracked, of the pixels in the first row. But they cannot help us with the pixels in the second, third, and other rows.

Discussion of the Point $P_{2,1}$

We turned next to a pixel in the second row, $P_{2,1}$, so that $(r,s) = (2,1)$. Carrying out the steps (i)-(v), we found that the double integral was a maximum, ι_1, for $(i,j) = (1,1)$. The integrals in the second, third, fourth and fifth place, $\iota_2, \iota_3, \ldots$, corresponded to $(i,j) = (1,2)$, $(2,1)$, $(1,3)$, $(2,2)$.

At high frequencies (equivalently, small skin depths), ι_1 was a good deal larger than $\iota_2, \iota_3, \ldots$, meaning that the photoinductive measurement at $P_{2,1}$ is sensitive primarily to the pixel (1,1).

At low frequencies (equivalently, large skin depths), ι_1 was moderately greater (not a good deal greater) than $\iota_2, \iota_3, \ldots$, meaning that the measurement is sensitive to several pixels, not merely the pixel (1,1). In particular, the measurement is sensitive to the pixel (2,1) which

is in the second row. Thus we found a point, $P_{2,1}$. such that a measurement there is useful data for inferring the condition of a pixel in the second row. The only proviso is that the skin depth should be large (equivalently the frequency should be low), say, 20-40% greater than $|\xi_{2,1}|$, the x-coordinate of the scan point $P_{2,1}$.

Why Vary the Frequency

In mathematical terms, Equation 8.5 reduces approximately to

$$\left[\mathbf{E}_0(\xi_{2,1},\eta_{2,1},0)+\sum_{(i,j)} p_{i,j} \iint_{Square\_i,j} \mathbf{G}_1(\xi_{2,1},\eta_{2,1},0,0,y',z')dy'dz'\right]^2 \approx \mathbf{E}^2(\xi_{1,1},\eta_{1,1},0) \quad (14.2)$$

where the indices $(i,j) = (1,1)$ at high frequencies, and $(i,j) = (1,1), (1,2), (2,1), (1,3), (2,2)$ at low frequencies. We paid particular attention to the double integrals corresponding to $(i,j) = (2,1), (2,2)$ in the double sum. These integrals were ι_3 and ι_5 If we could make ι_3 and ι_5 large, then the measurement at $P_{2,1}$ would be sensitive to the presence or absence of a crack in the pixels (2,1), (2,2), *i.e.*, pixels in the second row.

By varying the frequency, we tried to realize the following two conditions:

$$\iota_3 \approx \iota_1 \quad (14.3)$$

$$\iota_3 >> \iota_5 \quad (14.4)$$

We shall indicate the significance of these two conditions next.

Significance of the First Condition

If the first condition is met, it means that the double integral over the pixel (2,1) is the largest possible, given that it cannot be larger than ι_1. The measurement would be sensitive

to the presence or absence of a crack in pixel (2,1). This condition is equivalent to achieving depth resolution beyond the first row, into the second row.

Significance of the Second Condition

To gain a better understanding of the second condition, consider the two cracks in Figure 14.2. In one, the pixel (2,1) is cracked and the pixel (2,2) intact, while in the other, it is the other way around. There is no other difference between the two cracks. Ideally, at least one measurement should be different between the two cracks. Clearly the measurements for the two cracks are widely different if ι_3 is a good deal greater than ι_5. This is the rationale for the second condition.

The Need for a Trade-Off

We found that the only way to realize the first condition was to make the frequency low. But this made it impossible to achieve the second condition. Similarly the only way to realize the second condition was to make the frequency high, which made it impossible to realize the first condition. Consequently, there was a need for a trade-off between the two conditions. The trade-off corresponded to the figure earlier cited, namely, the skin depth should be, say, 20-40% greater than $|\xi_{2,1}|$, the x-coordinate of the scan point $P_{2,1}$.

The Trade-Off and the Ill-Posedness

The very phrase "trade-off" indicates that the second condition cannot be met exactly. Therefore ι_3 is only moderately greater than ι_5. Therefore the measurements associated with the two cracks shown in Figure 14.2 are nearly the same. The existence of two cracks with nearly the same set of photoinductive measurements is indicative of ill-posedness.

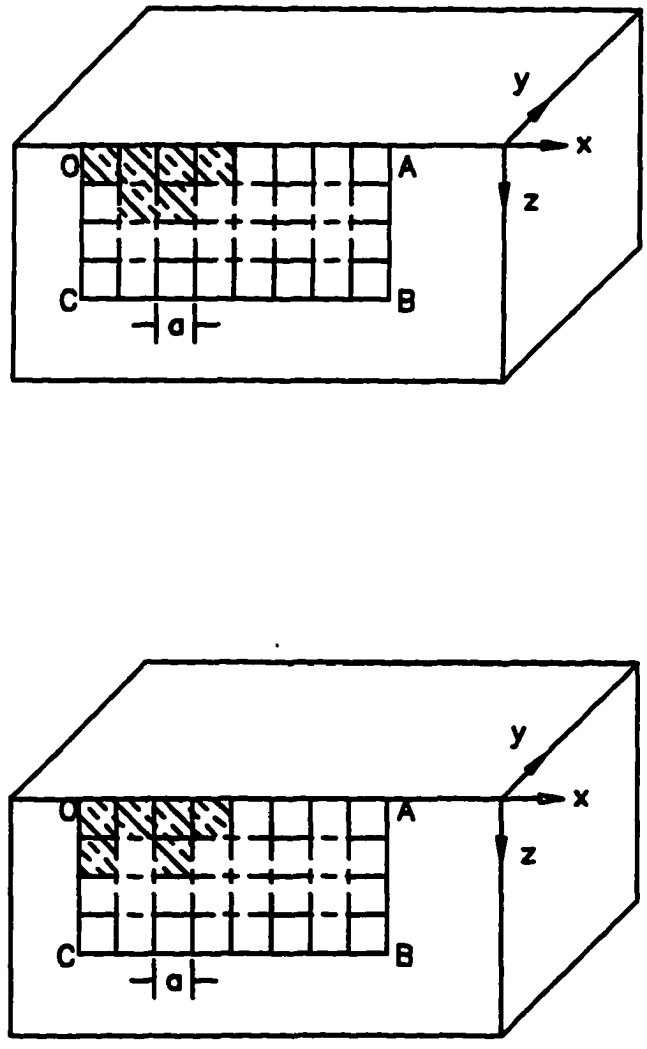

Figure 14.2. Different cracks should ideally give rise to different photoinductive data

CHAPTER 15. INTERLEAVING MEASUREMENT AND RECONSTRUCTION

Scope of the Chapter

The results and discussion presented in Chapter 14 has an impact on the reconstruction procedure. This chapter first shows why reconstruction can be begun even when only one measurement has been completed. The chapter explains what inputs should be given in such a case, what the objective function should be and how the results should be analyzed. The chapter closes by pointing out how more and more reconstruction can be done, as additional measurements become available

Possibility of Interleaving Measurement and Reconstruction

In Chapter 14, we saw that a single photoinductive measurement at a particular laser focus point (or scan point), labeled $P_{1,1}$ in Figure 14.1, is adequate for determining the condition, whether intact or cracked, of the pixel 1,1. Therefore if we make this measurement, and immediately run our reconstruction algorithm (the minimization algorithm), we should at least know what the condition of the pixel 1,1 is. After this, we can make the measurement at the laser focus point $P_{1,2}$, run our inversion algorithm, and determine the condition, whether intact or cracked of the pixel 1,2. In short, we should be able to interleave measurement and minimization.

The Inputs to the Computer Program

Suppose that the αth measurement has just been made. The inputs to the computer program are as follows.

(i) ξ_α, η_α -- the xy coordinates of the αth laser focus point (or scan point)

(ii) y_{coil_α} -- the y coordinate of the center of the base of the coil

(iii) f_α -- the frequency of the current source

(iv) π_α -- the photoinductive measurement $\mathbf{E}_{off}^2$

(v) I'_α = the set of the pixels i, j which are known to be intact from previous minimizations

(vi) C'_α = the set of the pixels i, j which are known to be cracked from previous minimizations

Items (i)-(iv) have already been mentioned in Chapter 8. Items (v) and (vi) are new. To illustrate them, set $\alpha = 1$, and consider the first minimization. There is no question of a previous measurement. Therefore $I'_\alpha = I'_1$ is an empty set. So is $C'_\alpha = C'_1$. Therefore items (v) and (vi) are each the empty set.

Objective Function

The objective function for the αth minimization is not the quantity F defined in Equation 11.3, but the quantity F_α defined by

$$F_\alpha = |M_\alpha|^2 + \sum_{i=1}^{m}\sum_{j=1}^{n}|N_{i,j}|^2 \tag{15.1}$$

where M_α and $N_{i,j}$ are defined in Equations 11.1-11.2.

Analysis of Reported Values

When the objective function in Equation 15.1 is minimized, the computer program reports $p_{i,j}$ for all indices i, j. The reported values are analyzed as follows.

(i) For those pixels which belong to the set I'_α, $p_{i,j}$ should be zero or, at least, very small. To illustrate, it may be small in comparison with the right-hand side of Equation 12.2.

(ii) For those pixels which belong to the set C'_α, $p_{i,j}$ should be nonzero. In fact it should be of the order of the right-hand side of Equation 12.2.

(iii) For the other pixels -- the pixels neither in I'_α nor in C'_α -- the analysis is more involved. Suppose, for concreteness, that the pixel 2,1 is one such pixel. We must first determine whether the computer program was able to calculate $p_{1,2}$ reliably. Roughly speaking, reliability means that the tradeoff discussed in connection with Equations 13.3-13.4 should be a good tradeoff. More precisely, the calculation of $p_{1,2}$ is reliable if the following condition are met:

(a) Compute the double integral over all the pixels that are neither in I'_α nor in C'_α. Let J denote the largest of these and K the largest but one. We verify that J is the double integral over the pixel 2,1 -- the pixel we are currently analyzing.

(b) When we write J in the place of ι_3 and K in the place of ι_5 , Equations 13.3-13.4 become

$$J = \iota_1 \tag{15.2}$$

$$J >> K \tag{15.3}$$

Here ι_1 has the same meaning as in Chapter 13. In general ι_1 is distinct from J, as ι_1 is greatest integral over *all* the pixels, not merely the ones that are neither in I'_α nor in C'_α. We verify that the trade-off between the relations (15.2) and (15.3) is good.

Assume that both conditions (a) and (b) are met. We now see whether the $p_{1,2}$ reported by the computer is small in comparison with the right-hand side of Equation 12.2, or of the same order. Accordingly, we decide whether the pixel 1,2 is intact or cracked.

Updating for the Next Computer Run

It is the sets $I'_{\alpha+1}, C'_{\alpha+1}$ that are updated at the end of each computer run. Suppose, for example, that the pixel 1,2 is found to be intact. Then we may update $I'_{\alpha+1}, C'_{\alpha+1}$ as follows.

$$I'_{\alpha+1} = I'_\alpha \cup \text{the pixel 1,2} \tag{15.4}$$

$$C'_{\alpha+1} = C'_\alpha \tag{15.5}$$

Or, if the pixel 1,2 is found to be cracked, we may update $I'_{\alpha+1}, C'_{\alpha+1}$ as follows.

$$I'_{\alpha+1} = I'_\alpha \tag{15.6}$$

$$C'_{\alpha+1} = C'_\alpha \cup \text{the pixel 1,2} \tag{15.7}$$

Either of these updates means that we are using the results of the αth computer run in the next computer run. We also have the option of not updating at all, so that

$$I'_{\alpha+1} = I'_\alpha \tag{15.8}$$

$$C'_{\alpha+1} = C'_\alpha \tag{15.9}$$

Flowcharts

At this stage, the theory behind our numerical procedure is complete. Therefore this would be an appropriate stage to insert the flowcharts for both the forward and the inverse problems (Figures 15.1-15.9)

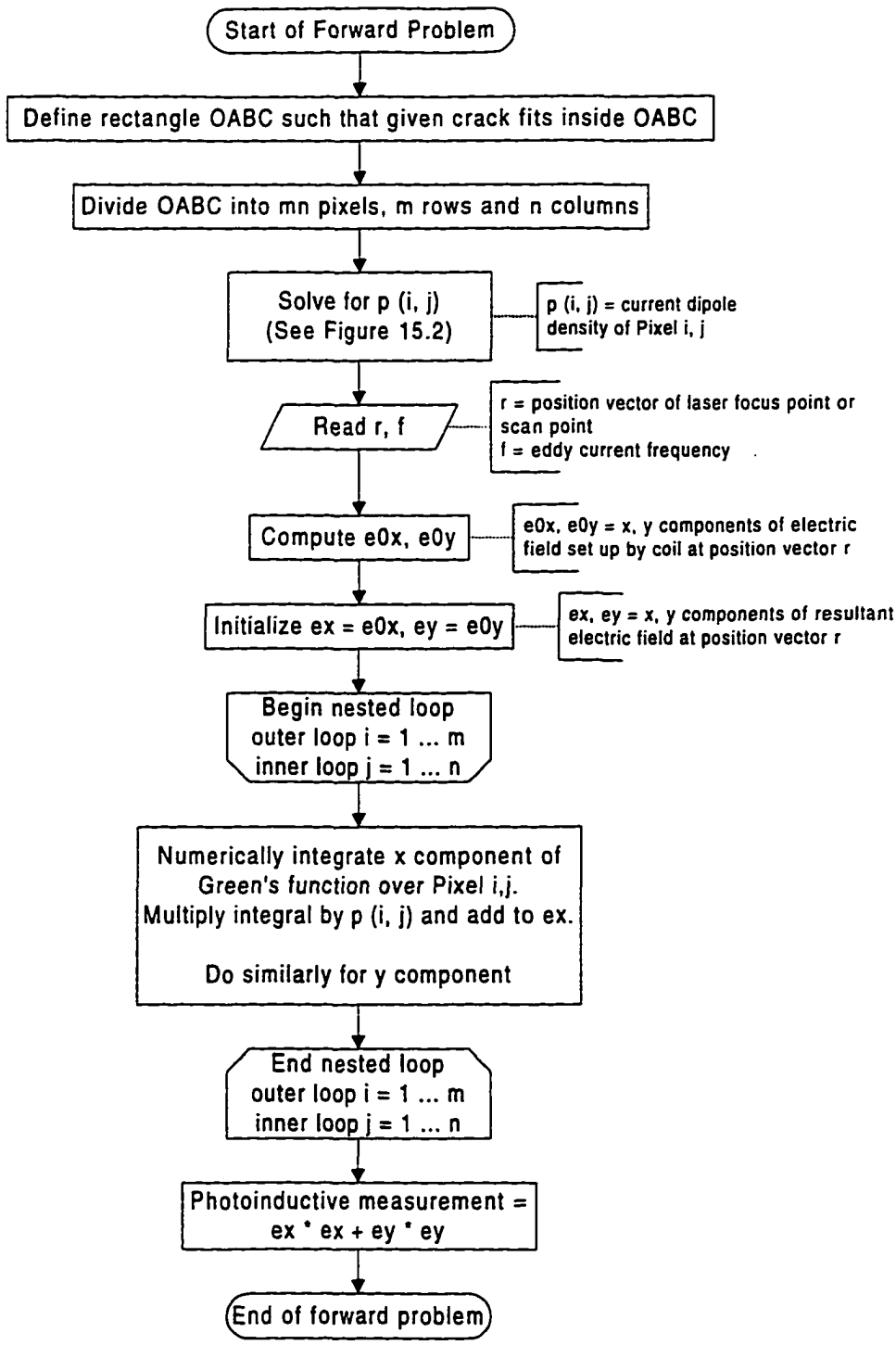

Figure 15.1. Flowchart for the forward problem used to generate synthetic photoinductive data

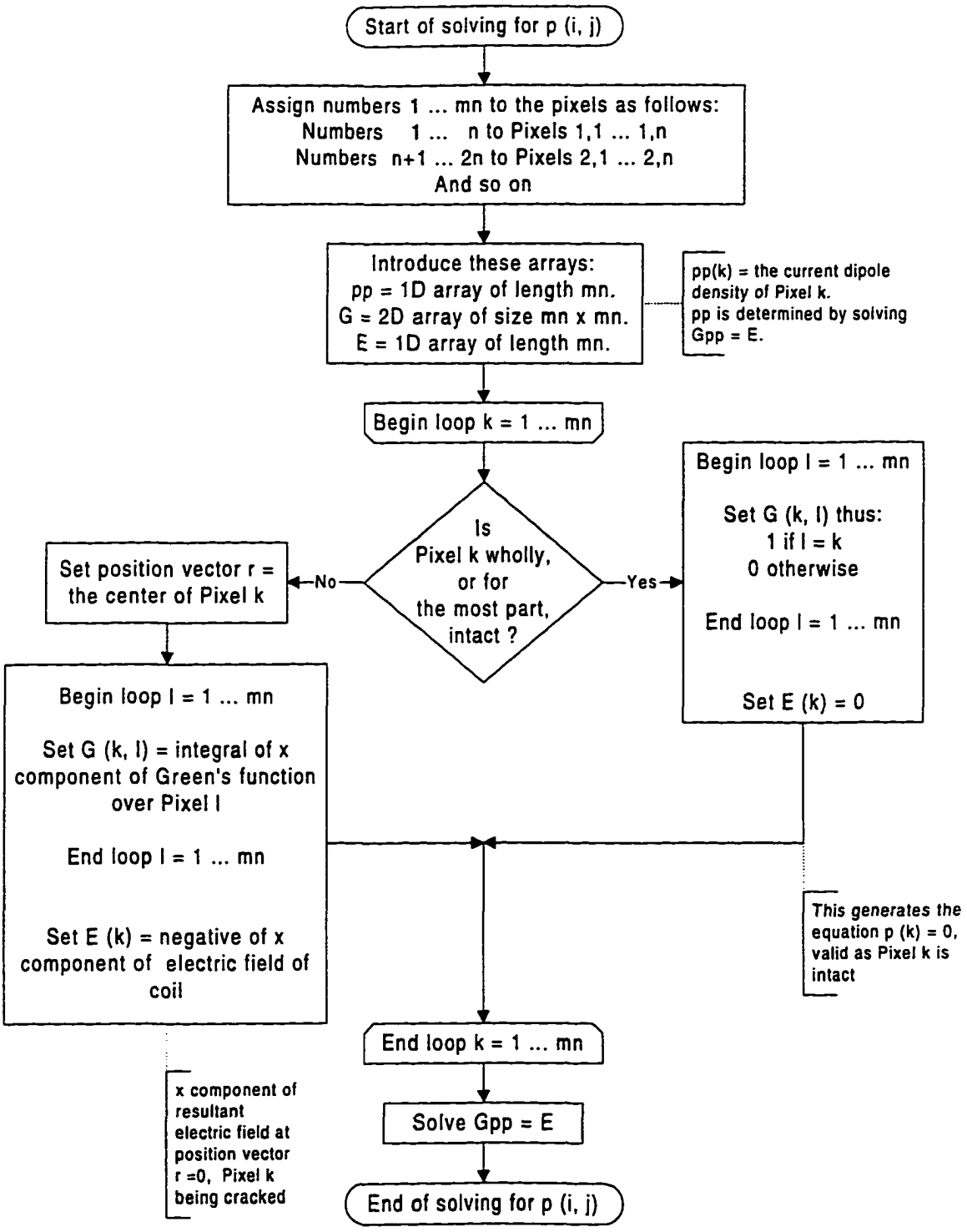

Figure 15.2. Flowchart for the obtaining the current dipole densities of all the pixels in the forward problem

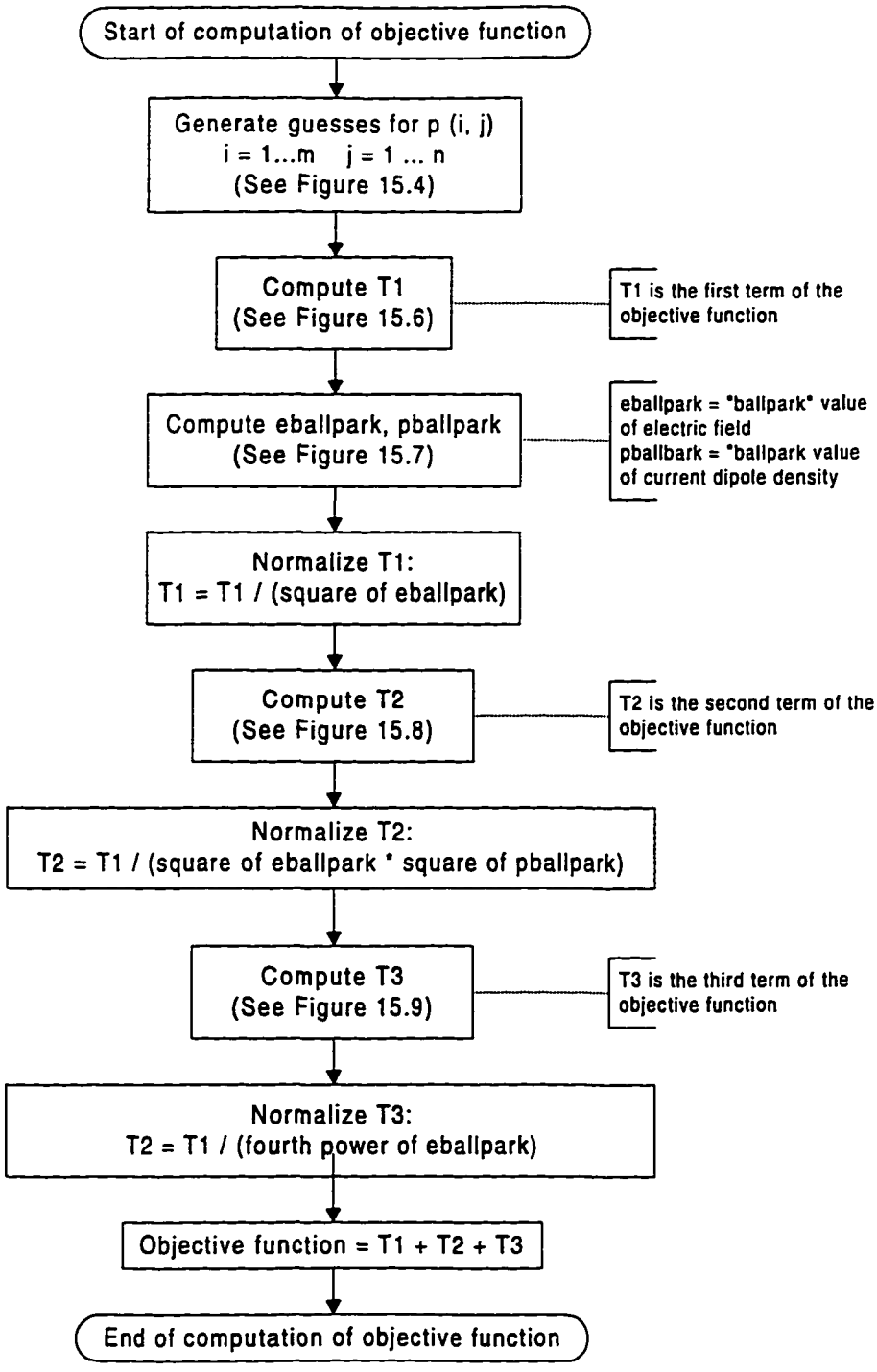

Figure 15.3. Flowchart for the computation of the objective function in the inverse problem

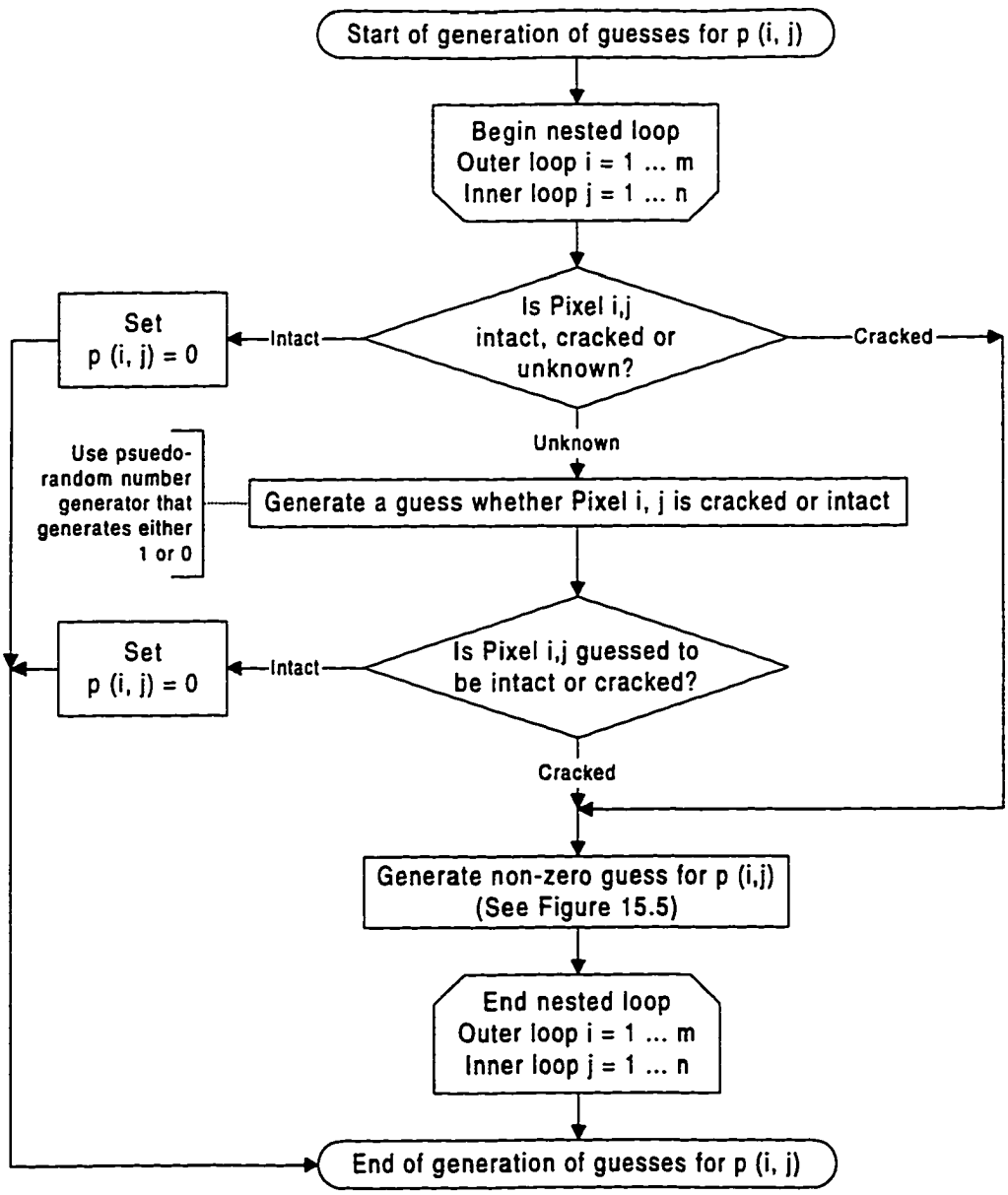

Figure 15.4. Flowchart for the generation of guesses for the current dipole densities of all the pixels in the inverse problem

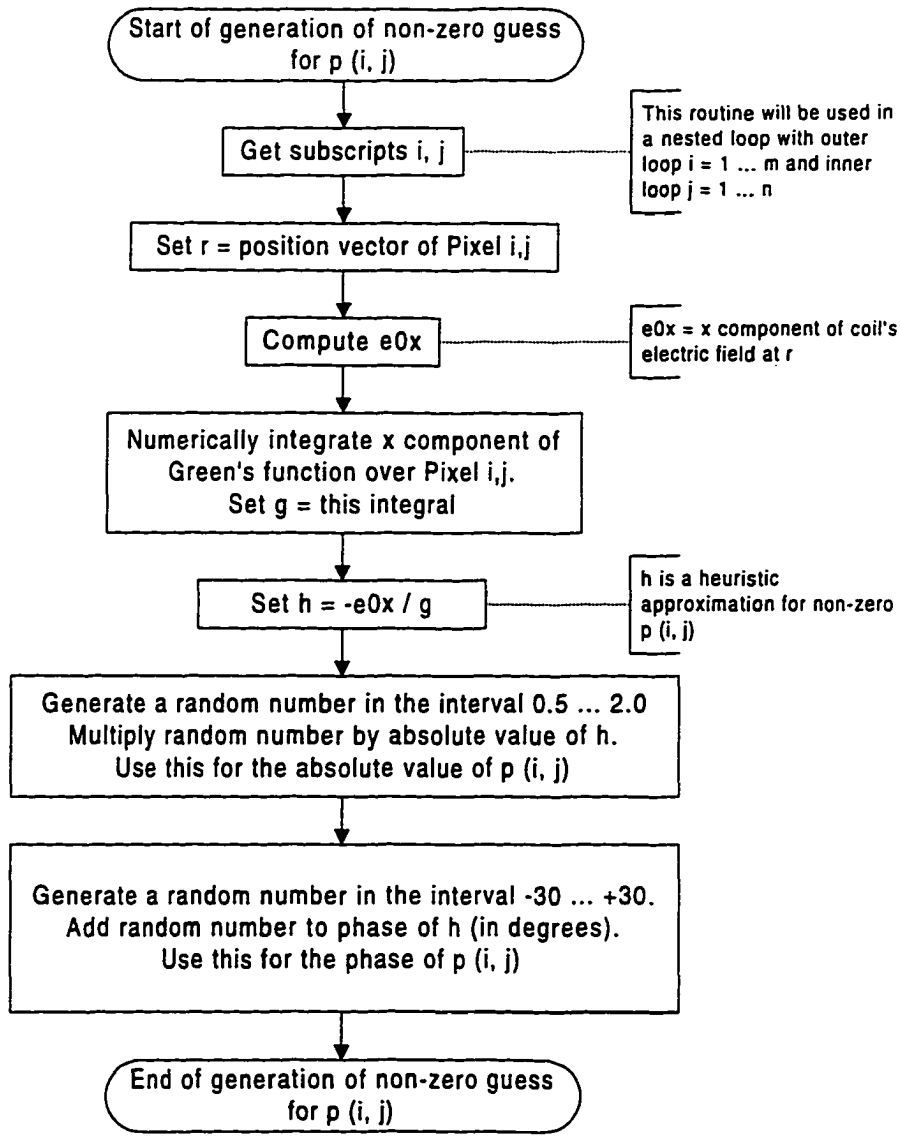

Figure 15.5. Flowchart for generating a non-zero guess for the current dipole density of a given pixel in the inverse problem

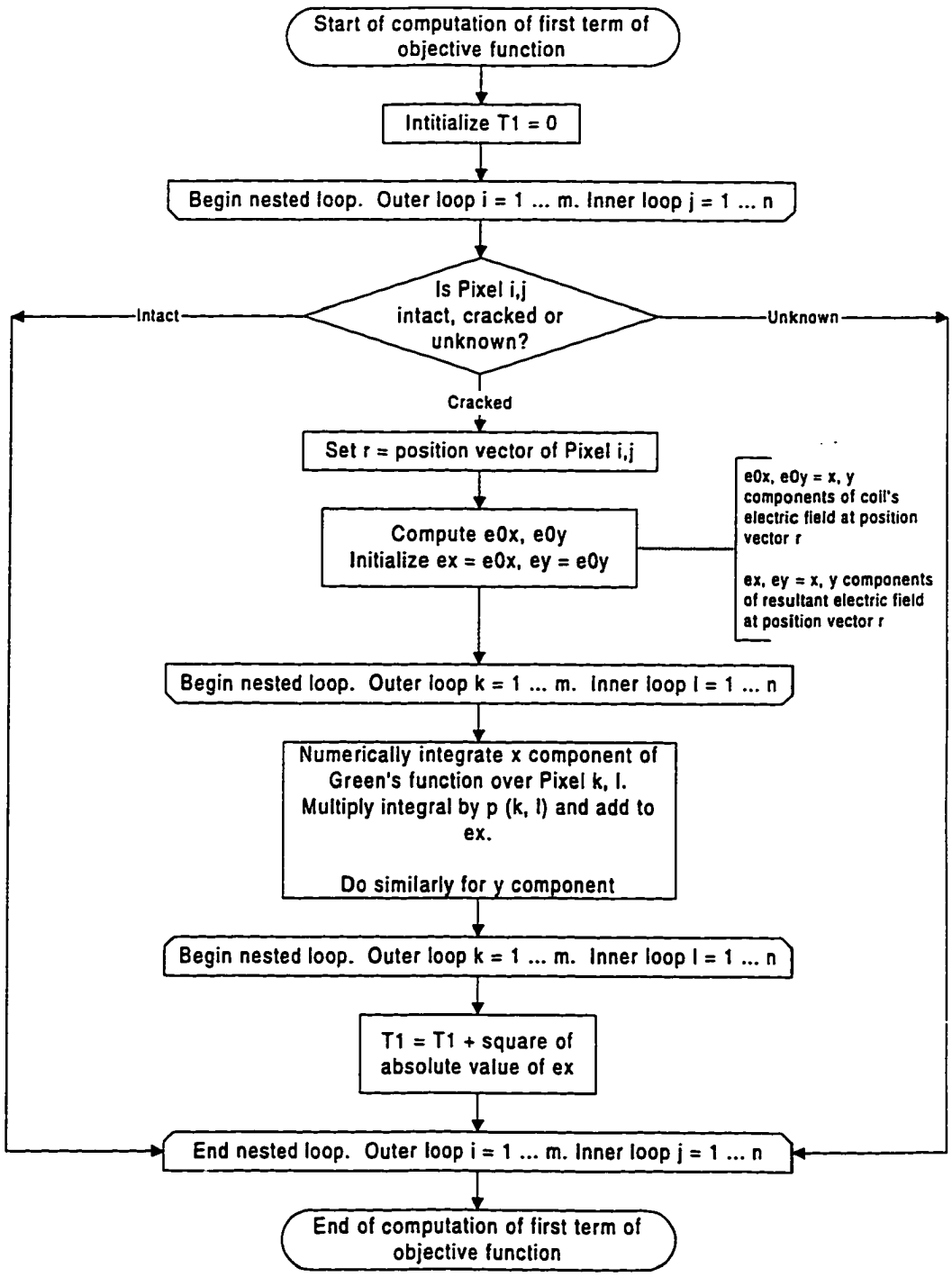

Figure 15.6. Flowchart for the computation of the first term in the objective function in the inverse problem

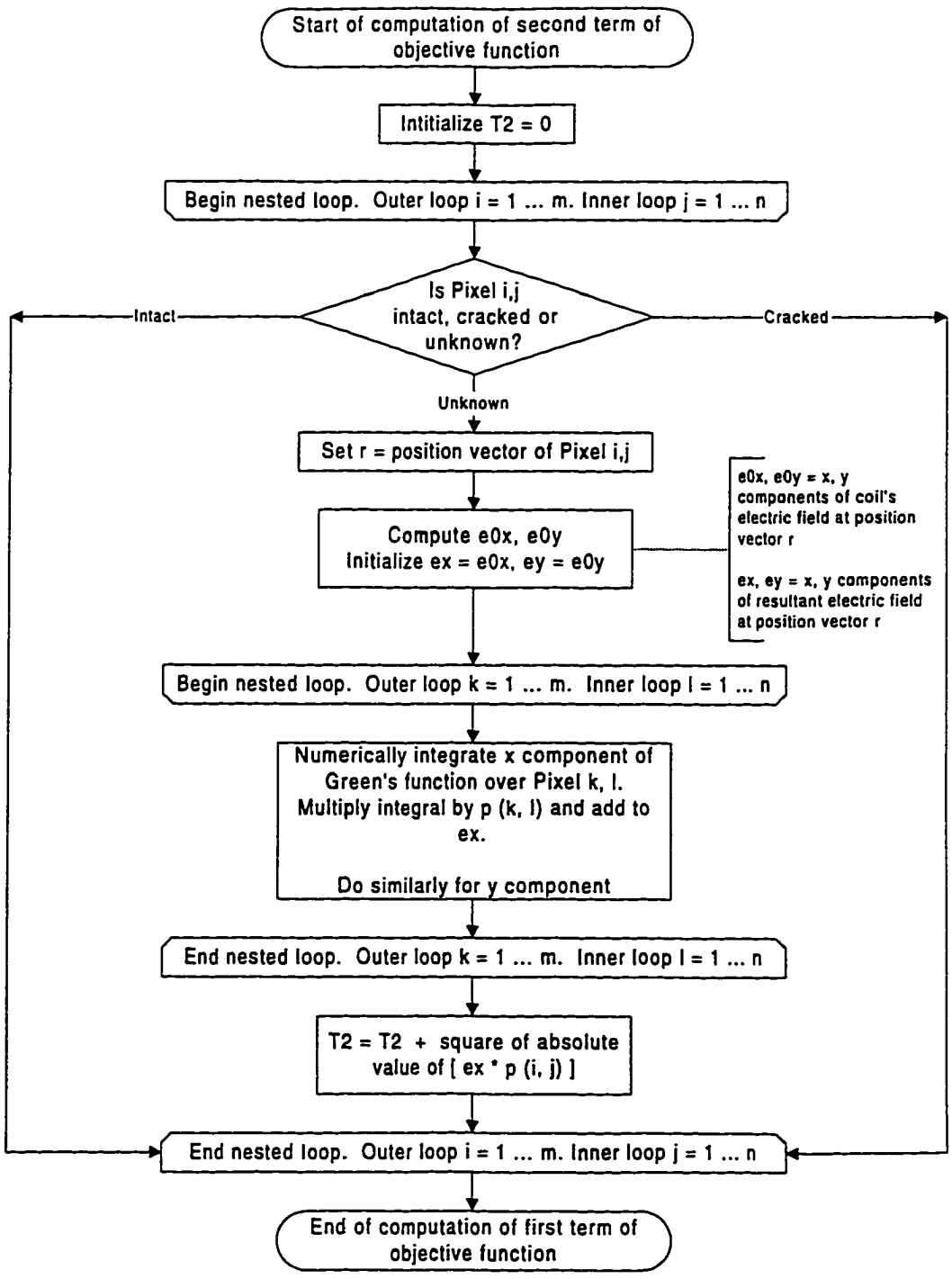

Figure 15.7. Flowchart for the computation of "ballpark" values of the electric field and the current dipole density

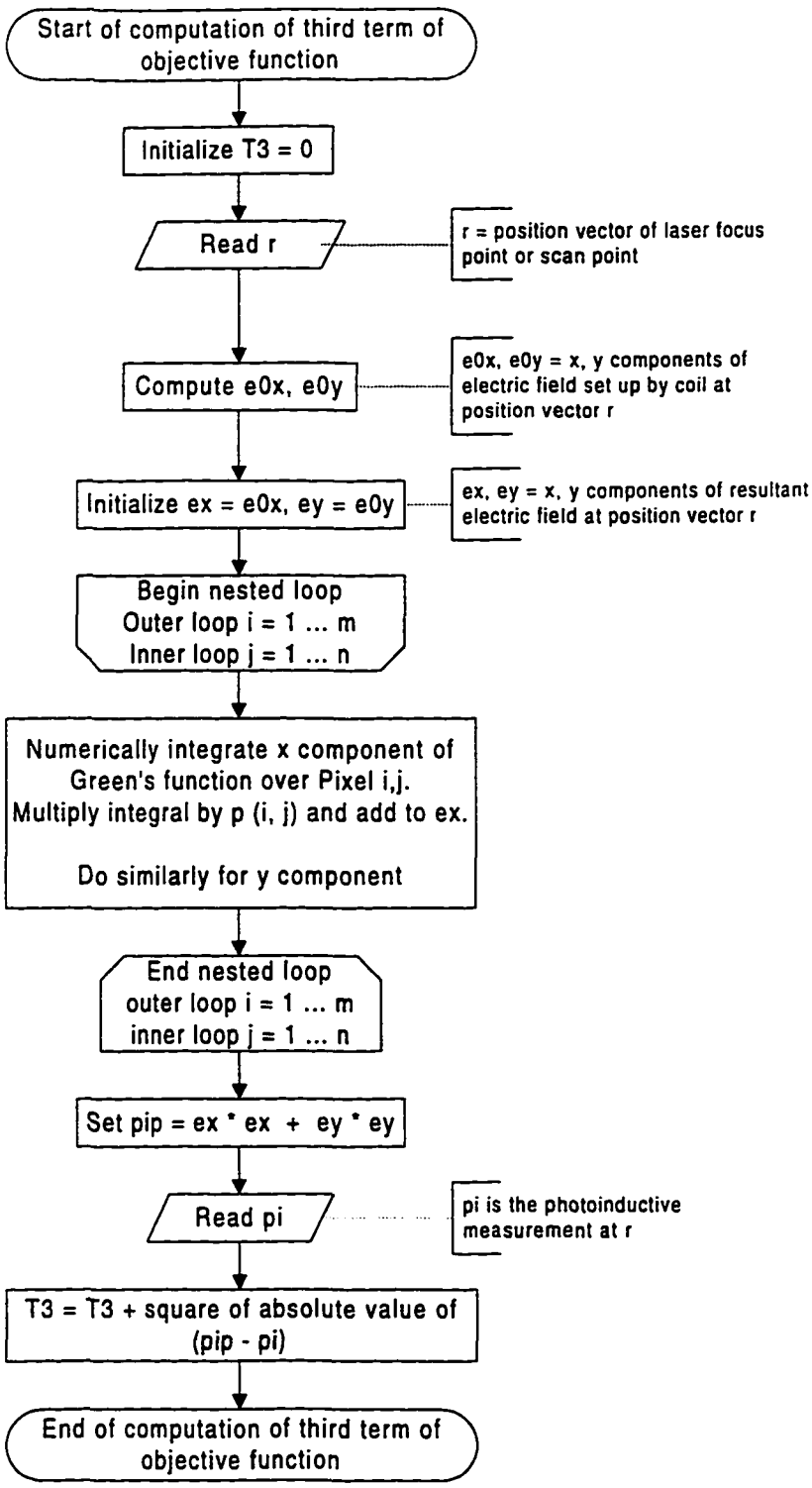

Figure 15.8. Flowchart for the computation of the second term of the objective function in the inverse problem

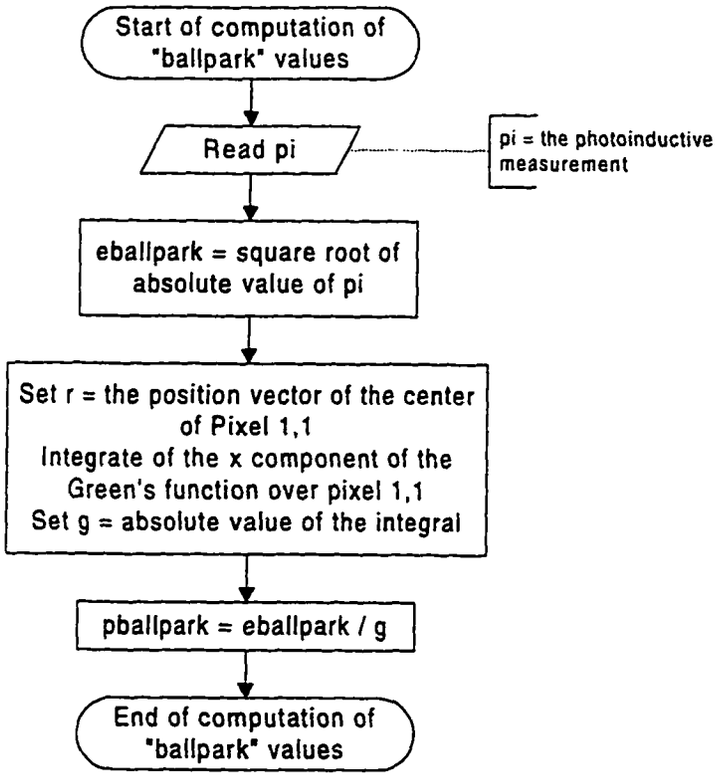

Figure 15.9. Flowchart for the computation of the third term of the objective function in the inverse problem

CHAPTER 16. ILLUSTRATING THE PROCEDURE

Scope of the Chapter

This chapter first notes a need for an illustrative example. After describing an example problem, it proceeds with certain details concerning the pixel size and the generation of synthetic photoinductive data. Next, it describes the first datum and the first computer run in detail. The stability of the crack reconstruction procedure with respect to the noise and the seed is also discussed. The chapter then shows how to determine in succession all the pixels in the crack. An instability, indicative of ill-posedness, is noticed and discussed.

An Illustrative Example

Chapters 10 and 15 show that solving Equations 8.5 and 9.1 to reconstruct the crack is a somewhat intricate procedure. We suggest that measurements and computer runs be interleaved. At the same time, there is a need to be alert to signs of ill-posedness. Given this intricacy, we shall describe the crack reconstruction procedure in some detail for a particular idealized crack in aluminum (Figure 16.1).

Pixel Size

The crack is assumed to lie within the rectangle $OABC$, which is divided into pixels of size $a = 100\mu$ m. Note that the pixel size is chosen to be of the order of the spatial resolution that can be achieved with the photoinductive method.

Synthetic Photoinductive Data

Experimental measurements are not yet available for the half space test specimen (Figure 7.1). Therefore, we used *synthetic* photoinductive data to test the crack reconstruction algorithm. These data were acquired by running the forward problem for the

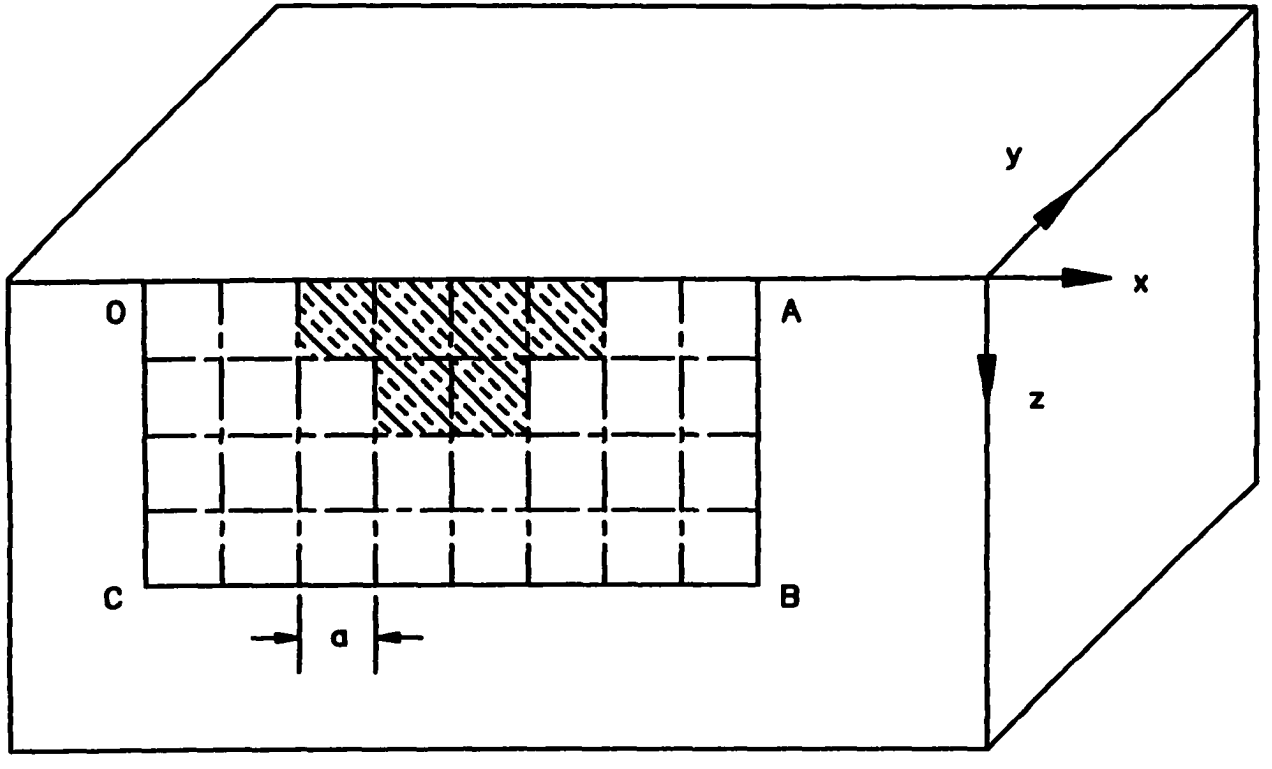

Figure 16.1. As an illustrative example, we endeavor to reconstruct the crack shown above

idealized crack shown in Figure 16.1, as described by Bowler [1], and computing $\mathbf{E}^2$. The scan plan is shown in Figure 16.2.

The First Synthetic Datum

For the first datum, corresponding to the index $\alpha = 1$, the laser focus point (or scan point) was $(\xi_1, \eta_1) = (0.5a, Y_{1,1})$ (In passing, we note that we are reverting to the use of single subscripts for ξ, η.) The frequency f_1 was chosen such that the skin depth was a little greater than $|\xi_1| = |0.5a|$, the perpendicular distance of the laser focus point and the top edge of the crack. Specifically, we set

$$\sqrt{\frac{2}{2\pi f_1 \mu_0 \sigma}} = skin\_depth = 1.15a = 1.15 \times 100 = 115 \quad \mu\,\mathrm{m}$$

Substituting $\sigma = 37.7$ MS/m for aluminum, we obtained f_1 = 508 kHz, or, say, 500 kHz.

The laser was set such that the center of its base was situated at $y_{coil} = Y_{1,1} - r_2$, where r_2 is the outer radius of the coil. Thus the coil is close to the pixel (1,1) (Figure 16.3). The coil attempts to drive a large current through this pixel. If the pixel were to be cracked, then that large current would be blocked, and the value of $\mathbf{E}^2$ would be considerably different from its value if the pixel (1,1) were intact. We generated a synthetic photoinductive datum, π_1, corresponding to these particulars.

Computer Run for the First Pixel

We indicated to the computer program that the condition, whether cracked or intact, of all the pixels was unknown, *i.e.*,

$$I_1' = C_1' = \text{the empty set} \tag{16.1}$$

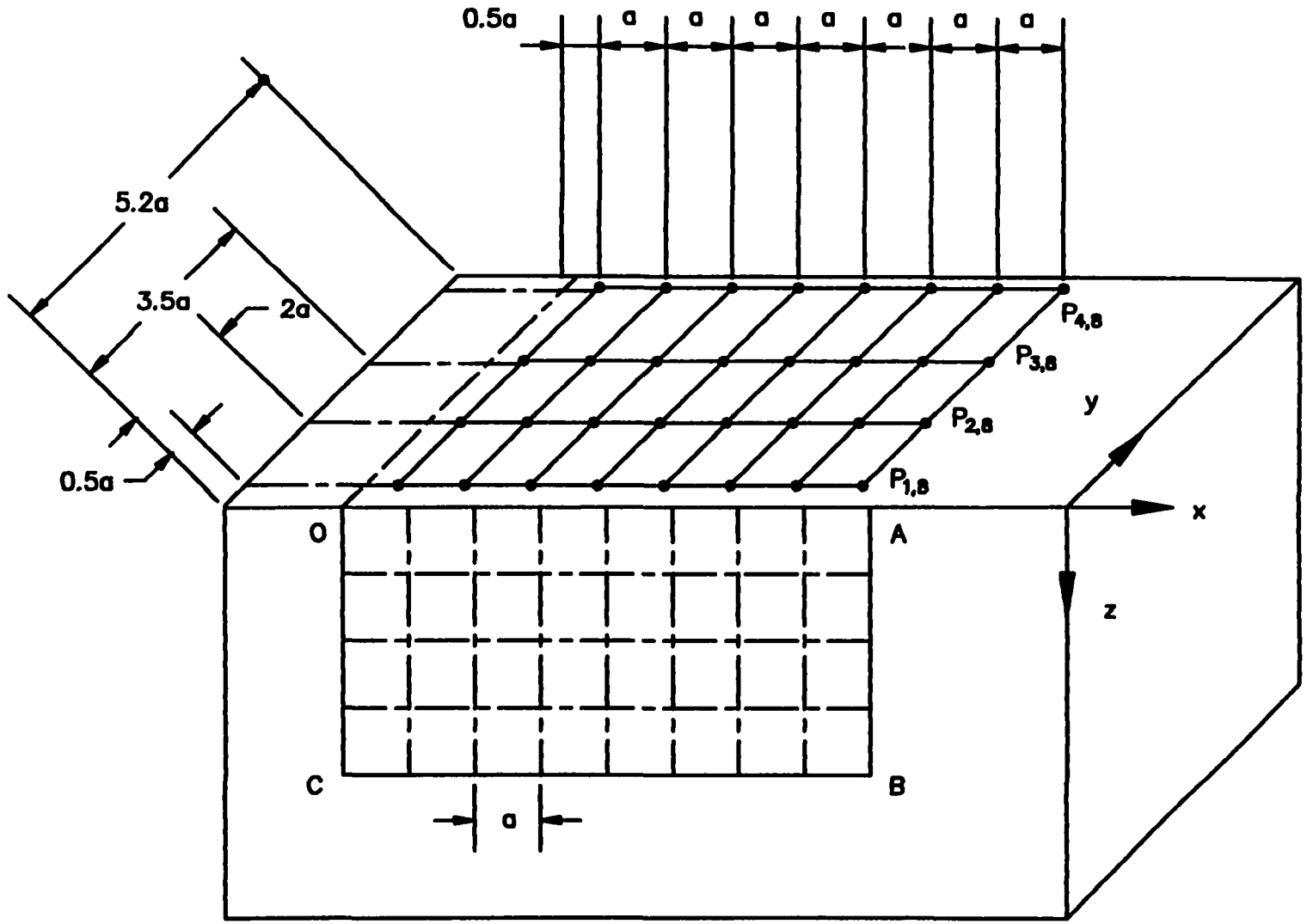

Figure 16.2. The scan plan used in the illustrative example

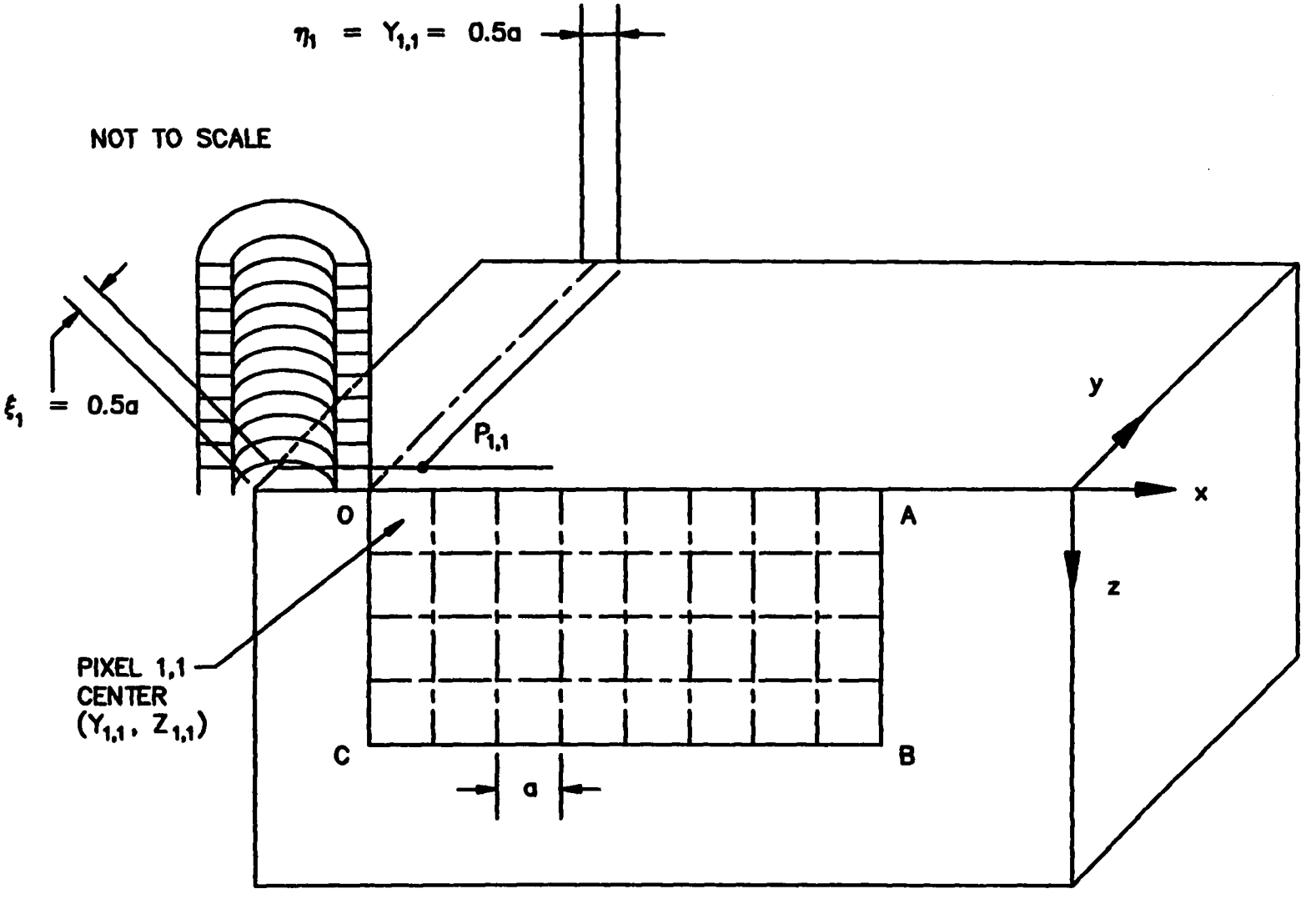

Figure 16.3. The photoinductive datum and the inversion for the pixel (1,1)

We provided the synthetic photoinductive data, π_1, and found that the computer program correctly predicted that the current dipole density for the pixel (1,1), $p_{1,1} = 0$; *i.e.*, the pixel (1,1) is intact.

Convergence

As mentioned in Chapter 12, our computer program was implemented using a Monte Carlo algorithm. The Monte Carlo algorithm operates by generating a sequence of N pseudorandom numbers, where N is an input to be provided by the user. We increased N in steps of 5000, beginning with 5000. We found that for $N > 20{,}000$, the final residual was consistently less than 0.001 times the initial residual.

Invariance with Respect to the Seed

To initiate the generation of a sequence of pseudorandom numbers, it was necessary for the user to supply a number known as the seed. The seed may be chosen arbitrarily. In the context of our optimization program, it was necessary to verify that the results of the computer program were the same, no matter what the seed. We found that this was indeed the case.

Stability with Respect to the Noise

We added a small number $\Delta\pi_1$ to the synthetic datum to simulate noise or repeatability error. Values were assigned to $\Delta\pi_1$ in the following way. In a crack-free test specimen, the photoinductive datum would have been $\mathbf{E}_0^2(\xi_1, \eta_1, 0)$. But the actual (synthetic) datum was π_1. We interpreted the difference $\mathbf{E}_0^2(\xi_1, \eta_1, 0) - \pi_1$ as the signal and $\Delta\pi_1$ as the noise. We let $\Delta\pi_1$ be a random number up to 10% of the signal, so that the signal-to-noise ratio was up to 10%. Using $\pi_1 + \Delta\pi_1$ as the datum, the program correctly obtained the same result, the current dipole density of the pixel (1,1) was zero, and thus this pixel (1,1) is intact (in the set I').

The result of the computer program was stable with respect to not only the seed, but also the noise. It is consistent with the discussion of the point $P_{1,1}$ in Chapter 14.

The Second Data and the Second Computer Run

For our next data, we shifted the coil as well as the laser a distance a to the right (Figure 16.4). The frequency was kept the same. The computer program reliably predicted that $p_{1,2}=0$, meaning that the pixel (1,2) was intact. This prediction was stable with respect to both the seed and the noise. Moreover, as in Equations 14.8-14.9, we could set

$$I_2' = I_1' \tag{16.3}$$

$$C_2' = C_1' \tag{16.4}$$

In other words, it was not necessary to supply the information learnt from the previous computer run, namely, the information that the pixel (1,1) was intact. Even so, the computer program correctly predicted the condition of the pixel (1,2). All this is consistent with the discussion about the point $P_{1,s}(s=1...n)$ in Chapter 14.

The Data and Computer Runs for the First Row

By moving the coil and the probe to the right in steps of a, and interleaving data generation with computer runs, we were able to predict the condition of all the pixels in the first row (Figure 16.5). In this way, the first n data helped to predict the condition of the pixels $(1,1),(1,2),...,(1,n)$.

The Data and the Computer Run for a Pixel in the Second Row

We set $\alpha = n+1$. The laser focus point was moved further from the crack; $(\xi_{n+1}, \eta_{n+1}) = (2a, Y_{2,1})$ (Figure 16.6). The frequency f_{n+1} was chosen such that the skin

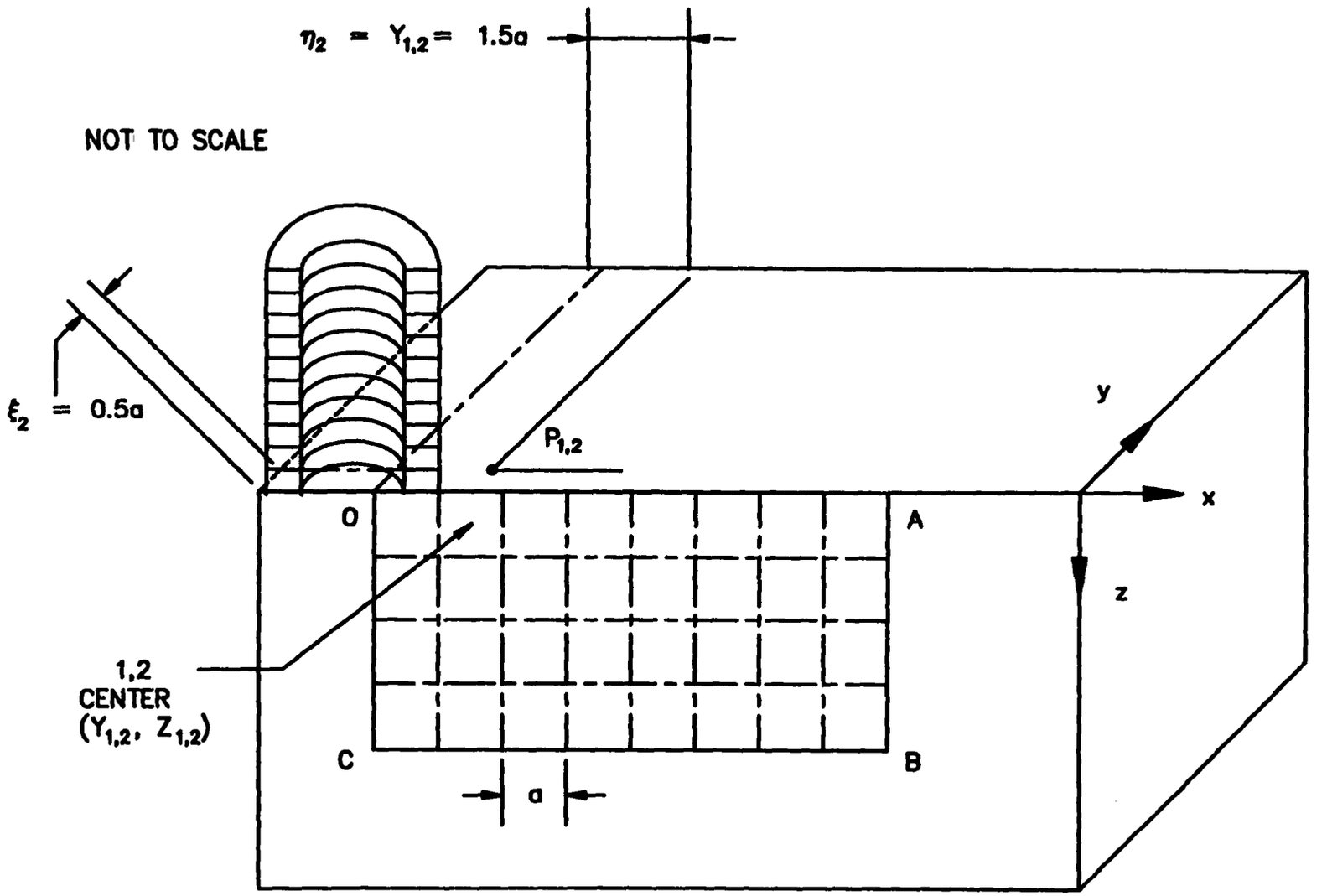

Figure 16.4. The photoinductive datum and the inversion for the pixel (1,2)

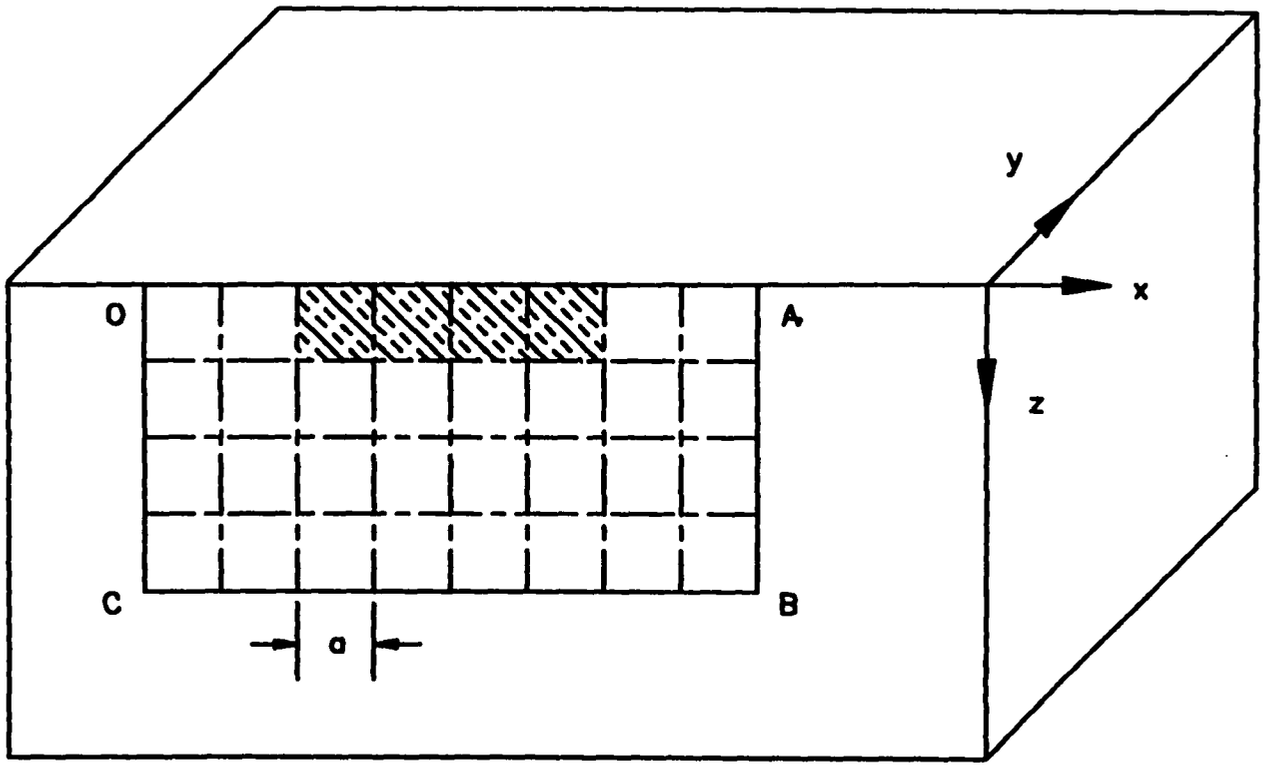

Figure 16.5. The inversion is accurate for the first row of pixels

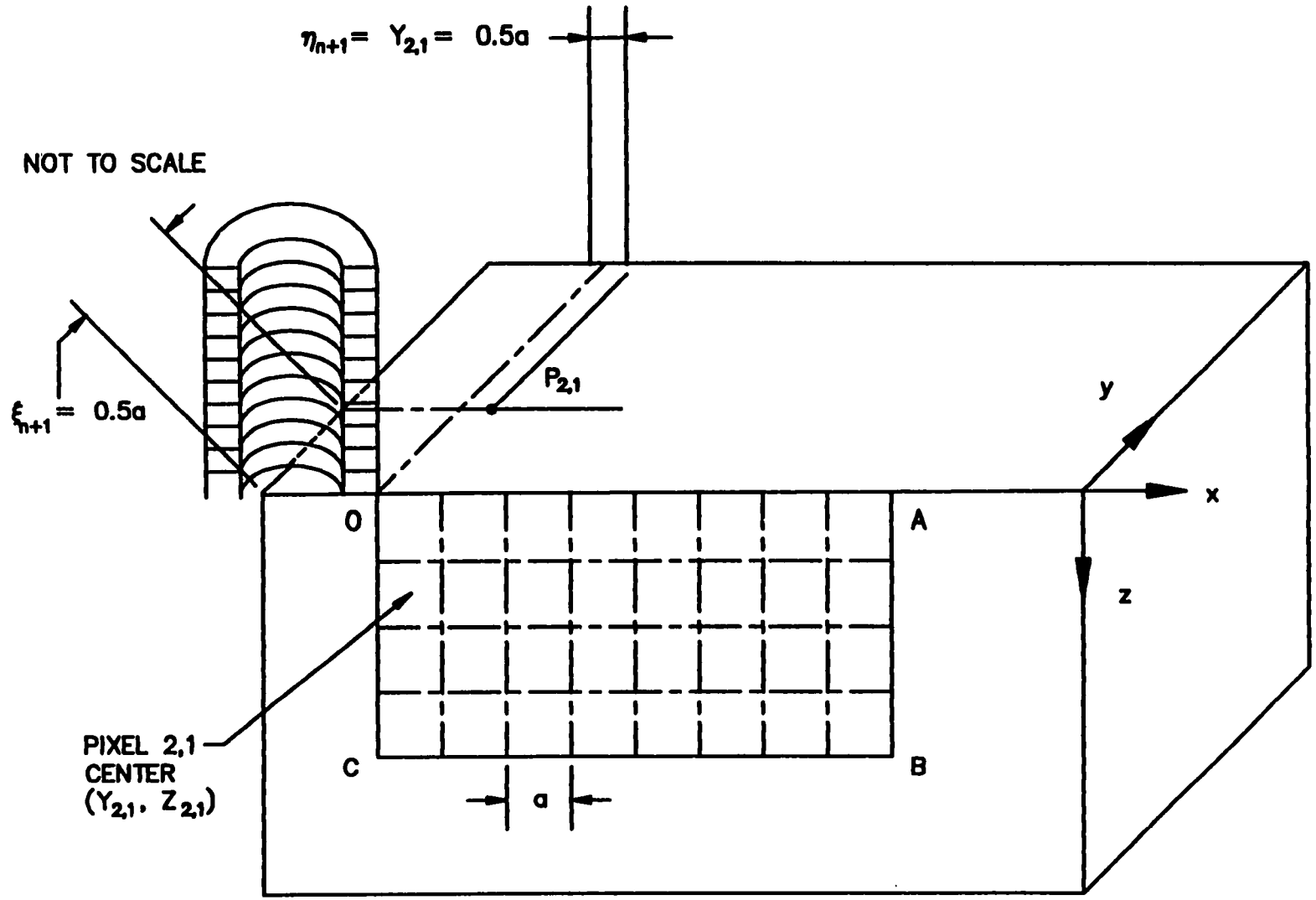

Figure 16.6. The photoinductive datum and the inversion for the pixel (2,1)

depth was a little greater than $|\xi_{n+1}|$, the perpendicular distance between the laser focus point and the top edge of the crack; specifically f_{n+1} = 125 kHz. We generated a synthetic photoinductive datum π_{n+1}, corresponding to these particulars. By appropriately defining the sets $I_\alpha^{'}, C_\alpha^{'}$, we supplied the computer program with the results that our computer program had obtained for the first row of pixels.

The computer program predicted that $p_{2,1} = 0$, meaning that the pixel (2,1) was intact. This is the correct prediction.

We shall speak of the stability with respect to the seed and with respect to the noise presently.

The Data and the Computer Runs for the Second Row of Pixels

By shifting the coil and the laser in steps of a to the right, and interleaving data with computer runs, we endeavored to reconstruct the condition of all the pixels in the second row. The correctness of the prediction was marred in some cases by an instability with respect to the seed and the noise, indicative of ill-posedness.

To illustrate, for some seeds, the computer program correctly predicted the condition of the pixel 2,5 to be cracked and the pixel 2,6 to be intact. For other seeds, it made the opposite prediction. As a result, not one, but two cracks emerged from our inversions (Figure 16.7). We ran the forward problem for both the cracks, *i.e.*, we computed what the photoinductive data $\mathbf{E}^2$ would be for these cracks. It turned out that both cracks gave nearly the same photoinductive data, indicating that the reconstruction problem was inherently ill-conditioned. All this is consistent with the discussion on the trade-off and the ill-posedness in Chapter 14.

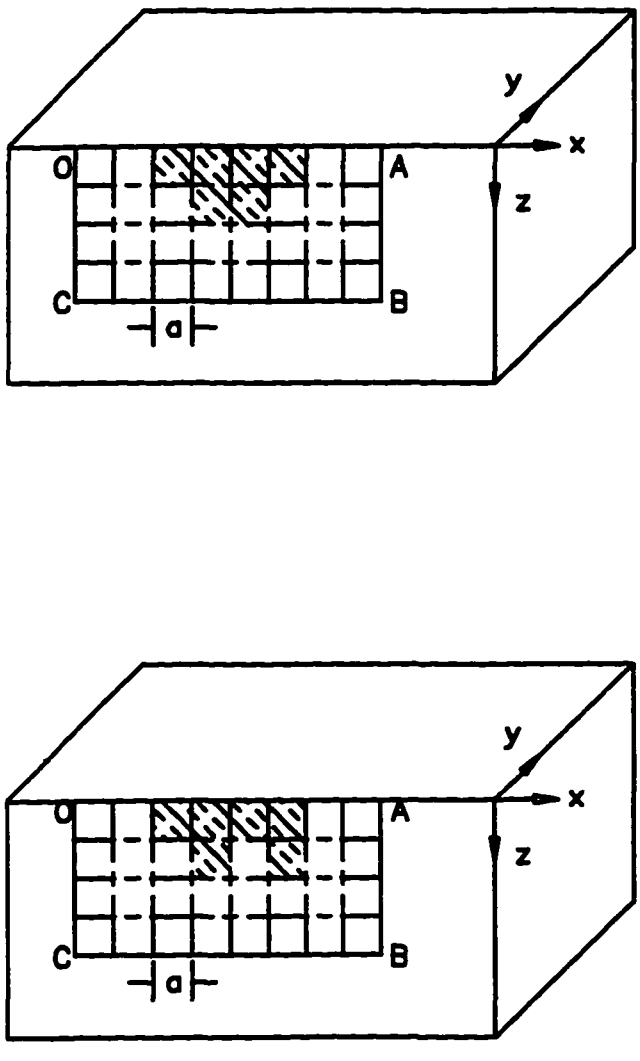

Figure 16.7. The reconstruction procedure yields more than one crack

Regularization

As discussed in Chapter 10, regularization involves imposing additional conditions or equations in an effort to eliminate ill-posedness. Using conventional eddy currents, Bowler, Norton and Harrison [3] imposed the additional condition that the area of the crack should be a minimum. Evidently, the minimum area condition helps to single out a crack with the least special shape.

We considered imposing the same condition in the dissertation problem also. But the two cracks shown in Figure 16.7 have the same area, indicating that the minimum area condition does not regularize the dissertation problem. Therefore we adjoined a different condition -- that of minimizing the perimeter of the crack. The minimum perimeter condition did help to select the correct crack from the two shown in Figure 16.7.

CHAPTER 17. RESULT AND DISCUSSION: CRACK RECONSTRUCTION

Scope

This chapter discusses some of the crack reconstructions which were carried out. The chapter indicates the metals considered and goes on to describe the crack sizes. After defining the pixel size and scan plan, the chapter presents the reconstruction results. The chapter closes with a discussion of ill-posedness, touching on regularization.

Metals Considered

We considered test specimens made of aluminum and titanium. Titanium ranks rather low among the metals in terms of electrical conductivity, while aluminum ranks rather high. The quality of the reconstruction presented below did not depend on the conductivity. Therefore, we believe that our results will be applicable to a broad range of nonmagnetic metals.

Magnetic materials were not considered. The signals from magnetic materials are not well-characterized, being dependent on factors like aging, exposure to atmosphere and surface damage [21].

Crack Size

A major point of this thesis is that the photoinductive method can deal with cracks that are smaller than the inner radius of the coil. The inner radii of typical coils range from 0.5 mm to several millimeters; for example, Moulder, Uzal and Rose cite a coil with an inner radius of 535 μ m [16, the L probe]. We will show that it is possible in principle to reconstruct cracks whose linear dimensions are on the order of hundreds of microns (Figures 17.1 - 17.2).

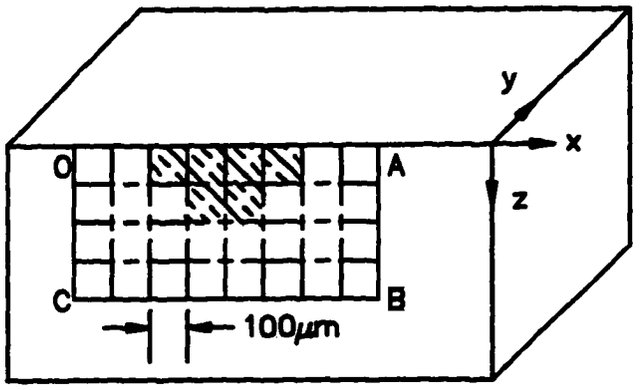

Figure 17.1. A test case with length greater than depth

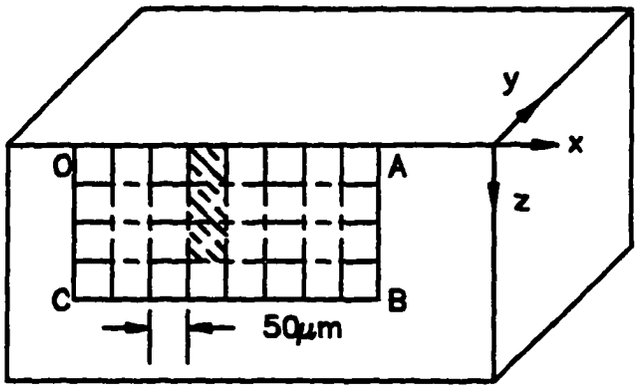

Figure 17.2. A test case with length less than depth

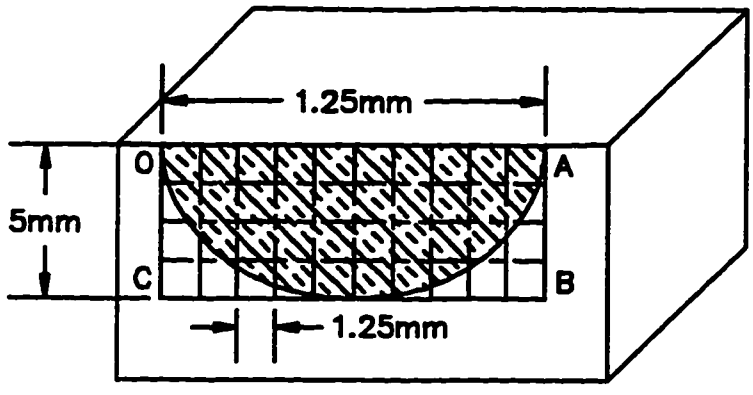

Figure 17.3. A crack of the order of the coil radius

We also inverted for the shape of a much larger crack, with a length of 12.5 mm (Figure 17.3) This particular crack is similar to the crack for which Bowler computed impedance changes [1, Table I, Expt 1].

Pixel Size

The pixels were 100μm by 100 μ m for the first trial crack (Figure 17.1), 50 μ m by 50μ m for the second trial crack (Figure 17.2), and 1.25 mm by 1.25 mm for the third trial crack (Figure 17.3).

Scan Plan

We used the scan plan of Figure 16.2 in all the cases, substituting the appropriate value for the pixel size a.

Reconstruction Results

Corresponding to the cracks in Figures 17.1 - 17.3, the reconstruction program yielded the cracks shown in Figures 17.4 -17.6 respectively. In each case, there were nonunique solutions, owing to ill-posedness. In each case, one of the nonunique solutions was in fact the actual crack. Running the forward problem on the other cracks as a check, we found that they gave nearly the same photoinductive measurements as the correct crack.

Stability with Respect to the Noise

For all the trial cases reported, the prediction for the pixels of the first row was stable with respect to the noise up to a signal-to noise ratio of 10%. Thus ill-posedness did not pose a problem in the first row.

It should be pointed out here that the seed was fixed whenever stability with respect to the noise was studied, since varying the seed itself can cause instability.

For the pixels in the second row, the prediction was stable if the signal-to-noise ratio was, say, 1%, but for 4% (or more), the prediction often lost stability, in consequence of ill-posedness.

The stability with respect to noise was still less for the pixels in the third, fourth, *etc.* rows, meaning that the ill-posedness was greater in these rows than in the second.

Results were identical for both aluminum and titanium.

Regularization

The cracks shown in Figure 17.4 have the same area. Therefore it is not possible to single out a unique crack, by adjoining the condition that the area of the crack should be a minimum. However, by adjoining a different condition, namely, that the perimeter should be a minimum, we can single out a unique crack. The crack so singled out is the correct crack, the

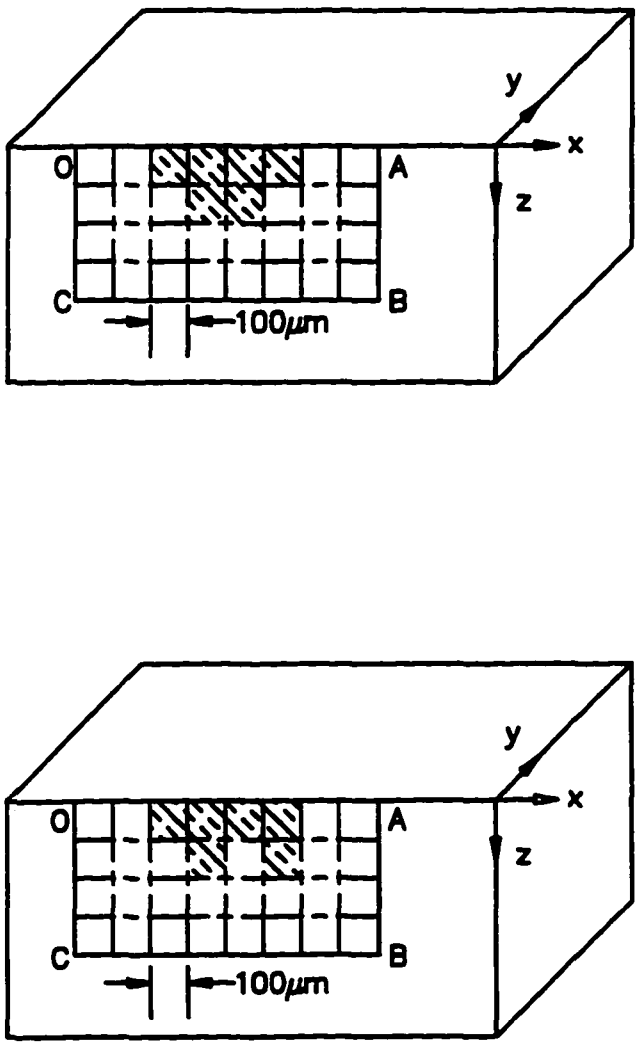

Figure 17.4. Reconstruction corresponding to Figure 17.1

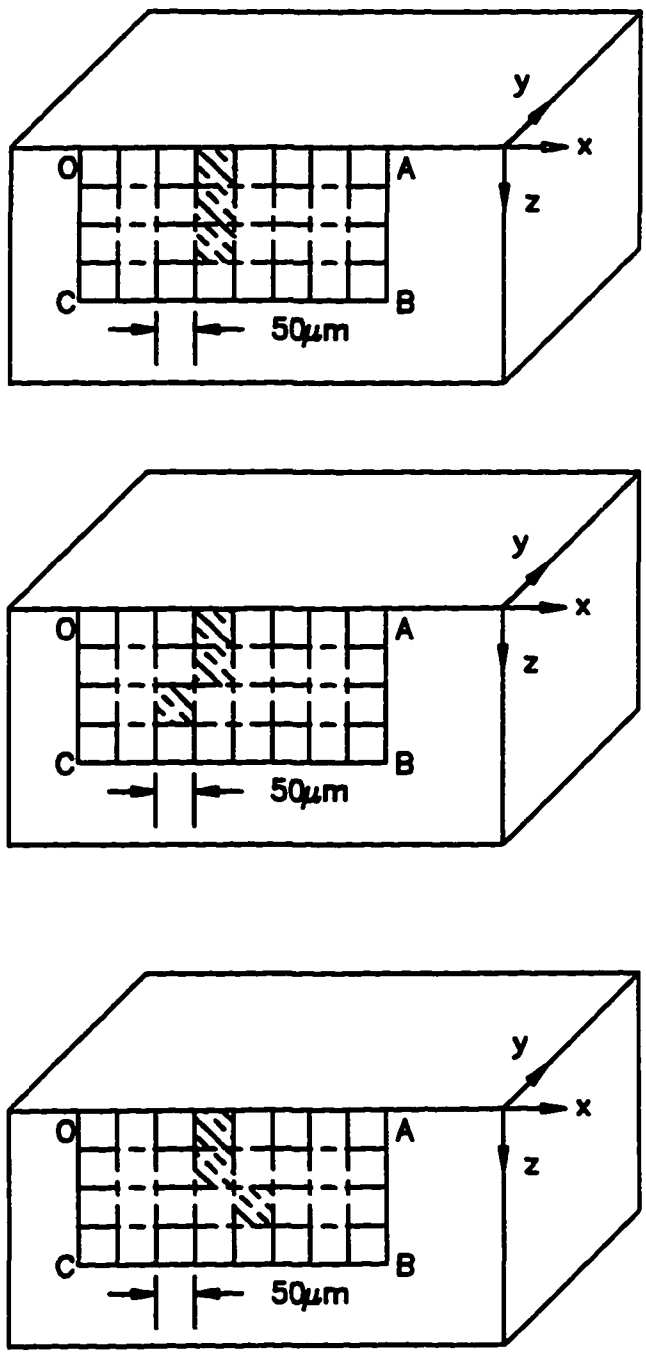

Figure 17.5. Reconstruction corresponding to Figure 17.2

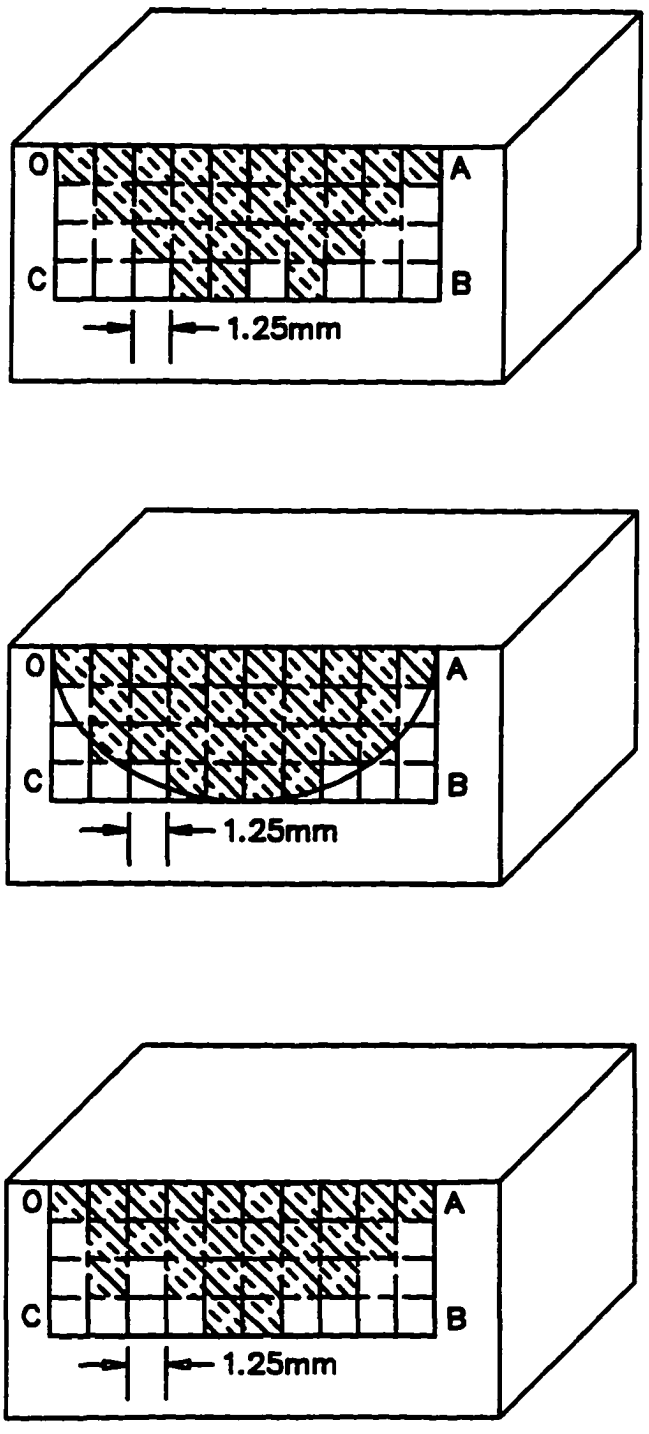

Figure 17.6. Reconstruction corresponding to Figure 17.3

crack shown in Figure 17.1. Evidently the minimum area condition singles out a crack with the least special shape.

Turning our atttention to Figures 17.5-17.6, the minimum perimeter condition helps to single out a unique crack in those figures also.

It appears that the minimum perimeter condition helps to regularize the dissertation problem.

CHAPTER 18. CONCLUSIONS

Scope of the Chapter

This chapter gives a brief statement of the work done, the main findings, the work for the future and the specific contribution of the dissertation.

What was Done

This dissertation has been concerned with reconstructing cracks from photoinductive measurements. We have developed the first inversion method for reconstructing the crack from photoinductive data. We tested the method on tight surface-breaking cracks in aluminum and titanium. These cracks ranged from hundreds to thousands of microns.

Findings

Crack reconstruction is inherently ill-posed, due to instability to small changes in the input data that manifests itself as a problem of nonuniqueness. Apart from this limitation, the crack reconstruction method was successful in all the test cases. By seeking a crack of minimum perimeter, we were able to single out from the nonunique solutions, a crack giving the correct estimate of the depth. All these results were weakly dependent on the conductivity of the metal; consequently the crack reconstruction method is likely to perform well with all nonmagnetic metals. Good estimates for the crack depth were obtained in all the cases tested. After regularization, the crack shape was also recovered for all the test cases.

Work for the Future

As bolt holes are subject to stress, they are prone to the development of small, tight-surface breaking cracks. Experimental photoinductve measurements are now available for a

set of laboratory specimens possessing bolt holes. Therefore it would be of considerable interest to extend this work to these test specimens. The technical problem is to derive formulas for the incident electric field $\mathbf{E}_0$ and the Green's function $\mathbf{G}_1$ (Equation 4.5) that are appropriate for bolt hole geometry. If this can be done, either analytically or numerically, the crack reconstruction method described here can be used with little or no modification.

The Specific Contribution of the Dissertation

As the photoinductive method is relatively new, the literature does not appear to contain any theoretical-numerical investigations of its potential in crack reconstruction. This dissertation has contributed such an investigation. More explicitly:

- The dissertation has contributed a numerical technique that reconstructs -- subject to the issue of ill-posedness -- small (*circa* 100 microns) tight surface-breaking cracks in nonmagnetic materials.
- Applying this numerical technique, the dissertation has shown that the depth of such cracks can be recovered from photoinductive measurements. In addition, the shape of the cracks can also be recovered if the problem is regularized.
- The dissertation has shown that the magnitude of the Green's function helps a user to judge beforehand at what laser focus points and at what eddy current frequencies photoinductive measurements will be useful for crack reconstruction.
- The dissertation has shown that three concepts occurring in Bowler's eddy current formulism – the current dipole density, the Green's function and the electric field set up by the coil – hold the key to reconstructing cracks from photoinductive measurements.

APPENDIX A. THE FORMULA FOR A PHOTOINDUCTIVE MEASUREMENT

Auld's Reciprocity Formula

Chapters 4-5 considered precision wound coils fed by a constant current source and set above a test specimen. In Chapter 4, the measured quantity was a difference of impedance: the difference between the no-crack impedance and the impedance with the crack. In Chapter 5, the measured quantity was a difference of voltage: the difference between the laser-high voltage and laser-low voltage. These differences are covered by Auld's reciprocity theorem [22, Chapter 3, Equation 3.14].

For Chapter 3, theAuld's reciprocity theorem can be quoted as follows:

$$Z - Z_0 = -\frac{1}{I^2} \iiint_{test\_specimen} \Delta\sigma \mathbf{E}_{crack} \cdot \mathbf{E}_{reference} dV \qquad \text{(A.1)}$$

where $\Delta\sigma$ is the difference between the conductivity of the crack (0 if the material of the crack is an insulator) and the conductivity of the metal. The quantity I is the current of the current source.

For Chapter 5, Auld's reciprocity theorem can be quoted as

$$\frac{U_{on} - U_{off}}{I} = -\frac{1}{I^2} \iiint_{test\_specimen} (\sigma_{on} - \sigma_{off}) \mathbf{E}_{on} \cdot \mathbf{E}_{off} dV \qquad \text{(A.2)}$$

The Born Approximation

As the laser increases the temperature only a little, $\mathbf{E}_{on} \approx \mathbf{E}_{off}$. Moreover, the quantity $\sigma_{on} - \sigma_{off}$ is nonzero only in the heated region shown in Figure 6.5. Therefore Equation A.2 reduces to

$$\frac{U_{on}-U_{off}}{I}=-\frac{1}{I^2}\iiint_{heated\_region}\left(\sigma_{on}-\sigma_{off}\right)\mathbf{E}_{off}\cdot\mathbf{E}_{off}dV \qquad (A.3)$$

If the heated region is very small, the integrand is practically a constant, and Equation A.3 further reduces to

$$\frac{U_{on}-U_{off}}{I}=-\frac{1}{I^2}\left(\sigma_{on}-\sigma_{off}\right)\mathbf{E}_{off}\cdot\mathbf{E}_{off}V \qquad (A.4)$$

which shows that the difference in voltage is a linear function of $\mathbf{E}_{off}\cdot\mathbf{E}_{off}$.

Wby the Frequency Domain?

Auld's formula depends on Lorentz's reciprocity theorem [12]. Since Lorentz's reciprocity theorem is quoted only in the frequency domain, Auld's formula must be also quoted in the frequency domain. Therefore the photoinductive method must be carried out only the frequency domain.

REFERENCES CITED

[1] J.R. Bowler, Eddy-current interaction with an ideal crack. I. The forward problem, Journal of Applied Physics, 75(12):8128 - 8137 (1994)

[2] J.R. Bowler, S.J. Norton, and D.J. Harrison, Eddy-current interaction with an ideal crack. II. The inverse problem, Journal of Applied Physics, 75(12):8138-8144 (1994)

[3] F.D.W. Charlesworth and W.D. Dover, Some aspects of crack detection and sizing using a.c. field measurement, In C.J. Beevers (editor), Advances in Crack Length Measurement, pages 253-276, Engineering Materials Advisory Services Ltd., Warley, West Midlands, UK (1982)

[4] W. Conley, Computer Optimization Techniques, Petrocelli Books Inc., New York (1980)

[5] C.V.Dodd and W.E.Deeds, Analytical solutions to eddy-current probe-coil problems, Journal of Applied Physics 6(6):2829-2835 (1968)

[6] W.D. Dover, R. Collins and D.H. Michael, The use of a.c. field measurements for crack detection and sizing in air and underwater, Philosophical Transactions of the Royal Society of London, A, 320:271-283 (1986)

[7] W.D. Dover, F.D. Charlesworth, K.A. Taylor, R.Collins and D.H. Michael, The use of a.c. field measurements to determine the shape and size of a crack in a metal, In G. Birnbaum and G. Free (editors), Eddy-current Characterization of Materials and Structures, pages 401-427, ASTM, Philadelphia (1981)

[8] L.C. Evans, Partial Differential Equations, Berkeley Mathematics Lecture Notes Vol. 3B, Center for Pure and Applied Mathematics, University of California, Berkeley, CA 94720 (1994)

[9] R. Kress, Linear Integral Equations, Springer-Verlag, Berlin (1989)

[10] C. Lanczos, Applied Analysis, Prentice-Hall, Englewood Cliffs, NJ (1956)

[11] L.D. Landau and E.M. Lifshitz, Electrodynamics of Continuous Media (2^{nd} edition), Permington, New York (1984)

[12] M. McIver, Characterization of surface-breaking cracks in metals sheets by using ac electric fields, Proceedings of the Royal Society of London, A, 421: 179-194 (1989)

[13] M. McIver, Inversion of voltage data to predict crack shape, In D.O. Thompson and D.E. Chimenti (editors) Review of Progress in Quantitative Nondestructive Evaluation, 9:367-373, Plenum Press, New York (1990)

[14] J.C. Moulder and N. Nakagawa, Characterizing the performance of eddy current probes using photoinductive field-mapping, Research in Nondestructive Evaluation. 4:221-236 (1992)

[15] J.C.Moulder, N.Nakagawa, K.S.No, Y.P.Lee and J.F.McClelland, Photoinductive imaging: a new NDE technique, In D.O.Thomson and D.E.Chimenti, editors, Review of Progress in Quantitative Nondestructive Evaluation, 8A: 599-606, Plenum, New York (1989)

[16] J.C. Moulder, E. Uzal and J.H. Rose, Thickness and conductivity of metallic layers from eddy current measurements, Review of Scientific Instruments 63(6):3455-3465 (1992)

[17] D.H. Michael, R.T. Waechter and R. Collins, The measurement of surface cracks in metals by using a.c. electric fields, Proceedings of the Royal Society of London, A, 381:139-157 (1982)

[18] N.Nakagawa, Theory of eddy current inspection of corner cracks, In D.O.Thomson and D.E.Chimenti, editors, Review of Progress in Quantitative Nondestructive Evaluation, 10A:249-254, Plenum, New York (1991)

[19] N.Nakagawa and J.C. Moulder, Eddy current probe calibration via the photoinductive effect, Review of Progress in Quantitative Nondestructive Evaluation, 13A:295-301, Plenum, New York (1994)

[20] A.P. Raiche and J.H. Coggon, Analytic Green's tensors for integral equation modelling, Geophysical Journal of the Royal Astronomical Society, 42:1035-1038 (1975)

[21] J.H. Rose, C.C. Tai and J.C. Moulder, Extreme sensitivity of eddy-curents to the surface conditions of nickel, Review of Progress in Quantitative Nondestructive Evaluation, 17, Plenum, New York (to be published in 1997)

[22] R. Satveli, Software modeling for flaw characterization of metals through eddy-currents, M.S. Thesis, Iowa State University, Ames, IA (1995)

[23] V.I. Smirnov, A Course of Higher Mathematics, (English translation by D.E. Brown), Permagon Press, Oxford (1964)

[24] C.C. Tai and J.C. Moulder, Photoinductive and eddy current imaging for bolt hole corner crack inspection (to be published)

[25] A.N. Tikhonov and V.Y. Arsenin, Solutions of Ill-Posed Problems, V.H. Winston and Sons, Washington D.C. (1977)